CHARACTERIZATION OF THE SKIN BARRIER TO CHEMICAL

PERMEATION BY IMPEDANCE SPECTROSCOPY

by

Erick A. White

A thesis submitted to the Faculty and the Board of Trustees of the

Colorado School of Mines in partial fulfillment of the requirements for the degree

of Doctor of Philosophy (Chemical Engineering)

Golden, Colorado

Date_____

Signed: _____

Eric A. White

Signed: _____

Dr. Annette L. Bunge

Thesis Advisor

Signed: _____

Dr. Mark E. Orazem

Thesis Advisor

Golden, Colorado

Date_____

Signed: _____

Dr. David W.M. Marr

Professor and Head

Department of Chemical Engineering

ii

ABSTRACT

Human skin is a heterogeneous composite membrane that acts as an effective barrier to permeation for most chemicals and ions. The barrier to ions is reflected in electrical impedance measurements, which are easily made, especially if measured at only one frequency. While measurements at a single frequency are useful, additional information about the skin barrier can be learned from measurements collected over a spectrum of frequencies. Despite the wide application of impedance measurements for the characterization of the skin barrier, the interpretation of those measurements remains nebulous.

The goals of this work were to develop a quantitative foundation for evaluating skin impedance measurements collected over a spectrum of frequencies and then to relate the results of the impedance data analysis to the effectiveness of skin samples in acting as barriers to chemical permeation. Toward this end, impedance spectra of undamaged and intentionally damaged samples of excised human skin, all fully hydrated, were analyzed using simple equivalent circuit models consisting of resistors and constant phase elements. In various experiments, including data from the literature, impedance results were compared with permeation measurements of tritiated water or two model lipophilic chemicals, 4-cyanophenol or parachloronitrobenzene.

Estimates of the effective capacitance calculated using parameters from the equivalent circuit models were remarkably similar for all samples studied, perhaps because water comprises a large volume fraction of fully hydrated skin. Moreover, the effective capacitance of skin treated with neat dimethyl sulfoxide

(DMSO), a polar aprotic solvent, for as long as one hour, did not change, although the skin resistance decreased as much as 150 fold. Impedance measurements for skin treated with DMSO for less than one hour were consistent with the presence of two layers in series: an undamaged layer with properties of the original skin sample, and a damaged layer with a thickness that was proportional to the square-root of the treatment time up to about 0.5 h, when the sample was fully damaged. For comparison, impedance spectra determined before and after the skin was punctured with a needle were adequately described by adding a low-resistance shunt in parallel with the skin that was otherwise unchanged. Significantly, the changes in impedance spectra collected before and after DMSO treatment for one hour could not be explained by a low resistance shunt parallel pathway.

Because the effective capacitance of hydrated skin is relatively constant, the DC skin resistance can be reliably estimated from single frequency impedance measurements reported in PAR mode at frequencies as large as 1000 Hz. By applying this analysis to four large data sets from three different laboratories comparing *in vitro* measurements of tritiated water permeability and impedance determined using an LCR databridge at 100 and 1000 Hz, the DC skin resistance was shown to be linearly proportional to the inverse of the tritiated water permeability coefficient. This result supports the hypothesis that water diffuses, to at least some significant extent, through the same polar pathway as ions.

The findings of this work illustrate the value of measuring impedance over a range of frequencies to examine skin barrier function. By analyzing the impedance spectrum, previously used methods of interpreting skin impedance measurements, especially for estimating the effective capacitance and DC resistance, were shown to not always reflect the true electrical properties of the skin. Also, insight into the mechanisms of chemical and physical damage can be deduced from a more complete analysis of the impedance spectrum.

TABLE OF CONTENTS

LIST OF FIGURES

LIST OF TABLES

ACKNOWLEDGMENTS

CHAPTER 1

INTRODUCTION

Human skin is a large and complicated organ. It is comprised of several layers each with different properties. The outer most layer, the stratum corneum (sc), is the primary barrier to permeation into and out of the body for many chemicals and is the main focus of this research. Unless stated otherwise in this thesis the word skin will refer to the sc. The sc is a formidable but not a perfect barrier to chemicals. The skin's excellent barrier properties are attributed to its composite structure. The sc can be visualized with a brick and mortar model where dead skin cells, corneocytes, are the bricks and a matrix of lamellar lipids form the mortar. It is widely accepted that chemical flux through the sc is a solution-diffusion process; however, the pathway of diffusion is still debated (Kasting et al., 2003; Wang et al., 2006, 2007).

The sc varies in thickness and composition with body region and between persons. To control for skin variability, one approach is to study permeation through skin from many subjects, but this is costly and time consuming. In skin penetration studies it is often difficult to distinguish between natural skin variability and actual damage. A common test for skin damage, also refered to as a skin integrity test, is to measure the permeability of tritiated water prior to or during the permeation experiment of the compound of interest. An 'acceptable' permeability of tritiated water is chosen above which the skin sample is deemed damaged and therefore unsuitable for permeation studies. This may result in an

unrepresentative sample population by discarding samples that are undamaged but have naturally high tritiated water permeability. Also, for samples with acceptable values of water permeability, the permeability of lipophilic compounds from water generally do not correlate with water permeability. This lack of correlation is attributed to a different pathway for skin permeation by lipophilic compounds than the pathway for polar compounds(Tang et al., 2002).

Single frequency impedance measurements are increasingly replacing tritiated water permeability measurements as skin integrity tests because they are inexpensive and quick compared to tritiated water permeability measurements. In these experiments, a value for skin impedance above which skin is deem acceptable is often chosen by comparing impedance measurements with established acceptance criteria for tritiated water permeability. A complication of single frequency impedance measurements is that the dielectric material in the skin causes the impedance to be a complex number that varies with the measurement frequency. As a result, except for measurements at low frequency, the relationship between single frequency impedance measurements and water permeability is nonlinear as observed by Fasano et al., (2002).

Chapters 2 and 3 of this thesis focus on the interpretation of single frequency impedance measurements made with a particular instrument, called the LCR data bridge, and the relationship between those measurements and the permeability coefficients of tritiated water and two hydrophilic compounds: urea and mannitol. In Chapter 4 the skin impedance measurements collected over a

range of frequencies are used to quantify the electrical properties of skin before and after skin is damaged either chemically or mechanically. These results are then compared with the steady-state flux of non-polar compounds through skin.

This chapter provides additional background and theory relevant to Chapters 2, 3 and 4, which because they are written in journal format, only contain brief descriptions of the most relevant background and theory. This chapter provides more detailed descriptions of the structure of human skin, the theory of dermal absorption, a model for chemical flux through skin, and the electrical properties of skin and impedance spectroscopy including the theory and modeling of impedance measurements. The last section is an overview of Chapters 2, 3 and 4.

1.1 Structure of Human Skin

Human skin is comprised of two macroscopic layers; the dermis is the inner layer and the epidermis is the outer layer. The dermis is a vascularized, essentially acellular layer approximately 1-2 mm thick (Rushmer et al., 1966) that contains hair follicles, muscles, sweat glands, sebaceous glands and blood vessels. The hair follicles and sweat glands, which occupy only 0.1-1% of the total skin surface area (Chien et al., 1989), originate in the dermis and penetrate through the epidermis. Blood vessels within the dermis provide a route to the systemic circulation for chemical to be cleared from the dermis.

The epidermis consists of two distinct avascular layers. The outermost layer, the sc, is a highly ordered, lipophilic layer of essentially dead cells. Below the sc is a hydrophilic layer of living cells called the viable epidermis (ve).

The sc is made of wide (20-40 μm), thin (~1 μm), and pentagonal or hexagonal shaped cells called corneocytes. The corneocytes have a dense cell wall of cross-linked proteins within which there are keratin filaments that are hydrophilic yet insoluble in water. Cells from healthy skin are exfoliated from the surface of the sc at a rate of about one cell layer per day, and replaced from the lower layers of the ve at the same rate to maintain a relatively constant sc thickness (10-40 μm).

The sc corneocytes are surrounded by highly organized lipid. The lipids are primarily made up of ceramides, saturated free fatty acids and cholesterol. The wall of the corneocytes contains covalently bound lipids that interact with the lipid bilayers which contributes to the mechanical strength of the sc (Wertz et al., 1989).

1.2 Dermal Absorption

Chemical penetration through the epidermis occurs via passive Fickian diffusion. Diffusion coefficients through the highly organized sc are much smaller than through the less organized ve. Thus, except for highly lipophilic solutes, which have low solubility in the hydrophilic ve, the sc controls the penetration of most chemicals through the skin.

Polar and ionic compounds appear to permeate the skin by a different path than nonpolar or lipophilic compounds. It has been argued that polar and ionic compounds permeate skin through a polar pathway at rates that depend primarily on molecular size, while non-polar compounds permeate through a non-polar pathway at rates that depend on both molecular size an lipophilicity (i.e.,

4

more lipophilic compounds permeate faster than less lipophilic compounds of the

same size) (Kasting et al., 1992). The lipopilicity of a compound is often

described by the octanol-water partition coefficient ($K_{o/w}$). It is possible that

lipophilic molecules diffuse through the sc via the extracellular lipids rather than

through the water-filled corneocytes (Michaels et al., 1975). The schematic

diagram in Figure 1.1 illustrates chemical permeation through the lipid bilayers

surrounding the corneocytes into the dermis where it is cleared by the blood.
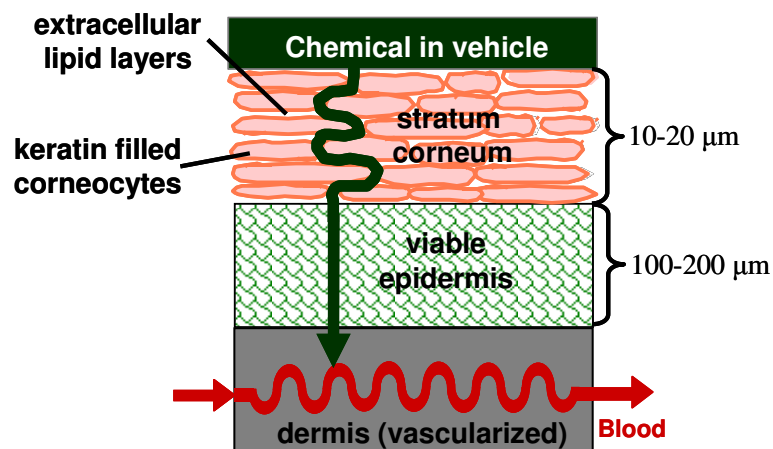
Figure 1.1 A schematic diagram illustrating the diffusion of a lipophilic compound from a donor solution to the systemic circulation via a tortuous path through the lamellar lipids.

In most cases solutes must first dissolve into the outermost layer of the sc

before it can diffuse through the sc. Penetration of solutes in the sc is slow

compared to diffusion of most compounds in liquids; thus, it is generally correct

to assume equilibrium between the solvent and the outermost layer of the sc.

Permeation through the epidermis to the dermis is usually slow relative to

clearance by the blood, resulting in low concentrations of the solute in the

dermis. For this reason, the dermis is often assumed to be a perfect sink for permeation across the epidermis.

Several chemicals are known to alter the barrier function of human sc. For example, Kurihara-Bergstrom demonstrated that dimethyl sulfoxide (DMSO) alters the barrier function of full-thickness excised skin (sc, ve and dermis) from hairless mouse by eluting sc lipids, and perhaps also by delaminating the sc and denaturing the sc proteins. However, when mixed with saline, DMSO had to exceed 50% strength (w/v) to alter the skin. In solutions containing 50% or less DMSO, the dermal absorption rates after adjusting for differences in thermodynamic activity were independent of DMSO concentration for methanol, 1-butanol and 1-octanol, which exhibit a wide range of octanol-water partitioning.

1.3 Chemical Flux Through Skin

The sc can be assumed to behave as a pseudo-homogeneous, isotropic membrane (Kasting et al., 1992). Under these conditions transport through the sc is described by Fick's second law

$$\frac{\partial C}{\partial t} = D \frac{\partial^2 C}{\partial x^2} \qquad 0 > x > L \qquad (1.1)$$

where C is the concentration of the solute within the sc, D is the effective diffusivity of the solute in the sc and L is the thickness of the sc. If initially there is no chemical within the skin then the initial condition is

$$t = 0 \qquad C = 0 \qquad 0 < x < L . \qquad (1.2)$$

Assuming equilibrium between the solution in contact with the outermost layer of the sc, the vehicle, also called the donor solution, then:

6

$$x = 0 \qquad C = C_v^o K \qquad t > 0 \qquad\qquad (1.3)$$

where C_v^o is the initial concentration of chemical in the vehicle, assumed to remain constant, and K is the equilibrium partition coefficient of the solute between the sc and the vehicle. If the concentration in the solution or tissue in contact with the innermost layer of the skin, the receptor solution or the ve, remains relatively small, then the boundary condition on the inside surface of the skin is

$$x = L \qquad C = 0. \qquad\qquad (1.4)$$

This is referred to as sink conditions, which is experimentally satisfied if the concentration in the receptor solution is less than 10% of saturation.

   With these restricting conditions, Fick's second law can be solved analytically (Crank, 1975) and the flux at $x = L$ integrated over time to give the following expression describing the cumulative mass of solute (M) that has diffused through an area (A) of the skin at time t:

$$M = a \left[tb - \frac{1}{6} - \frac{2}{\pi^2} \sum_{n=1}^{\infty} \frac{(-1)^n}{n^2} e^{-n^2 \pi^2 bt} \right] \qquad (1.5)$$

Equation (1.5) depends on two parameters, defined as:

$$a = K C_v^o A L \qquad\qquad (1.6)$$

and

$$b = \frac{D}{L^2}. \qquad\qquad (1.7)$$

which respectively quantify the solution (a) and diffusion (b) mechanisms of dermal absorption.

In diffusion cell experiments, excised skin is clamped between two chambers, one containing the donor solution and the other the receptor solution, which is kept close to sink conditions. In these experiments, concentration is measured in the receptor chamber solution from which the cumulative mass permeated is calculated. Eq (1.5) can be regressed to the cumulative mass as a function of time using the terms in the infinite series that contribute significantly. The lag time (t_{lag}) is calculated as

$$t_{lag} = \frac{L^2}{6D} = \frac{1}{6b}$$

(1.8)

and the permeability coefficient (P) is calculated as

$$P = \frac{KD}{L} = \frac{ab}{AC_v^o}$$

(1.9)

Note that here, as in most literature on skin penetration, the permeability coefficient is a function of the skin thickness. In other membrane literature P is called permeance.

After a delay that is approximately 2.4 times the t_{lag}, M in the receptor solution increases linearly with t (Bunge et al., 1995a). The rate that M per unit skin area (i.e. M/A) increases after 2.4 t_{lag} is the steady-state flux (J_{ss}) and is calculated from parameters a and b by Eq. (1.10)

$$J_{ss} = \frac{ab}{A}$$

(1.10)

If there is not sufficient data early in the experiment to model the rate of appearance of M in the receptor solution during transient period, J_{ss} and t_{lag} are

derived from regression of Eq. (1.11) to data in the linear portion of the M/A

versus t curve.

$$M / A = J_{ss}t - J_{ss}t_{lag} \qquad \text{for } t > 2.4 \ t_{lag} \qquad (1.11)$$

The slope of the regression line is J_{ss} and t_{lag} is the ratio of the intercept to the

J_{ss}. Experimental estimates for J_{ss} derived by linear regression to Eq. (1.11) will

be systematically lower than the actual value for J_{ss} if measurements of M/A at

times less than about 2.4 t_{lag} are included in the linear regression (Bunge et al.,

1995b).

1.4 Electrical Properties of Skin

Electrical resistivity (ρ) is the intrinsic material property that characterizes

the flux of ions through the the sc. Resistivity, which has units of Ω-cm, is related

to the DC resistance of the skin membrane (R_m) as:

$$\rho = \frac{R_m A}{L} \qquad (1.12)$$

where A is the area of the skin measured and L is the thickness of the sc barrier,

which is not normally known. It is convenient, therefore, to report the product of

ρ and L, which is equal to $R_m \cdot A$ and has units of $\Omega \ cm^2$. Thus, measurements of

the ionic transport barrier of skin samples should be represented by the DC

resistance multiplied by the sample area. Because skin is a heterogeneous

membrane, ($R_m \ A$) is proportional to the average resistivity over the area of the

skin sampled.

Likewise, the dielectric constant (ε), which is non-dimensional, is the intrinsic property of a membrane like the sc that has a capacitive component. The value of the effective capacitance (C_{eff}) is related to the dielectric constant by

$$C_{\text{eff}} = \frac{\varepsilon \, \varepsilon_{\text{o}} A}{L} \qquad (1.13)$$

where $\varepsilon_{\text{o}} = 8.8542 \times 10^{-5}$ nF/cm is the permittivity of vacuum. As with resistivity, since L is not known, it is typical to report $\varepsilon\varepsilon_{\text{o}} / L$ which is equal to C_{eff} / A with units of nF / cm^2.

Mass transfer across the sc is through either polar or non-polar pathways depending upon the $K_{\text{o/w}}$ of the penetrating molecule (Bennett and Barry, 1985). This is supported by experiments that show that the electrical resistance of skin is linearly related to the permeability of ionic and polar compounds (Burnette and Bagniefski, 1988; DeNuzzio and Berner, 1990; Oh et al., 1993). For example, as shown in Figure 1.2, the permeability of a polar compound (urea) is correlated with skin resistance while the permeability of a lipophilic compound (corticosterone) is independent of skin resistance. Since resistance measures the inverse of ionic mobility, decreasing values of resistance should correspond with easier penetration though the polar pathway. Further, the lack of correlation between the lipophilic compound and the resistance suggests that the lipophilic compound takes a different path than the charge conducting species.

Investigators have suggested that the skin capacitance arises from the highly ordered sc lipid layers (the major component of the lipophilic pathway),

which act as the dielectric material in the skin (DeNuzzio and Berner, 1990; Oh et al., 1993).
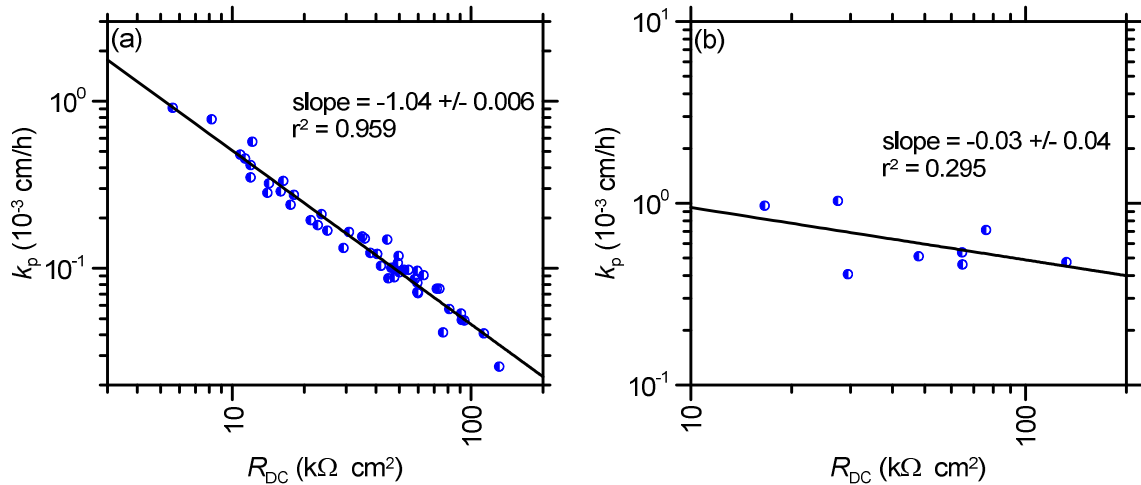
Figure 1.2 Plots of permeability as a function of resistance for (a) urea ($\log K_{o/w}$ = -2.11) and (b) corticosterone ($\log K_{o/w}$ = 1.94) reproduced from Peck et al. (1995).

Several studies have been conducted in which the skin was treated in such a way that the lipid structure was altered and the impedance was measured. For example, Kim and Oh (2011) applied non-ionic surfactants that were thought to increase the fluidity of the sc lipids to hairless mouse skin and observed an increase in skin capacitance. They also found that the surfactant treatment enhanced penetration of a nonpolar drug, ketoprofen, suggesting that capacitance may characterize the lipid pathway. Oh et al. (1993) found that the capacitance of hairless mouse skin increased with increasing temperature (between 20°C and 60°C) while the resistance decreased. They attributed the increase in skin capacitance to changes in the intercellular lipids presumed to be related to increased lipid fluidity and the decrease in skin resistance at elevated temperatures to the increased ionic mobility. They observed that at the gel-to-

liquid crystalline phase transition temperature of hairless mouse skin the impedance became indistinguishable from that of the electrolyte solution (Oh et al., 1993).

1.5 Impedance Spectroscopy

Skin impedance (Z) is measured by applying a small-amplitude oscillating current or potential signal across the skin and measuring the responding potential or current. The impedance is the ratio of the change in potential (V) to the change in current (I). Electrical resistance (R) is the direct current (DC) analog to Z. Like R, Z has units of Ohms (Ω) and is an extrinsic property, which depends on the area (A) and thickness (L) of the sample as well as the skin resistivity (ρ). Skin impedance also depends on the frequency of the applied signal. Measuring the impedance of a sample over a range of frequencies is called impedance spectroscopy.

The time variation, also known as the waveform, of the modulated signal can have different shapes, although sinusoidal variations are common. For potentiostatic impedance, the sinusoidal time oscillation of the potential (or voltage) E can be described as:

$$E(t) = E_\text{o} \cos(2\pi f t) \tag{1.14}$$

where t is time, and E_o is the amplitude and f is the frequency, respectively of the potential signal. The current response to this oscillating potential is expressed as:

$$I(t) = I_\text{o} \cos(2\pi f t - \phi) \tag{1.15}$$

where ϕ is the phase shift and I_o is the amplitude of the measured current response signal. The impedance (Z) is related to the potential and current by Ohms law (i.e., $Z = E / I$). Thus,

$$Z = \frac{E_o \cos(2\pi f t)}{I_o \cos(2\pi f t - \phi)} = \frac{E_o}{I_o} e^{j\phi} = |Z| e^{j\phi} \tag{1.16}$$

in which $|Z|$ is the frequency-dependent magnitude (i.e., the modulus) of the impedance and $j = \sqrt{-1}$. Using Euler's relationship,

$$e^{j\phi} = (\cos\phi + j\sin\phi) \tag{1.17}$$

the impedance can be written as the sum of real and imaginary components (Z_r and Z_j, respectively):

$$Z = Z_r + j Z_j \tag{1.18}$$

where

$$Z_r = |Z|\cos\phi \quad \text{and} \quad Z_j = |Z|\sin\phi \tag{1.19}$$

are related to the modulus and phase as follows:

$$|Z| = \sqrt{Z_r^2 + Z_j^2} \tag{1.20}$$

$$\phi = \arctan\frac{Z_j}{Z_r} \tag{1.21}$$
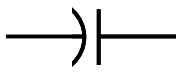
If the phase shift is zero, the impedance of the system is independent of the applied frequency and only a function of the amplitude of the perturbation (i.e. $Z = E_o / I_o$). This occurs for systems that only contain ideal resistors.

In general, non-zero values for the phase shift arises from time-dependant processes within the system. In skin the phase shift is likely due to a

13

capacitance that arises from the polarization and subsequent relaxation of the insulating material within the skin (DeNuzzio and Berner, 1990; Yamamoto and Yamamoto, 1976b).

Impedance measurements from physical systems like skin are commonly interpreted by relating them to the impedance that would arise from an electrical circuit, called an equivalent circuit model, comprised of passive elements that represent the impedance of the skin. Circuit elements that are commonly used in models applied to skin are a resistor (with resistance R), a capacitor (with capacitance C), and a constant-phase element (CPE) that is characterized by the parameters Q and α. The functional form of the impedance (Z) that arises from each of these elements is summarized in Table 1.1. The impedance of the resistor is independent of the frequency, while, as mentioned above, the impedance for the capacitor and the constant phase element (CPE) vary with frequency. Thus, the system resistance affects the magnitude of the impedance signal while components that behave like a capacitor or CPE affect the phase angle of the signal.

Table 1.1 Typical circuit elements and corresponding impedance

Element	Symbol	Impedance
Resistor	⌇	R
Capacitor	⊣⊢	$\dfrac{1}{j\omega C}$
Constant Phase Element	⊣⊢	$\dfrac{1}{Q(j\omega)^{\alpha}}$

Often, the equivalent circuit model required to represent the observed impedance-frequency response involves two or more circuit elements connected in either series or parallel. For circuits containing a number of elements (n) in series, the total impedance is the sum of the impedances as represented by Eq. (1.22).

$$Z = \sum_{i=1}^{n} Z_i \qquad (1.22)$$

For circuits with n elements in parallel, the reciprocal of the total impedance is the sum of reciprocals of the impedances as in Eq. (1.23).

$$\frac{1}{Z} = \sum_{i=1}^{n} \frac{1}{Z_i} \qquad (1.23)$$

The diagrams of two equivalent circuits that have been used to model skin impedance are displayed in Figure 1.3. The R-C circuit is comprised of a parallel resistor (R_m) and capacitor (C) that represent the skin membrane, in series with a resistor (R_e) representing the electrolyte resistance. The R-CPE circuit is similar to the R-C circuit except that the capacitor is replaced with a CPE.
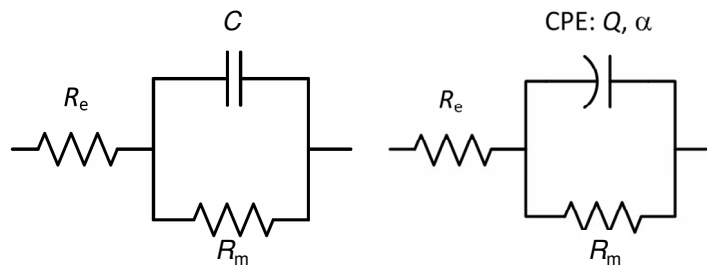
Figure 1.3 Two equivalent circuit models that have been used to model skin impedance. The R-C circuit (left) is a parallel resistor (R_m) and capacitor (C) in series with an electrolyte resistance (R_e). The R-CPE circuit (right) is similar to the R-C circuit except that a constant phase element (CPE) replaces the capacitor.

15

Expressions describing the complex impedance for the R-C and R-CPE circuits depicted in Figure 1.3 are given in Eqs. (1.24) and (1.25), respectively.

$$Z = R_e + \frac{R_m}{1 + R_m C (2\pi f \, j)} \qquad (1.24)$$

$$Z = R_e + \frac{R_m}{1 + R_m Q (2\pi f \, j)^{\alpha}} \qquad (1.25)$$

The R-C circuit is characterized by a single characteristic frequency (f_c)

$$f_c = \frac{1}{2\pi R_m C} \qquad (1.26)$$

which has units of Hz.

CPE behavior is attributed to a normal distribution of relaxation processes, characterized by the parameter α, which, for skin, is a number less than or equal to 1. If α is 1, then the R-CPE circuit is equivalent to the R-C circuit.

The R-CPE circuit represents the skin impedance better than the R-C circuit. This might be expected because the pathway for ions (and current) through skin consists of multiple paths of varying length and area, combined with the various sources of skin capacitance, which would result in a continuous distribution of characteristic frequencies. Integration over the distribution of characteristic frequencies results in the R-CPE equivalent circuit, which exhibits a single characteristic frequency (i.e. $f_{c,CPE}$) (Orazem and Tribollet, 2008; Yamamoto and Yamamoto, 1976b).

$$f_{c,CPE} = \frac{1}{2\pi (R_m Q)^{1/\alpha}} \qquad (1.27)$$

The CPE behavior of skin should be related to the dielectric constants and geometric configurations of the sc components, which are not yet known, that produce the frequency dependent impedance response. For the purpose of comparing skin samples, it is convenient to estimate an *effective* capacitance (C_{eff}). Hsu and Mansfeld (2001) suggested that because the characteristic frequency of the R-CPE circuit is independent of α, an expression relating C_{eff} to the R-CPE parameters R_{m}, Q and α can be derived by equating f_{c} and $f_{\text{c,CPE}}$ (Eq. (1.26) and Eq. (1.27) respectively) and substituting C_{eff} for C, resulting in Eq. (1.28)

$$C_{\text{eff}} = \left(Q R_{\text{m}}^{1-\alpha} \right)^{1/\alpha} \tag{1.28}$$

As discussed in Chapter 4 of this thesis, estimates of C_{eff} for skin calculated using Eq. (1.28) are unrealistically large by one or two orders of magnitude.

Recently, Hirschorn et al. (2010) demonstrated that the R-CPE behavior of skin impedance is consistent with a power-law decay of resistivity with depth into the skin while the dielectric constant is independent of position. There are published experimental results supporting this possibility (Kalia et al., 1996; Yamamoto and Yamamoto, 1976a). In this case, C_{eff} is defined as:

$$C_{\text{eff}} = g^{1/\alpha} Q^{1/\alpha} R_L^{(1-\alpha)/\alpha} \tag{1.29}$$

where R_{L} is the resistance of the inner most interface of the dominant resistive layer, which in this case is the stratum corneum, and the parameter g is defined by Eq. (1.30).

$$g = 1 + 2.88 \left(1 - \alpha \right)^{2.375} \tag{1.30}$$

Depending on the magnitude R_L, which is always smaller than R_m, values for C_{eff} estimated according to the Eq. (1.29) are more physically realistic than the Hsu and Mansfeld approach.

It is convenient (and common) to present impedance-frequency data on an *impedance-plane* plot (also called a Nyquist plot), which displays the negative of the imaginary part of the impedance ($-Z_j$) as a function of the real part of the impedance (Z_r) determined at each frequency. In Figure 1.4 an impedance plane plot of the impedance measured for an actual R-C circuit, configured as shown in Figure 1.3, is compared to the impedance of a theoretical R-CPE with the same characteristic frequency as the R-C circuit. The R-C circuit was comprised of resistors and capacitors such that $R_e = 0.100 \pm 1\%$ kΩ, $R_m = 115 \pm 1\%$ kΩ and $C = 47 \pm 20\%$ nF (RadioShack, Ft. Worth, TX). The impedance was measured under sinusoidal potentiostatic modulation, 10 mV rms perturbation, over a frequency range of 0.1 Hz to 20 kHz. The impedance of the R-CPE circuit also shown in Figure 1.4 was calculated using Eq. (1.25) with $R_e = 0.1$ kΩ, $R_m = 115$ kΩ, $\alpha = 0.80$ and $Q = 20.9$ nF, which corresponds to $C_{eff} = 47$ nF calculated using Eq. (1.28). These values of R_e, R_m and Q are typical to those observed in a 1.77-cm^2 sample of human skin when $\alpha = 0.80$ which is a reasonable value for skin. In Figure 1.4, the solid circles designate measurements collected (or calculated in the case of the R-CPE circuit) at the indicated frequencies and the symbol X designates the characteristic frequency for each circuit.
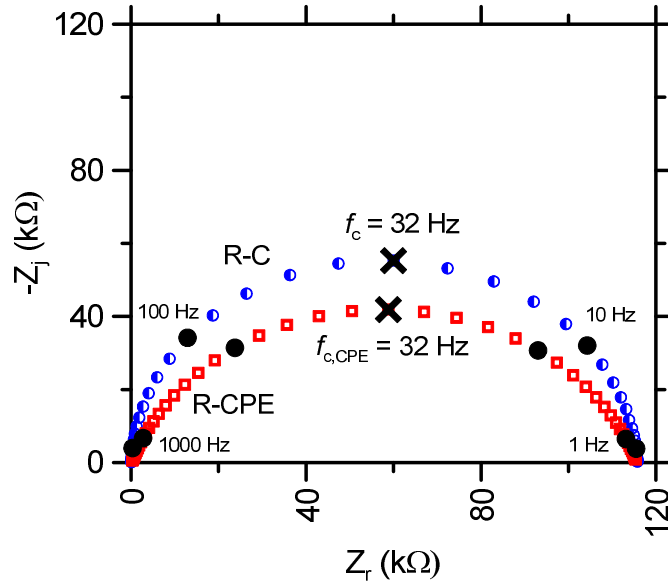
Figure 1.4 The impedance-plane plots of the experimental R-C circuit (half-filled circles, R_e = 0.100 kΩ, R_m = 115 kΩ and C = 47 nF) and the theoretical R-CPE circuit with the same characteristic frequency (R_e =0.100 kΩ, R_m = 115 kΩ, α = 0.80 and Q = 20.9 nF, which corresponds to C_{eff} = 47 nF calculated using Eq. (1.28)). The filled circles designate impedance at 1, 10, 100 and 1000 Hz.

1.6 Error Analysis of Impedance Data

Analysis of error in impedance data is important for assessing experimental technique and for analysis of experimental data (Agarwal et al., 1995a). Minimizing the systematic experimental error and quantifying the stochastic error in the impedance measurement increases the amount and quality of information that can be obtained from the EIS measurements. The Measurement Model Toolbox for impedance spectroscopy, developed by Mark Orazem, was used in this work to model the stochastic error of the measurements and to check the measurements for Kramers-Kronig consistency (Orazem, 2001). The method summarized here is described elsewhere in more

detail (Agarwal et al., 1995a; Agarwal et al., 1995b; Agarwal et al., 1992, 1996; Orazem, 2004; Orazem et al., 1996).

The frequency dependant residual error, ε_{res}, in the impedance data is defined by Eq. (1.31)

$$\varepsilon_{res}(\omega) = Z(\omega) - \hat{\hat{Z}}(\omega) \tag{1.31}$$

where ω is the radial frequency equal to $2\pi f$, $Z(\omega)$ is the measured value of the impedance and $\hat{\hat{Z}}(\omega)$ is the model value of the impedance. The residual error in turn depends on the systematic error due to lack of fit of the model (ε_{fit}), the systematic experimental (bias) error (ε_{bias}), and the random stochastic error (ε_{stoch}) as described by Eq. (1.32)(Orazem, 2004):

$$\varepsilon_{res}(\omega) = \varepsilon_{fit}(\omega) + \varepsilon_{bias}(\omega) + \varepsilon_{stoch}(\omega). \tag{1.32}$$

Bias errors are a result of instrumental artifacts or experimental factors described below. The measurement model method of error analysis identifies the frequency range of a spectrum that is affected by the bias error and provides a weighting strategy for regression based on the stochastic error of the data.

Inconsistency with the Kramers-Kronig relations indicates bias error in the impedance measurement. The Kramers-Kronig relations are a set of integral equations from which the imaginary component of the impedance can be predicted from the real component and vice versa, as expressed by Eqs. (1.33) and (1.34) respectively.

$$Z_j(\omega) = -\left(\frac{2\omega}{\pi}\right)\int_0^\infty \frac{Z_r(x) - Z_r(\omega)}{x^2 - \omega^2}\,dx \tag{1.33}$$

$$Z_r(\omega) = Z_r(\infty) + \left(\frac{2}{\pi}\right)\int_0^\infty \frac{xZ_j(x) - \omega Z_j(\omega)}{x^2 - \omega^2}\,dx \tag{1.34}$$

where *x* represents all frequencies between zero and infinity. The problem with applying the Kramers-Kronig relationships directly is that it requires measuring the impedance at a sufficient number of frequencies to approximate a continuous function between zero and infinity which is often unattainable in practice.

Satisfaction of the Kramers-Kronig relations is a necessary but not sufficient requirement of a system that is causal, stable and stationary. A system is causal if the response of the system is caused by a perturbation to the system. A system is stable if the response to a perturbation decays to its un-perturbed value with time. In the case of EIS, a stationary system means a system that does not change with time.

The electrochemical systems are rarely stationary; thus, the stationary condition is defined on three time scales. The first is non-stationary in which the system changes while collecting one data point (i.e., datum at one frequency in a spectrum). Impedance spectroscopy is generally not applicable to systems in this regime. The second is pseudo-stationary in which the system changes negligibly over the time required to collect an entire spectrum but significantly over the course of the experiment. This is the typical regime for electrochemical systems. The third time scale is stationary in which the system does not change with time during the entire experiment. To satisfy the Kramers-Kronig relations, the changes in the skin must be slow enough to be at least pseudo-stationary.

Non-stationary impedance behavior of human skin may indicate time variation in the hydration of the skin, a gradient in the concentration of charge-carrying ions across the skin, or skin damage caused by the measurement. Kramers-Kronig consistency is not sufficient to prove that the measured spectrum reflects only the properties of the system because some instrument artifacts may result in impedance features that are consistent with the Kramers-Kronig relations (Orazem, 2004).

To evaluate the data for bias errors, the magnitude of the stochastic errors must be determined. The magnitude of the stochastic error for skin impedance measurements cannot be determined by calculating the standard deviation of replicate measurements because the pseudo-stationary behavior of the skin introduces bias errors to the estimate of the stochastic error. The measurement model approach described below enables determination of the magnitude of the stochastic error by using a Kramers-Kronig consistent circuit model as a filter for experimental bias, baseline drift and fitting errors in the impedance measurements. Following Agarwal et al. (Agarwal et al., 1995a; Agarwal et al., 1995b; Agarwal et al., 1992, 1996) and Orazem et al. (Orazem et al., 1996), the measurement model chosen for this work consists of Voigt elements, composed of a parallel resistor and capacitor, in series with a resistor, representing the solution resistance, as expressed by the following equation

$$\hat{\tilde{Z}}(\omega) = R_e + \sum_{k=1}^{n} \frac{R_k}{\left(1 + j\tau_k\omega\right)} \qquad (1.35)$$

where R_e is the electrolyte resistance, R_k and τ_k are the resistance and the time constant (equal to $1/(2\pi f_k)$ where f_k is the characteristic frequency) of the kth Voigt element.

The stochastic error is determined by fitting the measurement model, Eq. (1.35), to several EIS scans, measured on the same experimental apparatus, by modulus-weighted, complex non-linear least squares regression. Each scan must have the same number of data points measured at the same frequencies. Also, each scan must be regressed to the same measurement model (i. e., the value of n in Eq. (1.35) must be the same for each scan). The value of n is the maximum number of Voigt elements that can be regressed to all of the scans such that the 95.4 % confidence interval for each fit parameter, R_k and τ_k, does not include zero. The value of n is determined iteratively by adding Voigt elements to the measurement model until the fit is no longer improved by the addition of further Voigt elements as determined by the 95.4% confidence interval.

The residual error between the data and the measurement model cannot be taken as the stochastic error because the error due to lack of fit could be significant. However, the standard deviation of the residuals, as expressed by Eq. (1.36), is an estimate of the stochastic error as a function of frequency.

$$\sigma_{Z_r}^2(\omega) = \frac{1}{n-1}\sum_{k=1}^{n}\left(\varepsilon_{\mathrm{res},Z_r,k}(\omega) - \bar{\varepsilon}_{\mathrm{res},Z_r}(\omega)\right)^2 \tag{1.36}$$

where $\varepsilon_{\mathrm{res},Z_r,k}(\omega)$ is the residual error, as defined by Eq. (1.31), of the real part of the impedance at frequency ω of scan k, $\bar{\varepsilon}_{\mathrm{res},Z_r}(\omega)$ is the mean of the residual

23

errors at frequency ω for n scans. The residual errors of the imaginary parts can be treated in the same way to estimate the standard deviation of the stochastic error. For Kramers-Kronig consistent data, σ_{Z_r} is indistinguishable from σ_{Z_j} (Durbha et al., 1997).

Agarwal et al. (1995a) suggested Eq. (1.37) as a general model for the stochastic error

$$\sigma_{Z_r} = \sigma_{Z_j} = \alpha \left| Z_j \right| + \beta \left| Z_r \right| + \gamma \frac{\left| Z \right|^2}{R_m} + \delta \tag{1.37}$$

where R_m is the known value of the current measuring resistor inside the instrument used for the experiment and α, β, γ, and δ are constants to be determined by regression (Agarwal et al., 1995a). Because the stochastic error is a characteristic of the impedance instrument, the stochastic error model can be used to weight all impedance scans of similar impedance magnitude measured by the same instrument over the same range of frequencies. For example, impedance measurements of damaged skin with low impedance can exhibit different stochastic errors than measurements of high impedance undamaged skin.

The stochastic error of eight impedance scans of human split-thickness skin is presented in Figure 1.5. The measurements were performed after twelve hours of equilibration in phosphate buffered saline solution and were regressed by the model of Eq. (1.37) as a function of frequency. The model of the stochastic error described by Eq. (1.37) and represented by the dashed curve in

Figure 1.5 does not capture all of the features of the error structure, particularly

the peak near 1000 Hz which is likely an artifact of the potentiostat.
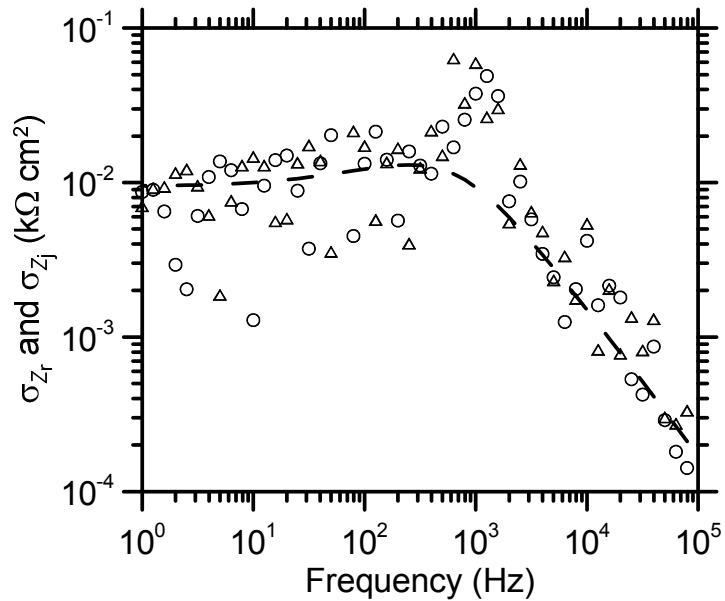
Figure 1.5 The standard deviation of the real (circles) and imaginary (triangles) residual errors for eight impedance scans of human split-thickness skin plotted as a function of frequency. The dashed curve represents the regression of Eq. (1.37) o the real and imaginary residual errors.

The general method to check for Kramers-Kronig consistency is to fit the

measurement model with the maximum number of statistically significant Voigt

elements to either the real or imaginary part of the impedance and use the

regression parameters to predict the other component. For example, in Figure

1.6 the measurement model regressed to the imaginary part of a skin impedance

spectrum, weighted by the model of the stochastic error shown in Figure 1.5, is

plotted as a function of frequency. The parameters derived from this regression

to the imaginary part were used to predict the real part of the impedance, which

is shown in Figure 1.7.

Weighting the regression of the data to the measurement model with the frequency-dependant stochastic error emphasizes data points with small stochastic error and de-emphasizes data points with large stochastic error (Agarwal et al., 1995a). The model of the stochastic error also provides criteria for a good fit of the measurement model to the data. The dashed curves in Figure 1.6 and Figure 1.7 represent the 95.4% confidence interval for the model obtained by Monte Carlo simulation using the calculated confidence intervals for the estimated parameters described elsewhere (Agarwal et al., 1995b).
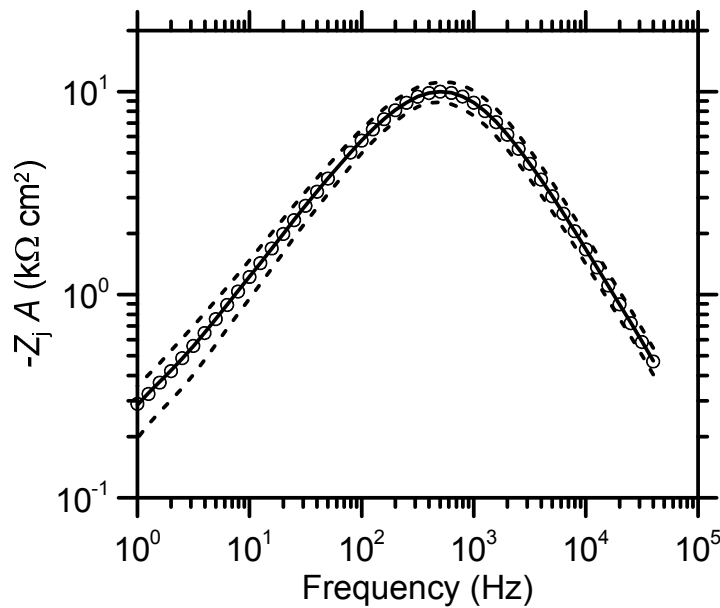
Figure 1.6 The results of the Voigt measurement model regressed to the imaginary part of a typical skin impedance spectrum plotted as a function of frequency. The circles are the imaginary part of the impedance of the scan. The solid curve is the regression result. The dashed curves represent the 95.4% confidence interval for the model.
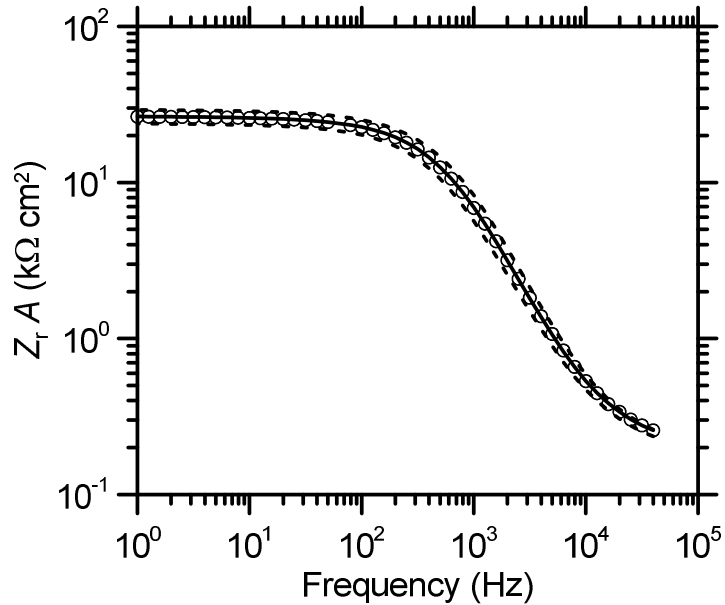
Figure 1.7 The real part of a typical impedance spectrum plotted as a function of frequency (circles). The solid curve represents the real part of the impedance predicted by the parameters from the regression fit to the imaginary part of the impedance spectrum shown in Figure 1.6. The dashed curves represent the 95.4% confidence interval for the model.

A more sensitive plot for assessing Kramers-Kronig consistency of the data is shown in Figure 1.8 in which the residuals of the regression to the imaginary data (circles) is plotted. The predicted residuals of the real data are shown in Figure 1.9. In both Figures 1.8 and 1.9, the dashed curves indicate the 95.4% confidence interval for the model obtained by Monte Carlo simulation using the calculated confidence intervals for the estimated parameters.

Data that fall outside of the 95.4% confidence interval for the model prediction are considered to be inconsistent with the Kramers-Kronig relations. All of the data shown in Figure 1.9 are within the 95.4% confidence interval of the fit, which confirms that the skin impedance data presented here are consistent with the Kramers-Kronig relations. Had there been data that were shown to be inconsistent with the Kramers-Kronig relations, the Kramers-Kronig inconsistent

data would be discarded and the entire process repeated. The remaining data, weighted with the variance of the stochastic error, is then regressed to the process model (e.g. the R-CPE model) using complex nonlinear least squares weighted by the stochastic error as described in more detail in Chapter 4. If the impedance data over a large portion of the frequency range were determined to be inconsistent with the Kramers-Kronig relations, then the experimental apparatus and procedure would need to be re-evaluated for sources of bias error.
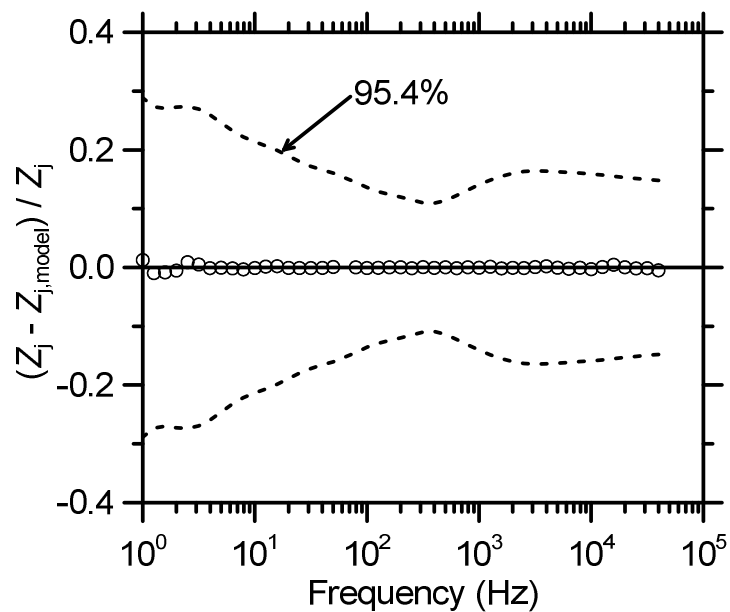
Figure 1.8 The relative residual errors for the regression fit of the measurement model to the imaginary part of the impedance data plotted as a function of frequency. The circles represent the relative residual errors of the regression as a function of frequency. The dashed curves represents the 95.4% confidence interval for the model obtained by Monte Carlo simulation using the calculated confidence intervals for the estimated parameters.
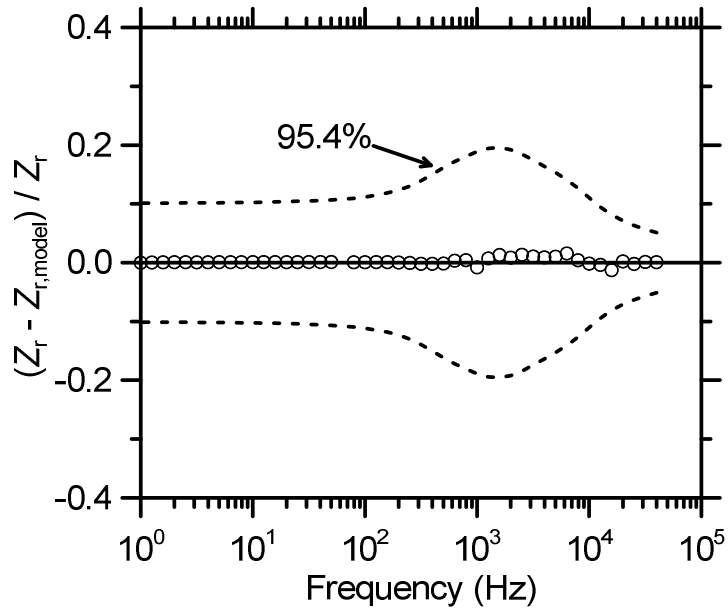
Figure 1.9 The relative residual errors for the real part of the impedance that is predicted by regression of the Voigt measurement model to the imaginary part of the impedance spectrum. The circles represent the relative residual errors of the real part of the regression as a function of frequency. The dashed curves represents the 95.4% confidence interval for the model obtained by Monte Carlo simulation.

1.7 Thesis Overview

The objective of this work is to establish a quantitative foundation for evaluating skin impedance measurements. In doing so, this work further develops impedance spectroscopy as a tool for measuring skin variability and skin damage in order to decrease the uncertainty in skin permeation experiments and thereby reduce the cost and duration of experimentation.

In Chapter 2 the theoretical interpretation of single frequency impedance measurements made with an LCR data bridge is clarified and demonstrated experimentally. Specifically, manipulations of the equations for a simple R-CPE equivalent circuit model are used to relate the measurements from an LCR data bridge to the DC skin resistance, which is the value that is most sensitive to skin

integrity. An average value for the effective capacitance, as determined by the Hsu and Mansfeld approach (Eq. (1.28)) is calculated from the impedance spectra of 145 skin samples and found to be relatively constant. Based on this analysis, it was shown that LCR databridge measurements at 100 Hz reported as R in parallel mode and C in series mode are more sensitive to skin integrity than R measured in series mode or C in parallel mode. Also, measurements at 100 Hz were superior to those collected at 1000 Hz.

In Chapter 3 the equations describing the frequency dependence of R reported in PAR mode developed in Chapter 2 are used to correlate LCR databridge impedance measurements with the permeability coefficient of tritiated water measured on the same piece of skin. The relationship between impedance measurements and the tritiated water permeability, which is based on the impedance of an R-CPE equivalent circuit, is extended to two other hydrophilic molecules. This relationship is used to compare previously published impedance criteria for identifying skin as acceptable for chemical absorption studies.

In Chapter 4, the skin impedance and the flux of moderately lipophilic compounds are quantitatively characterized before and after two treatments known to alter skin either chemically, with the polar solvent dimethyl sulfoxide (DMSO), or mechanically by puncture with a needle. The impedance spectrum of skin treated with DMSO for less than 0.5 h appears to consist of an undamaged layer and a damaged layer but the flux of p-chloronitrobenzene does not change after DMSO treatments for 0.25 or 1 h.

The pinhole experiments provide a quantitative test for the Hsu and Mansfeld formula (Eq. (1.28)) for estimating the effective capacitance of skin when there are other features not associated with the electrical properties of the skin itself. Before and after pinhole, the skin impedance is consistent with a single R-CPE circuit, the characteristic frequency of the skin changes in a way that is predicted by the theory recently published by Hirshchorn (2010). After the puncture, the flux of 4-cyanophenol increases by a small but significant amount that is not correlated with the estimated area of the pinhole calculated from the change in the resistance of the system.

REFERENCES

Agarwal, P., Crisalle, O., Orazem, M.E., Garcia-Rubio, L., 1995a. Application of measurement models to impedance spectroscopy, II. Determination of the stochastic contribution to the error structure. Journal of the Electrochemical Society 142, 4149-4158.

Agarwal, P., Orazem, M.E., Garcia-Rubio, L., 1995b. Application of measurement models to impedance spectroscopy, III. Evaluation of consistency with Kramers-kronig relations. Journal of the Electrochemical Society 142, 4159-4168.

Agarwal, P., Orazem, M.E., Garcia-Rubio, L.H., 1992. Measurement Models for Electrochemical Impedance Spectroscopy 1. Demonstration of Applicability. Journal of Electrochemical Society 139, 1917-1926.

Agarwal, P., Orazem, M.E., Garcia-Rubio, L.H., 1996. The influence of error structure on interpretation of impedance spectra. Electrochim. Acta 41, 1017-1022.

Bennett, S.L., Barry, B.W., 1985. Effectiveness of skin penetration enhancers propylene glycol, azone, decylmethylsulphoxide and oleic acid with model polar (mannitol) and nonpolar (hydrocortisone) penetrants. J. Pharm. Pharmacol. 37, 84P.

Bunge, A.L., Cleek, R.L., Vecchia, B.E., 1995a. A new method for estimating dermal absorption from chemical exposure. 3. Compared with steady-state methods for prediction and data analysis. Pharm. Res. 12, 972-982.

Bunge, A.L., Cleek , R.L., Vecchia, B.E., 1995b. A new method for estimating dermal absorption from chemical exposure. 3. Compared with steady-state methods for prediction and data analysis. Pharm. Res. 12, 972-982.

Burnette, R.R., Bagniefski, T.M., 1988. Influence of constant current iontophoresis on the impedance and passive Na+ permeability of excised nude mouse skin. J. Pharm. Sci. 77, 492-497.

Chien, Y.W., Siddiqui, O., Shi, W.M., Lelawongs, P., Liu, J.C., 1989. Direct current iontophoretic transdermal delivery of peptide and protein drugs. J. Pharm. Sci. 78, 376-383.

Crank, J., 1975. The Mathematics of Diffusion, Second Edition ed. Oxford University Press, Oxford.

DeNuzzio, J.D., Berner, B., 1990. Electrochemical and iontophoretic studies of human skin. J. Controlled. Release 11, 105-112.

Durbha, M., Orazem, M.E., Garcia-Rubio, L.H., 1997. Spectroscopy Applications of the Kramers-Kronig Transforms: Implications for Error Structure Identification. Journal of The Electrochemical Society 144, 48-55.

Fasano, W.J., Manning, L.A., Green, J.W., 2002. Rapid integrity assessment of rat and human epidermal membranes for in vitro dermal regulatory testing: correlation of electrical resistance with tritiated water permeability. Toxicol. In Vitro 16, 731-740.

Hirschorn, B., Orazem, M.E., Tribollet, B., Vivier, V., Frateur, I., Musiani, M., 2010. Determination of effective capacitance and film thickness from constant-phase-element parameters. Electrochim. Acta 55, 6218-6227.

Hsu, C.H., Mansfeld, F., 2001. Technical note: Concerning the conversion of the constant phase element parameter Y0 into a capacitance. Corrosion 57, 747-748.

Kalia, Y.N., Pirot, F., Guy, R.H., 1996. Homogeneous transport in a heterogeneous membrane: Water diffusion across human stratum corneum in vivo. Biophys. J. 71, 2692-2700.

Kasting, G.B., Barai, N.D., Wang, T.-F., Nitsche, J.M., 2003. Mobility of water in human stratum corneum J. Pharm. Sci. 92, 2326-2340.

Kasting, G.B., Smith, R.L., Anderson, B.D., 1992. Prodrugs for dermal delivery: solubility, molecular size, and functional group effects, In: Sloan, K.B. (Ed.), Prodrugs: Topical and Ocular Drug Delivery. Marcel Dekker, New York, pp. 117-161.

Kim, H.S., Oh, S.Y., 2011. Effect of Polyoxyethylene Alkyl Esters on Permeation Enhancement and Impedance of Skin. Biomolecules & Therapeutics 19, 109-117.

Kurihara-Bergstrom, T., Flynn, G.L., Higuchi, W.I., 1986. Physicochemical study of percutaneous absorption enhancement by dimethyl sulfoxide: kinetic and thermodynamic determinants of dimethyl sulfoxide mediated mass transfer of alkanols. J. Pharm. Sci. 75, 479-486.

Michaels, A.S., Chandrasekaran, S.K., Shaw, J.E., 1975. Drug permeation through human skin: Theory and in vitro experimental measurement. American Institute of Chemical Engineers' Journal 21, 985-996.

Oh, S.Y., Leung, L., Bommannan, D., Guy, R.H., Potts, R.O., 1993. Effect of current, ionic strength and temperature on the electrical properties of skin. J. Controlled. Release 27, 115-125.

Orazem, M.E., 2001. User Manual for the Measurement Model Toolbox for Impedance Spectroscopy. University of Florida, Gainesville, FL.

Orazem, M.E., 2004. A systematic approach toward error structure identification for impedance spectroscopy. Journal of Electroanalytical Chemistry 572, 317-327.

Orazem, M.E., Moustafid, T.E., Deslouis, C., Tribollet, B., 1996. The Error Structure of Impedance Spectra for Systems with a Large Ohmic Resistance with Respect to the Polarization Impedance. Journal of The Electrochemical Society 143, 3880-3890.

Orazem, M.E., Tribollet, B., 2008. Electrochemical Impedance Spectroscopy. Wiley-Interscience, Hoboken, NJ.

Peck, K.D., Ghanem, A.H., Higuchi, W.I., 1995. The effect of temperature upon the permeation of polar and ionic solutes through human epidermal membrane. J. Pharm. Sci. 84, 975-982.

Rushmer, R.F., Buettner, K.J.K., Short, J.M., Odland, G.F., 1966. The Skin The Most Accessible Tissue of the Body Serves as a Potential Focus for Multidisciplinary Research. Science 154, 343-348.

Tang, H., Blankschtein, D., Langer, R., 2002. Prediction of steady-state skin permeabilities of polar and nonpolar permeants across excised pig skin based on measurements of transient diffusion: Characterization of hydration effects on the skin porous pathway. J. Pharm. Sci. 91, 1891-1907.

Wang, T.F., Kasting, G.B., Nitsche, J.M., 2006. A multiphase microscopic diffusion model for stratum corneum permeability. I. Formulation, solution, and illustrative results for representative compounds. J. Pharm. Sci. 95, 620-648.

Wang, T.F., Kasting, G.B., Nitsche, J.M., 2007. A multiphase microscopic diffusion model for stratum corneum permeability. II. Estimation of physicochemical parameters, and application to a large permeability database. J. Pharm. Sci. 96, 3024-3051.

Wertz, P.W., Madison, K.C., Downing, D.T., 1989. Covalently bound lipids of human stratum corneum. J. Invest. Dermatol. 92, 109-111.

Yamamoto, T., Yamamoto, Y., 1976a. Dielectric constant and resistivity of epidermal stratum corneum. Med. Biol. Eng. Comput. 14, 494-500.

Yamamoto, T., Yamamoto, Y., 1976b. Electrical properties of the epidermal stratum corneum. Med. Biol. Eng. 14, 151-158.

CHAPTER 2

A CRITICAL ANALYSIS OF SINGLE-FREQUENCY LCR

DATABRIDGE IMPEDANCE MEASUREMENTS OF HUMAN SKIN

The content of this chapter was published in Toxicology in Vitro (White et al., 2011) and reproduced here with consent from the publisher.

Testing whether the barrier of skin samples has sufficient integrity for meaningful measurements of *in-vitro* chemical permeability is usually required when data are generated for regulatory purposes. Recently, skin integrity has been assessed using LCR databridge measurements, which are reported as resistances determined in either series (SER) or parallel (PAR) modes at a single frequency, typically 100 or 1000 Hz. Measurements made at different combinations of mode and frequency are known to differ, although the skin literature reveals confusion over the meaning of these differences and the impact on the interpretation of integrity test results. Here, the theoretical meanings of resistance and capacitance measurements in PAR and SER mode are described and confirmed experimentally. SER-mode resistances are equal to the real part of the complex impedance; whereas, PAR-mode resistances are the inverse of the real part of the admittance. Capacitance measurements reported in SER and PAR modes are similar manipulations of the imaginary parts of the complex impedance and admittance. A large body of data from human cadaver skin is used to show that the PAR-mode resistance and SER-mode capacitance

measured at 100 Hz are sensitive to skin resistivity, which is the electrical

measurement most closely related to skin integrity.

2.1 Introduction

Measurement of electrochemical impedance has been shown to be a

convenient method for characterizing many different materials, including human

or animal skin. The method involves applying small-amplitude sinusoidal

modulation of an input current or potential and measuring the responding

potential or current. Impedance is the ratio of the change in potential to the

change in current. Because the phase difference between the measured and

input signals depends on the modulation frequency, it is convenient to express

the impedance as a complex number that varies with the frequency of the time

variation. In the limit of low frequency, the impedance measurement should

approach the direct current (DC) resistance (R_{DC}).

Percutaneous absorption data are required for risk assessments of

potentially toxic chemicals. *In-vitro* measurements of human skin can be used to

avoid testing on human volunteers or animals. However, the collection and

handling of excised skin can introduce damage, which may affect the

percutaneous absorption measurements (Scott et al., 1991). Therefore, testing

whether the barrier function of skin samples has sufficient integrity for meaningful

measurements of *in-vitro* chemical permeability is common and usually required

when data are generated for regulatory purposes (Heylings and Esdaile, 2007;

International Programme on Chemical Safety (IPCS), 2006; OECD, 2004a).

Measurement of skin impedance is faster and less expensive than measuring

tritiated water permeation (Davies et al., 2004; Fasano and Hinderliter, 2004; Fasano et al., 2002), which has been the conventional skin integrity test (Franz and Lehman, 1990; Kasting et al., 1994; Scott et al., 1992). For the same reason, *in-vitro* impedance measurements are also used to identify chemicals and chemical mixtures that cause irreversible (or corrosive) damage to the skin (OECD, 2004a).

Several papers have described impedance measurements of *in-vitro* skin samples determined using an LCR databridge; e.g., from PRISM (Davies et al., 2004; OECD, 2004b) or Tinsley (Fasano et al., 2002). According to their manufacturers, these instruments measure inductance (L), capacitance (C) or resistance (R) in either a parallel (PAR) or series (SER) mode determined at one of two user-selected frequencies, usually 100 or 1000 Hz. Nearly always, the reported resistance values measured by PAR and SER modes (i.e., R_{PAR} and R_{SER}, respectively) at a given frequency are different. Also, R_{PAR} and R_{SER}, determined at different frequencies, are different, clearly indicating that these instruments are not reporting the DC skin resistance (Fasano and Hinderliter, 2004).

In assessing skin integrity or corrosion, the meaningful quantity is the electrical resistivity of the skin (ρ), which quantitatively characterizes the pathway for transport of ions. Consistent with this, the permeability of polar and ionic chemicals through skin has been shown to be inversely proportional to the resistivity (Kasting and Bowman, 1990; Peck et al., 1994, 1995). Low resistivity, therefore, indicates high permeability to ions or polar chemicals, which is

consistent with damage. Because the thickness of the stratum corneum (ℓ), the

skin layer primarily responsible for electrical resistance, is not usually measured,

it is convenient to report the product of ρ and ℓ, which is equal to the DC

resistance of the skin (R_{skin}) multiplied by the area for charge transfer (A). LCR

databridge measurements of skin will meaningfully assess skin integrity or

damage only if the resistance measured represents a reliable estimate of the DC

resistance.

The strategy is to reject skin samples with resistivity below a specified

acceptance criterion as being too damaged for determining reliable chemical

permeation parameters. Typically, the acceptance criterion is selected by

comparing electrical measurements on a series of samples to the percutaneous

absorption measurements for tritiated water (Davies et al., 2004; Fasano et al.,

2002), other polar compounds (Peck et al., 1995), or ionized salts (Kasting and

Bowman, 1990). Peck et al. (1995) and Kasting and Bowman (1990)

recommended that DC resistance values of 20 and 35 kΩ cm^2, respectively, were

suitable acceptance criteria. Proposed minimum acceptable values in R_{PAR} from

LCR databridge measurements, derived by comparing R_{PAR} measurements to

the same maximum acceptable tritiated water absorption of 1.5 mg cm^{-2} h^{-1}

(which is equal to a permeability coefficient of 1.5 x 10^{-3} cm/h), differ depending

on the frequency of the R_{PAR} measurement. Fasano et al. (2002) suggested that

skin samples be rejected if they have a resistance, measured at 1000 Hz and

normalized for area, less than 11 kΩ cm^2. Davies et al. (2004) recommended

using a criterion of 25 kΩ cm^2 based on measurements at 100 Hz. (Note that

Davies et al. (2004) incorrectly listed the measuring frequency as 100 kHz rather

than 100 Hz (Heylings, 2009).) The OECD 430 guidelines for identifying

corrosive chemicals used measurements at 100 Hz in SER mode in validation

studies, and recommend measurement frequencies between 50 and 1000 Hz

(OECD, 2004b).

Given that skin integrity is characterized by the resistivity, equal to

$R_{skin} \cdot A/\ell$, it is important to know the extent to which LCR databridge

measurements at 100 or 1000 Hz, reported in either PAR or SER modes, are

correlated with the DC skin resistance. The objective of this work is to explain

and establish experimentally the electrical quantities represented by R_{PAR} and

R_{SER} and also the capacitance reported in PAR and SER modes (i.e., C_{PAR} and

C_{SER}, respectively). A large quantity of skin impedance data is used to

demonstrate the significant advantage of using the PAR resistance

measurements at 100 Hz or the SER capacitance measurements at 100 Hz to

estimate the skin resistivity, and therefore, integrity. These data are also used to

derive equations relating the DC resistance to R_{PAR} at 100 and 1000 Hz and C_{SER}

at 100 Hz. In a companion study, measurements of tritiated water permeation

are shown to be linearly correlated with estimates of DC resistance derived from

LCR databridge measurements determined at either 100 or 1000 Hz in three

different laboratories (White, 2011).

2.2 Theory

Impedance (Z) is the alternating current (AC) analog to the DC resistance (R_{DC}), which is expressed in terms of real (Z_r) and imaginary (Z_j) parts as

$$Z = Z_r + j\, Z_j \qquad (2.1)$$

where $j = \sqrt{-1}$. The inverse of the impedance is the admittance (Y), which is the AC analog of DC conductance. Like the impedance, the admittance can be written in terms of real (Y_r) and imaginary (Y_j) parts as

$$Y = \frac{1}{Z} = Y_r + j\, Y_j \qquad (2.2)$$

Notably, Z_r is only equal to the inverse of Y_r when the imaginary part of the impedance is zero.

The complex capacitance is defined to be the admittance (or the inverse of the impedance) divided by the angular frequency (ω), i.e.,

$$C = \frac{Y}{j\omega} = \frac{1}{j\,Z\omega} = C_r + j\, C_j \qquad (2.3)$$

in which ω is equal to $2\pi f$, where f is the number of cycles per time. It is important to note that the complex capacitance depends on frequency and is not the intrinsic dielectric property of the material.

The presence of dielectric material in the skin causes a phase lag in the response to a periodic electrical signal. As a result, Z, Y and C measured for skin vary with frequency and include imaginary parts. It has been suggested that highly ordered stratum corneum lipids are the dielectric material (DeNuzzio and

40

Berner, 1990; Oh et al., 1993). If skin were to behave as a simple resistor, there would be no phase shift and no imaginary parts, and Z and Y would be independent of frequency (Fasano and Hinderliter, 2004).

The references to 'parallel' and 'series' in the LCR databridge measurements is nomenclature from older technology in which a variable resistor and capacitor in either parallel or series circuits were used on one side of a Wheatstone bridge circuit. The electrochemical cell on which measurements are being made is connected to the other side of the Wheatstone bridge circuit, and the magnitudes of the capacitor and resistor are adjusted to balance the potential drop across the Wheatstone bridge. The values of the resistor and capacitor in the balanced circuit gave the real and imaginary parts of the impedance. If the configuration of the balancing circuit is a resistor and capacitor in series, then the impedance, referred to as Z_{SER} is given by:

$$Z_{SER} = R_{SER} + j\frac{-1}{\omega C_{SER}} = Z_r + j Z_j \qquad (2.4)$$

It follows that the real part of the impedance, $Z_r = R_{SER}$, and the imaginary part of the impedance, $Z_j = -1/\omega C_{SER}$.

Similarly, when the balancing circuit is configured as a resistor and capacitor in parallel, then the inverse of the impedance of the parallel circuit $(1/Z_{PAR})$ is equal to the inverse of the impedance for the resistor and capacitor as follows:

$$\frac{1}{Z_{PAR}} = Y_{PAR} = \frac{1}{R_{PAR}} + j\omega C_{PAR} = Y_r + j Y_j \qquad (2.5)$$

Therefore, the measured R_{PAR} is equivalent to $1/Y_r$ and the measured C_{PAR} is equivalent to Y_j/ω.

Unlike Wheatstone bridge devices, LCR databridge instruments do not contain an actual resistor-capacitor (R-C) measuring circuit. Instead, the LCR databridge instruments use a phase-sensitive analog-to-digital converter to determine the magnitude of the resulting voltage that is in-phase with the perturbation and the magnitude of the voltage that is out-of-phase with the perturbation. The corresponding current is measured with a current-to-voltage converter (H. Tinsley & Co, 1996). The measurement theory and practice is described in detail in the 6401 LCR Databridge Users Manual (H. Tinsley & Co, 1996).

A physical model of skin impedance is not available because the source of the skin impedance is not well understood. As a result, it is customary to use equivalent circuits, comprised of simple circuit elements, to model the skin impedance. A common circuit model of *in-vitro* skin impedance, depicted in Figure 2.1, is a resistor that represents the frequency-independent (Ohmic) resistance containing contributions from the electrolyte, wires, and possibly the dermis (R_e) in series with a parallel resistor (R_{skin}) and capacitor (C_{skin}) that represent the skin polarization resistance and skin capacitance, respectively. Although this simple R-C circuit model does not represent actual skin impedance spectra as well as alternative circuit models like a resistor in parallel with a constant phase element (Hirschorn et al., 2010; Kontturi and Murtomaki, 1994; Yamamoto and Yamamoto, 1976b; Yamamoto and Yamamoto, 1976a;

42

Yamamoto and Yamamoto, 1976c, 1981a, b) , it is presented here because it does capture the important features.
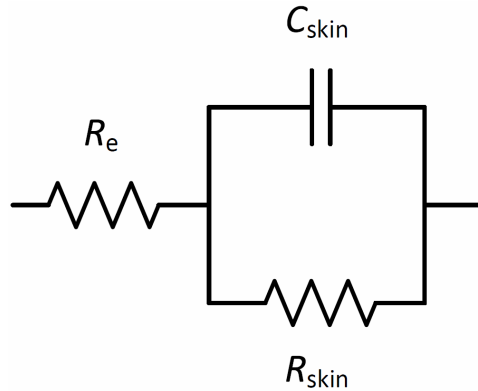
Figure 2.1 A simple R-C circuit model of skin

The impedance response of the R-C circuit presented in Figure 2.1 is similar to that of human skin, determined either *in vitro* or *in vivo*, in that the Z_r in both cases approach asymptotic values at high and low frequencies. As the alternating current (AC) frequency approaches zero, Z_j approaches zero and Z_r approaches the DC resistance of the system; thus, $Z = Z_r = R_{DC} = R_e + R_{skin}$. For large frequencies, the impedance of the skin becomes negligibly small and $Z = Z_r$ $= R_e$ (Orazem and Tribollet, 2008). The equations presented in Table 2.1 for R_{PAR}, R_{SER}, C_{PAR} and C_{SER}, corresponding to the R-C circuit in Figure 2.1, can be obtained by algebraic rearrangements of the expressions describing the complex impedance provided in the Appendix. The equations describing R_{PAR}, R_{SER}, C_{PAR} and C_{SER} for a circuit with a resistor in series with a resistor in parallel with a constant phase element (R-CPE circuit) also are listed in the Appendix.

Table 2.1 Equations for the PAR and SER modes of R and C for the R-C model circuit shown in Figure 1.

	PAR	SER
R	$R_{PAR} = \dfrac{1}{Y_r} = \dfrac{R_{skin}\left[\left(1+\dfrac{R_e}{R_{skin}}\right)^2 + \left(\omega R_e C_{skin}\right)^2\right]}{R_e R_{skin}\left(\omega C_{skin}\right)^2 + 1 + \dfrac{R_e}{R_{skin}}}$	$R_{SER} = Z_r = R_e + \dfrac{R_{skin}}{1+\left(\omega R_{skin} C_{skin}\right)^2}$
C	$C_{PAR} = \dfrac{Y_j}{\omega} = \dfrac{C_{skin}}{\left(1+\dfrac{R_e}{R_{skin}}\right)^2 + \left(\omega R_e C_{skin}\right)^2}$	$C_{SER} = -\dfrac{1}{Z_j \omega} = C_{skin} + \dfrac{1}{\omega^2 R_{skin}^2 C_{skin}}$

2.3 Materials and Methods

Impedance and LCR databridge measurements were performed on a "dummy cell" circuit constructed of resistors and capacitors to confirm the interpretation of the LCR databridge results in terms of a full spectrum impedance analysis. Impedance measurements on human skin were then used to simulate LCR databridge readings and, thereby, to establish the relationship between LCR databridge measurements and skin integrity.

2.3.1 Dummy Cell

A dummy cell electrical circuit, constructed to mimic approximately the impedance behavior of skin, was used to test the theoretical definitions of R_{PAR},

44

R_{SER}, C_{PAR} and C_{SER}. Specifically, measurements of R_{PAR}, R_{SER}, C_{PAR} and C_{SER}

from an LCR databridge (Tinsley Model 6401 LCR Databridge, Croydon, UK)

measured at 100 and 1000 Hz were compared to the complex impedance and

admittance spectra determined for frequencies from 0.1 Hz to 20 kHz using a

Gamry potentiostat (model PCI4/300, Warminster, PA). The dummy cell (Radio

Shack, Fort Worth, TX) was assembled on a modular integrated circuit

breadboard socket with a resistor ($R_e = 100 \pm 1\ \Omega$) placed in series with a second

resistor ($R_{skin} = 115 \pm 1\ k\Omega$) that was in parallel with a capacitor ($C_{skin} = 47.0 \pm$

9.4 nF). The impedance electrode leads were connected to the circuit in a two

electrode configuration with solderless breadboard jumper wires. The LCR

databridge data were provided by C. Roper (Charles River Laboratories,

Edinburgh, UK). For the Gamry potentiostat measurements, the potential was

modulated 10 mV rms with a mean applied potential of zero (i.e. no DC bias was

applied) at 10 frequencies per logarithmic decade over the frequency range.

2.3.2 Chemicals and Materials

Phosphate buffered saline (0.01 M) with 0.138 M NaCl, 0.0027 M KCl (pH

7.4, Sigma P-3813) was prepared in de-ionized (DI) water (Millipore Corporation,

Bedford, MA). Split-thickness human cadaver skin (approximately 300 μm thick),

harvested from the back or abdomen within 24 hours post mortem, was

purchased from National Disease Research Interchange (NDRI, Philadelphia,

PA). The skin was immediately frozen after collection and stored at

temperatures less than -60° C until used.

2.3.3 Skin Impedance

Impedance was measured across skin samples mounted between two horizontally oriented chambers in one of three configurations. Most experiments were conducted in glass Side-Bi-Side^{TM} cells from PermeGear, Inc. (Hellertown, PA), which have an exposed skin area of 1.77 cm^2 and a 13-mL volume for each chamber. Other impedance experiments were conducted in custom-made, polycarbonate cells (0.64-cm^2 area and a chamber volume between 9 and 15 mL each), or in Side-Bi-Side^{TM} cells modified to hold a customized frame assembly (PDM Services, Golden, CO), in which the skin is mounted (area and nominal volume are 1.70 ± 0.14 cm^2 and 13 mL, respectively). Both chambers of the three cell configurations were designed to accommodate two Ag/AgCl electrodes (In Vivo Metric, Healdsburg, CA), one working and one reference. The working electrodes were 12 mm diameter discs oriented with the face parallel to the skin surface. The cylindrical reference electrodes (1.5 mm diameter and 3 mm long) were oriented such that the long axis is parallel to the skin surface. During an experiment, both chambers were filled with PBS solution and the temperature was maintained at 32°C in either a temperature-controlled environmental chamber (Electro-Tech Systems, Inc., PA) or by circulating water through the water jacket from a temperature-controlled bath.

Spectra of impedance-frequency scans were measured for 145 skin samples from 6 subjects (all Caucasian, 4 males, ages 51 to 78 years, average of 68.5 years) using the Gamry potentiostat at the same operating conditions used in the dummy cell experiment. The frequency range was from 1 Hz to 10

kHz, except for a few scans for which the frequency was as low as 0.1 Hz or as high as 300 kHz. Impedance scans were collected hourly during an equilibration period of 8 to 12 h to establish a baseline for the electrical properties of the skin as well as to verify that the skin was at equilibrium as indicated by insignificant differences between subsequent spectra. The frequency dependence in the measurements was consistent among the six subjects. No distinguishable effect of age or gender was observed; e.g., the subjects with the highest and lowest average impedance values (85 and 17 kΩ cm^2) were males of 78 and 76 years, respectively.

2.4 Results and Discussion

Experiments performed on a "dummy cell" circuit constructed of resistors and capacitors provided confirmation of the relationship between LCR databridge values and impedance results at the same frequency. This correspondence was used to assess the use of LCR databridge values to estimate skin resistivity and as a measure of skin integrity.

2.4.1 Dummy Cell Measurements

Measurements of the dummy cell determined using the LCR databridge are compared in Figure 2.2 to the Z_r and $1/Y_r$ spectra measured with the Gamry potentiostat. In agreement with the equations presented in Table 2.1, Z_r and $1/Y_r$ asymptotically approach the sum $R_e + R_{skin}$ at low frequency and R_e at high frequency. At intermediate frequencies, Z_r and $1/Y_r$ both decrease with frequency, although the rate of decrease for Z_r is greater than $1/Y_r$. Consistent

with the definitions provided in Table 2.1 for LCR databridge measurements, values of R_{SER} measured at 100 Hz and 1000 Hz are indistinguishable from the corresponding Z_r values. Likewise, R_{PAR} measured at 100 Hz and 1000 Hz are indistinguishable from the corresponding $1/Y_r$ values.
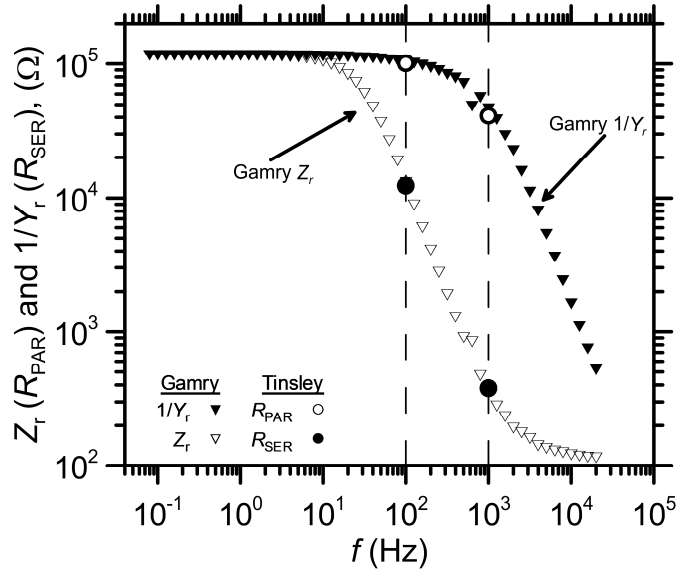
Figure 2.2 R_{PAR} and R_{SER} measured by the Tinsley LCR databridge at 100 and 1000 Hz compared with Z_r and $1/Y_r$ spectra measured by the Gamry potentiostat for the dummy cell (R_e = 100 Ω, R_{skin} = 115 kΩ, C_{skin} = 47 nF).

Values for C_{PAR} and C_{SER} reported by the Tinsley 6401 at 100 Hz and 1000 Hz are compared in Figure 2.3 to ($-1/\omega Z_j$) and Y_j/ω calculated from the complex impedance spectra measured with the Gamry potentiostat. The values of C_{SER} and C_{PAR} determined at 100 Hz and 1000 Hz with the Tinsley instrument are indistinguishable from values of ($-1/\omega Z_j$) and Y_j/ω, respectively, which confirms the definitions of the C_{SER} and C_{PAR} measurements presented in Table 2.1. For an ideal R-C circuit, C_{skin} is the asymptotic limit for ($-1/\omega Z_j$) at high frequency and also for Y_j/ω at low frequency if $R_e \ll R_{skin}$ (Table 2.1). For the

48

dummy cell, the asymptotic limits of Y_j/ω and $(-1/\omega Z_j)$ are the same and approximately 40 nF, which is within the component tolerance reported by the manufacturer. The small but evident frequency dependence at low and high frequency for Y_j/ω and $(-1/\omega Z_j)$, respectively, indicates that the electrical components of the dummy cell were not perfectly ideal capacitors.
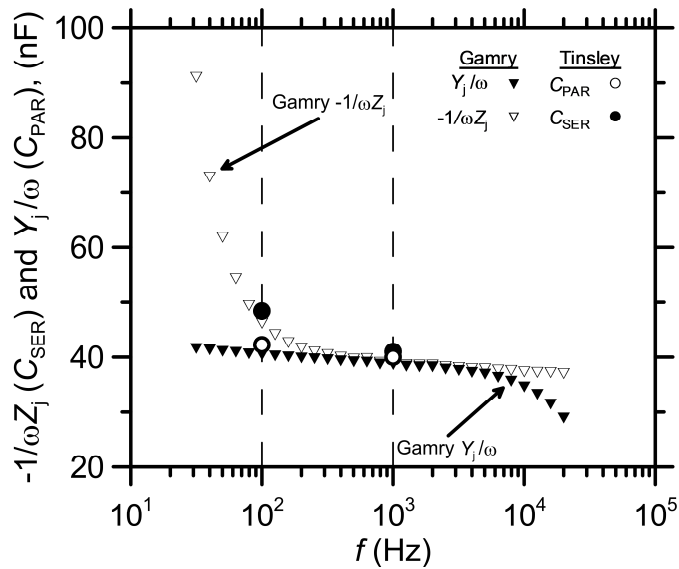
Figure 2.3 C_{PAR} and C_{SER} measured by the Tinsley LCR databridge compared with Y_j/ω and $-1/\omega Z_j$ spectra measured by the Gamry potentiostat for the dummy cell (R_e = 100 Ω, R_{skin} = 115 kΩ, C_{skin} = 47 nF).

2.4.2 Application to Human Skin

The results presented in the previous section confirm that impedance measurements at 100 and 1000 Hz can be used to estimate the values of R_{PAR}, R_{SER}, C_{PAR}, and C_{SER} measured by a Tinsley LCR databridge. Values of R_{SER} and R_{PAR} calculated from the complex impedance measured as a function of frequency for two samples of human cadaver skin are presented in Figure 2.4 as examples of skin exhibiting low and high impedance values. The frequency

variation of C_{PAR} and C_{SER} are presented in Figure 5 for the same two pieces of skin.
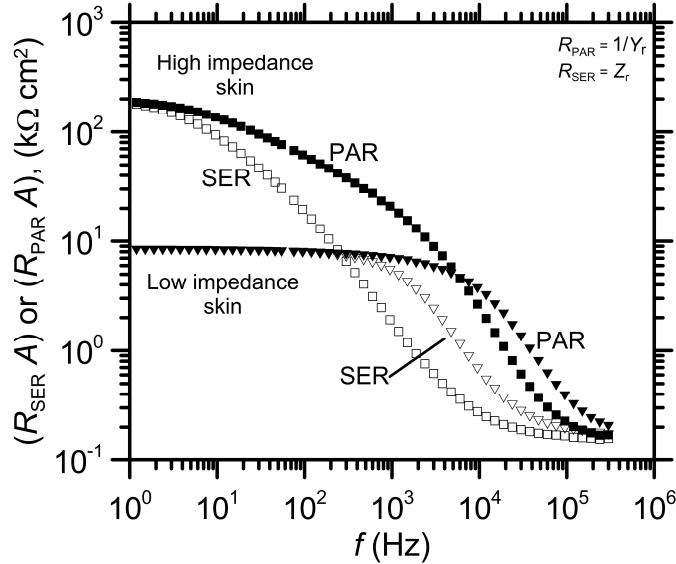
Figure 2.4 Area-normalized values of R_{SER} (open symbols) and R_{PAR} (filled symbols) calculated from the complex impedance measured with the Gamry potentiostat as a function of frequency for a high impedance skin sample (squares) and a low impedance skin sample (triangles).

The features of the R_{SER} and R_{PAR} spectra for human skin are similar to those observed for the dummy R-C circuit shown in Figure 2.2. At low frequency, R_{SER} and R_{PAR} asymptotically approach the DC resistance of the total cell (*i.e., R_e + R_{skin}*), which is approximately 9 and 180 kΩ cm^2 for the low and high impedance samples, respectively. As with the dummy cell, R_{PAR} and R_{SER} both asymptotically approach R_e at higher frequencies. Also, like the dummy cell, at a given intermediate frequency, R_{PAR} is larger than R_{SER} for both the high and low impedance skin. For both R_{SER} and R_{PAR}, the magnitude of any deviation from the DC resistance of the cell is reduced when measurements are made at lower frequency.

50

Notably, although the frequency dependence is similar for skin and the dummy cell, the maximum slope of the R_{PAR} and R_{SER} spectra is smaller for the skin samples than would be expected for an ideal R-C circuit. This is consistent with many other skin impedance studies (Hirschorn et al., 2010; Kontturi and Murtomaki, 1994; Membrino et al., 1997; Yamamoto and Yamamoto, 1976c), which found that, while the frequency dependence of the impedance for a simple R-C circuit model is similar to that measured in skin, a good quantitative fit of the skin data with an R-C circuit is not possible.

The C_{SER} and C_{PAR} spectra of the cadaver skin samples shown in Figure 2.5 and the dummy cell shown in Figure 2.3 also have similar features. The C_{PAR} spectra for the high and low impedance skin samples almost overlap, indicating little sensitivity to the large difference in DC resistance of the skin. Furthermore, the C_{PAR} values are nearly independent of frequency over most of the measured spectrum, decreasing significantly only at the higher frequencies. The rate of change of C_{SER} with frequency is large for both skin samples at frequencies less than about 100 Hz and relatively independent of frequency at frequencies of about 1000 Hz and higher. Overall, the C_{SER} spectra for the high impedance skin is shifted to the left relative to the C_{SER} spectra for low impedance skin, suggesting that C_{SER} is sensitive to variations in the DC cell resistance, although this will not be apparent if C_{SER} is measured at a higher frequency. At higher frequencies, C_{SER} for both pieces of skin approach a similar asymptotic value, which is related to, but not normally equal to, the effective capacitance of the skin sample (which is defined and discussed in the Appendix). Despite the more than

20-fold difference in the low frequency impedance values, the asymptotic values of C_{SER} at high frequency for the low and high impedance skin samples shown in Figures 2.4 and 2.5 differ by only a factor of about two, which is consistent with the typically small variation in the effective capacitance for fully hydrated skin in diffusion cell experiments.
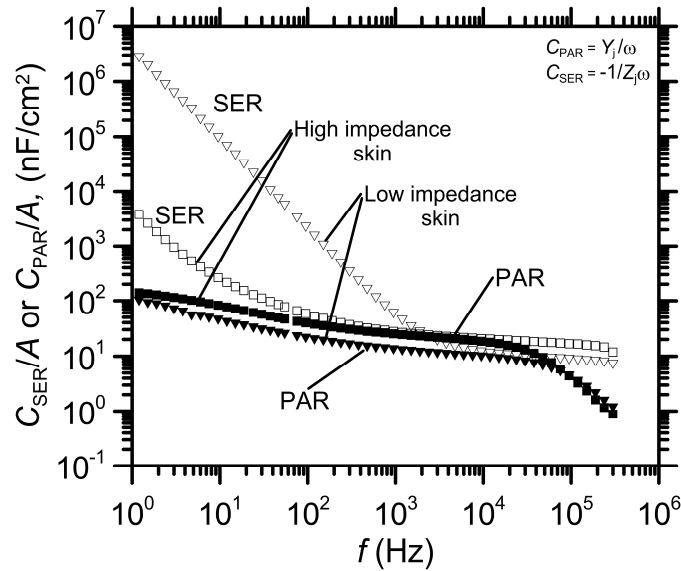
Figure 2.5 Area normalized values of C_{SER} (open symbols) and C_{PAR} (filled symbols) calculated from the complex impedance measured with the Gamry potentiostat as a function of frequency for a high impedance skin sample (squares) and a low impedance skin sample (triangles).

The frequency-dependent *in-vitro* measurements presented in Figures 2.4 and 2.5 are consistent with measurements collected over a similar range of frequencies on human subjects *in vivo*, including the effects of treatments that caused skin damage; e.g., (Curdy et al., 2001; Curdy et al., 2004; Kalia et al., 1996; Rosell et al., 1988). Quantitative *in vitro-in vivo* comparisons to these published data are not possible due to differences in the experimental protocols.

There are a few commercial instruments designed to assess human skin hydration *in vivo* through measurement of the total magnitude of the impedance, the reciprocal of the resistance of the impedance, or the capacitance contribution of the impedance (Barel and Clarys, 2006; Gabard et al., 2006; Nicander et al., 2006; Tagami, 2006). Quantitative comparisons of the measurements among these instruments are impossible due to differences in the measurement frequencies, the nature of the skin-electrode contact, and the electrode type, shape and configuration (Nicander et al., 2006). Compared with *in-vitro* impedance measurements, which are made across known skin layers, the skin depth measured by these commercial instruments is unknown and different for each. Also, some of the devices (e.g., the Corneometer from Courage-Khazaka Electronic) only report results in arbitrary units related to skin hydration. Moreover, in contrast to the LCR databridge and Gamry measurements presented here, these commercial devices measure at frequencies that are large, at least 1 kHz and often greater than 1 MHz (Barel and Clarys, 2006; Gabard et al., 2006; Nicander et al., 2006; Tagami, 2006). Most probably the observations from these measurements are related to factors other than stratum corneum resistivity.

2.4.3 Estimation of Skin Resistivity

The resistance of skin is usually much larger than the Ohmic resistance (i.e., $R_{skin} >> R_e$), and, therefore, the low-frequency asymptote of the real part of the impedance approximates the DC resistance of the skin sample (R_{skin}). If the lowest frequency measured is sufficiently small, the low-frequency asymptote

can be estimated by the real part of the impedance at the lowest frequency measured, designated as $Z_{r,lf}$. Values of R_{SER} and R_{PAR} calculated from the complex impedance measured at either 100 or 1000 Hz were normalized by $Z_{r,lf}$ for 145 samples of human cadaver skin. The corresponding ratios $R_{SER}/Z_{r,lf}$ and $R_{PAR}/Z_{r,lf}$ are presented in Figure 2.6 as functions of R_{SER} and R_{PAR}, respectively. For all the samples shown in this and subsequent figures, the estimated difference between $Z_{r,lf}$ and the true value of R_{skin} is less than 4%.
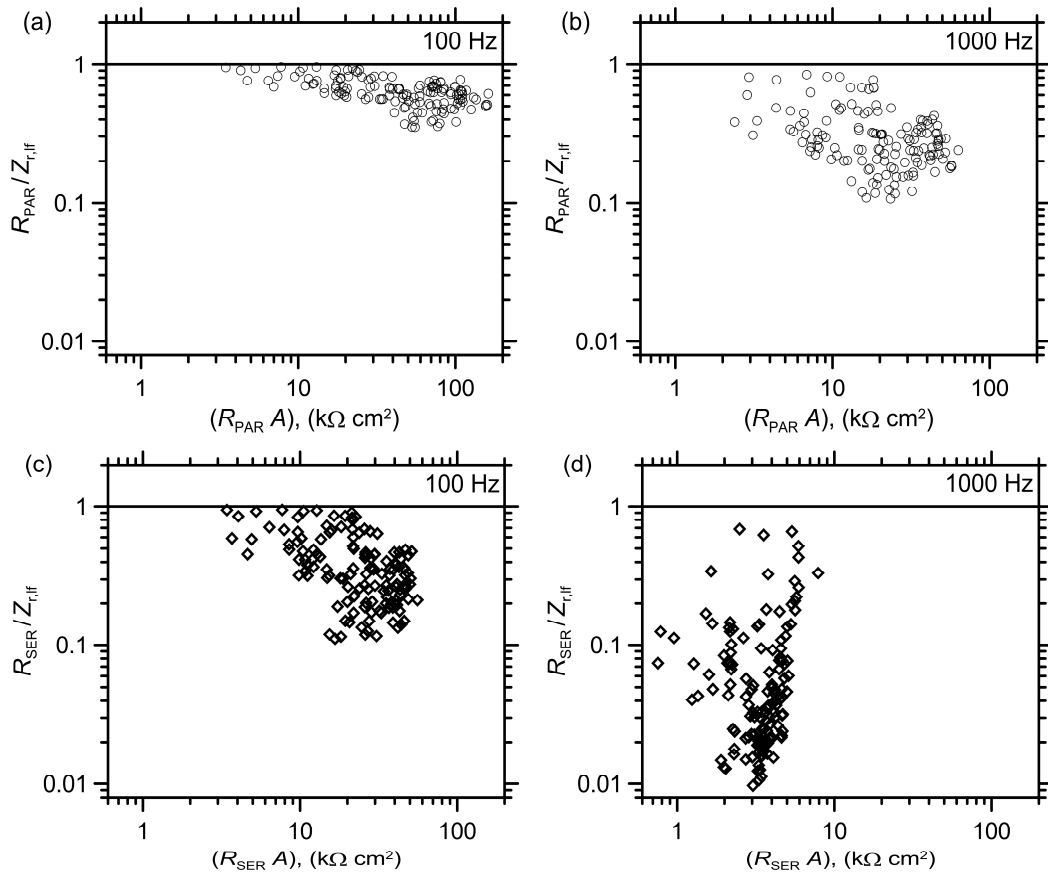
Figure 2.6 Ratios of R_{PAR} and R_{SER} to the low frequency real impedance ($Z_{r,lf} \cong R_{skin}$) plotted as a function of R_{PAR} and R_{SER}, respectively for 145 samples of human cadaver skin measured at 100 or 1000 Hz.

Consistent with the results in Figure 2.4 for two representative pieces of skin, the data presented in Figure 2.6 show that R_{PAR} is a better estimate for $Z_{r,lf}$ than is R_{SER} at both frequencies (i.e., measurements of $R_{PAR}/Z_{r,lf}$ are close to 1 more often than are measurements of $R_{SER}/Z_{r,lf}$). Also, R_{PAR} more closely estimates $Z_{r,lf}$ when R_{PAR} is smaller; the same applies to R_{SER}. At 100 Hz, R_{PAR} and R_{SER} can underestimate $Z_{r,lf}$ by factors of 3 and 10, respectively. This increases to factors of 13 and 100 for R_{PAR} and R_{SER}, respectively when measured at 1000 Hz.

Overall, the skin impedance results shown in Figure 2.6 indicate that skin resistivity and, therefore, its barrier function to ions or polar molecules is estimated better by impedance measurements at lower frequency, and that measurements at higher frequency may show little correlation with skin resistivity. This is consistent with observations from others. For example, Kalia et al. (1998) found that changes in measurements of *in-vivo* transepidermal water loss (TEWL) during skin barrier function development in premature infants correlated with the modulus of the impedance measured at 1.6 Hz but not with impedance measured at 486 Hz. Also, in experiments comparing *in-vitro* measurements of tritiated water permeability with R_{PAR} determined at 1000 Hz for heat-separated human epidermal membranes, Fasano et al. (2002) observed that the natural logarithm of the tritiated water permeability was not linearly related to the natural logarithm of R_{PAR} measured at 1000 Hz. Their observation is consistent with the results presented in Figure 2.6b and d, which shows that

the ratios of $R_{PAR}/Z_{r,lf}$ and $R_{SER}/Z_{r,lf}$ measured at 1000 Hz were not equal to one or independent of the measured skin impedance.

The OECD guidelines for identifying chemicals that irreversibly damage skin recommend measuring impedance in SER mode at frequencies between 50 and 1000 Hz (OECD, 2004b). Based on the present, more thorough, examination of the frequency dependence of skin impedance measurements, the skin barrier to polar and ionic compounds is best assessed at a frequency that is not larger than 100 Hz.

Values of C_{SER}/A and C_{PAR}/A calculated from Gamry potentiostat measurements at 100 and 1000 Hz are presented in Figure 2.7 as a function of $(Z_{r,lf}\,A)$ for the same skin samples shown in Figure 2.6. As expected from the results shown in Figure 2.5, C_{PAR} determined at either 100 or 1000 Hz is insensitive to variations in $(Z_{r,lf}\,A)$. In contrast, C_{SER} decreases with increasing $Z_{r,lf}$, although the data scatter for the measurements at 1000 Hz are too large to derive a meaningful correlation. However, measurements of C_{SER} at 100 Hz are obviously correlated with $(Z_{r,lf}\,A)$ with only a little scatter for skin samples having area-normalized values of $Z_{r,lf}$ between about 20 and 80 kΩ cm^2; for these, C_{SER}/A is related to $(Z_{r,lf}\,A)$ by

$$\log\left(C_{SER}\,/\,A\right) = -1.07\,\log\left(Z_{r,lf}\cdot A\right) + 3.85 \qquad r^2 = 0.94 \qquad (2.6)$$

where the units for C_{SER}/A and $(Z_{r,lf}\,A)$ are nF/cm^2 and kΩ cm^2, respectively.

Figure 2.7 Area-normalized values of C_{SER} and C_{PAR} calculated from the complex impedance of 145 cadaver skin samples measured using the Gamry potentiostat at either 100 or 1000 Hz and plotted as a function of $(Z_{r,lf} A)$.

Two factors make C_{SER} measured at 100 Hz for human skin more sensitive to changes in the skin resistance than C_{SER} measured at 1000 Hz. First, the variation in the effective capacitance of most skin samples is relatively small. Second, 100 Hz is usually within a factor of about four of the characteristic frequency (f_c) for human skin, defined here as the frequency at which the negative of the imaginary component of the impedance is maximized. For an R-C model circuit, f_c is related to the skin resistance and capacitance as (Orazem and Tribollet, 2008):

$$f_c = \frac{1}{2\pi R_{skin} C_{skin}} \qquad (2.7)$$

For an R-CPE circuit model, C_{skin} in Eq. (2.7) is the effective skin capacitance, $C_{skin,eff}$, which is described in the Appendix.

When C_{SER} is measured at a frequency close to the characteristic frequency, it varies strongly with R_{skin} but minimally with small variations in the effective skin capacitance. When measured at a frequency that is more than an order of magnitude larger or smaller than the characteristic frequency, C_{SER} is nearly insensitive to R_{skin} but affected by variations in the effective capacitance.

The variation of C_{SER} at 100 Hz and 1000 Hz with R_{skin} is illustrated in Figure 2.8, in which predictions from the R-CPE model circuit (described by Eqs. (A.7)and (A.8) in the Appendix) are presented and compared to the 145 experimental values from Figure 2.7. The model predictions were calculated at the mean value in the effective skin capacitance plus and minus one standard deviation assuming a log mean distribution of the effective capacitance values for the 145 skin samples shown in Figures 2.6 and 2.7. Specifically, the mean ± one standard deviation in the logarithm of $C_{skin,eff}/A$ was equal to 1.60 ± 0.30, which corresponds to a mean of 39.8 nF/cm^2 with upper and lower bounds at 75.8 nF/cm^2 and 20.2 nF/cm^2, respectively. The α parameter in the R-CPE model was assumed to be 0.8, which is a typical number for skin (Hirschorn et al., 2010; Poon and Choy, 1981). The predicted dependence of C_{SER} with R_{skin} is in excellent agreement with the experimental results at both 100 and 1000 Hz.
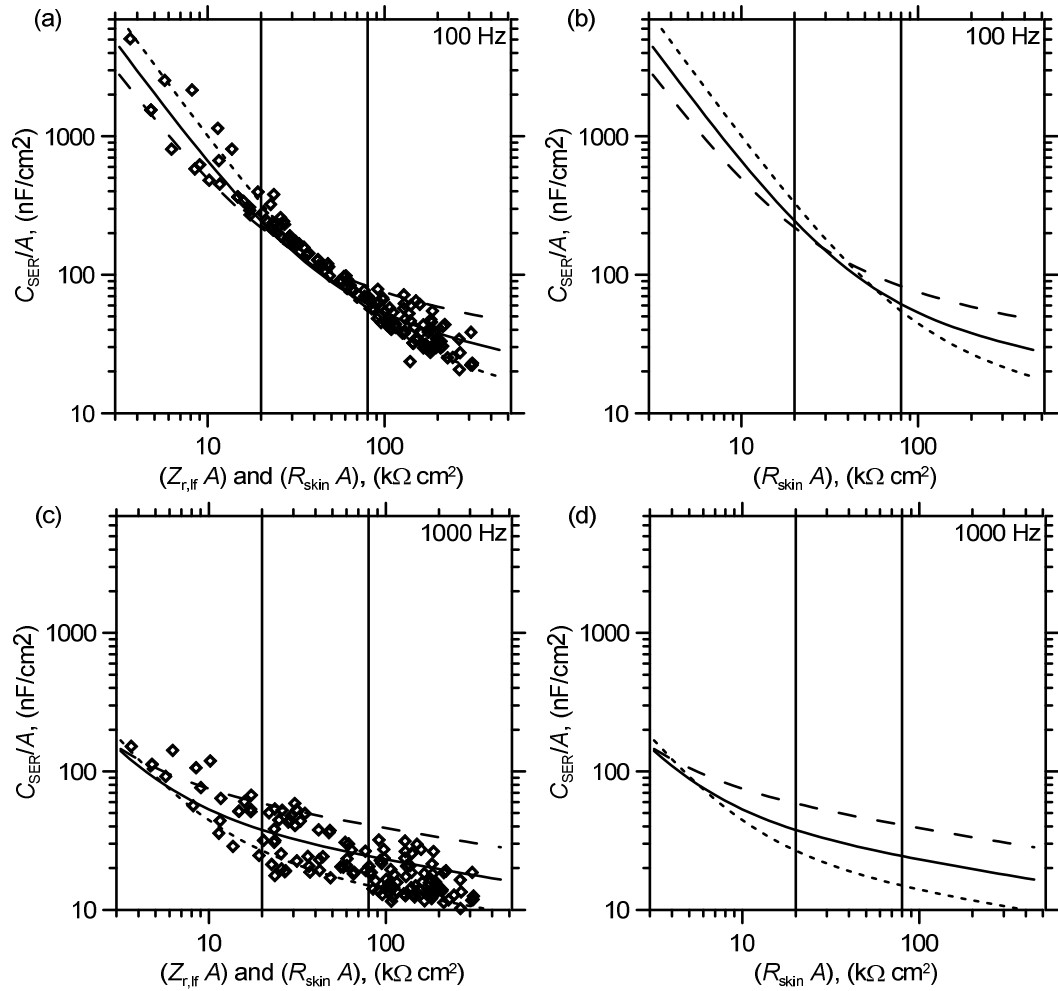
Figure 2.8 Area-normalized values of C_{SER} calculated from the complex impedance of 145 cadaver skin samples measured using the Gamry potentiostat plotted as a function of the $Z_{r,lf}$ compared with C_{SER}/A predicted by the R-CPE model circuit plotted as a function of R_{skin} for the mean value of $C_{skin,eff}/A$ (solid curve) plus and minus one standard deviation (long and short dashed curves respectively) assuming a log mean distribution of $C_{skin,eff}/A$ for the 145 skin samples shown in Figures 2.6 and 2.7: data compared with model at 100 Hz (a) and 1000 Hz (c); and model alone at 100 Hz (b) and 1000 Hz (d).

The values of $(Z_{r,lf} A)$ at 20 and 80 kΩ cm^2 indicated on Figure 2.8 designate the interval over which C_{SER} measured at 100 Hz appears to be approximately linear with $(Z_{r,lf} A)$. The characteristic frequencies for skin samples within the 20 to 80 kΩ cm^2 interval are approximately 25 to 400 Hz. For these samples, 100 Hz is within a factor of 4 smaller or larger than f_c, whereas, 1000

59

Hz is larger than f_c by 2.5 to 40 fold, which is consistent with the greater effect of skin resistance on C_{SER} measured at 100 Hz. Typically, f_c is less than 100 Hz for samples with $(R_{skin} A) > 80$ kΩ cm^2 and greater than 100 Hz for samples with $(R_{skin} A) < 20$ kΩ cm^2. Skin samples considered acceptable for diffusion cell determinations of chemical permeability generally have $(R_{skin} A)$ that are 20 kΩ cm^2 or a little larger, which is within the approximately linear interval for C_{SER} and R_{skin}.

Interestingly, from the model predictions at 100 Hz (Figure 2.8b) for a fixed effective skin capacitance, it is evident that C_{SER} actually is not linear with R_{skin} over the interval between 20 and 80 kΩ cm^2. The apparent linear relationship of C_{SER} and R_{skin} between 20 and 80 kΩ cm^2 is caused by the intersections of the C_{SER} versus R_{skin} curves at various values of the effective skin capacitance.

2.4.4 Application for Assessing Skin Integrity

Often the goal of LCR databridge measurements is to test the integrity of skin samples used for *in-vitro* determinations of chemical permeation through skin. For this purpose, the meaningful test quantity is electrical resistivity, the magnitude of which, for LCR databridge instruments reporting R_{PAR}, R_{SER}, C_{PAR} and C_{SER} values at 100 and 1000 Hz, is most closely represented by R_{PAR} at 100 Hz. However, the correlation between C_{SER} and $Z_{r,lf}$ observed in Figures 2.7 and 2.8 suggests that C_{SER} measured at 100 Hz might also be used as a surrogate measure for resistivity. Therefore, using the 145 cadaver skin measurements presented in Figures 2.6 through 2.8, the suitability of using $(R_{PAR} A)$ and

(C_{SER}/A) determined at 100 Hz as surrogates for identifying skin samples with acceptable and unacceptable resistivity was explored.

The evaluation scheme is illustrated in Figure 2.9. For the selected test value of the area-normalized DC skin resistance ($R_{skin} A$)$_{test}$, the test value of the surrogate measurement is chosen. For the chosen surrogate test value, the number of skin samples was determined that, according to the area-normalized surrogate measure, was either acceptable or unacceptable. By comparing ($R_{skin} A$)$_{test}$ to values of ($Z_{r,lf} A$), assumed to represent ($R_{skin} A$) for each skin sample, results identified as acceptable according to the surrogate measurements were then categorized as either true acceptable (designated TA), meaning ($R_{skin} A$) $\geq$ ($R_{skin} A$)$_{test}$, or true unacceptable (designated TU), meaning ($R_{skin} A$) < ($R_{skin} A$)$_{test}$. Similarly, results identified by the surrogate measurements as unacceptable were categorized as either false acceptable, FA, or false unacceptable, FU, according to ($R_{skin} A$) compared with ($R_{skin} A$)$_{test}$. For ($R_{PAR} A$) as the selected surrogate test measurement, skin samples are deemed acceptable if ($R_{PAR} A$) $\geq$ ($R_{PAR} A$)$_{test}$, and unacceptable if ($R_{PAR} A$) < ($R_{PAR} A$)$_{test}$. Since (C_{SER}/A) decreases with increasing skin resistance, skin samples are deemed acceptable if (C_{SER}/A) $\leq$ (C_{SER}/A)$_{test}$, and unacceptable if (C_{SER}/A) > (C_{SER}/A)$_{test}$. The performance results for four surrogate criteria are reported in Table 2.2 as the percentage of the 145 skin samples identified as TA, FA, TU or FU for values of ($R_{skin} A$)$_{test}$ between 10 and 36 kΩ-cm^2, which represents the range of previously proposed test values for R_{PAR} or R_{skin}.
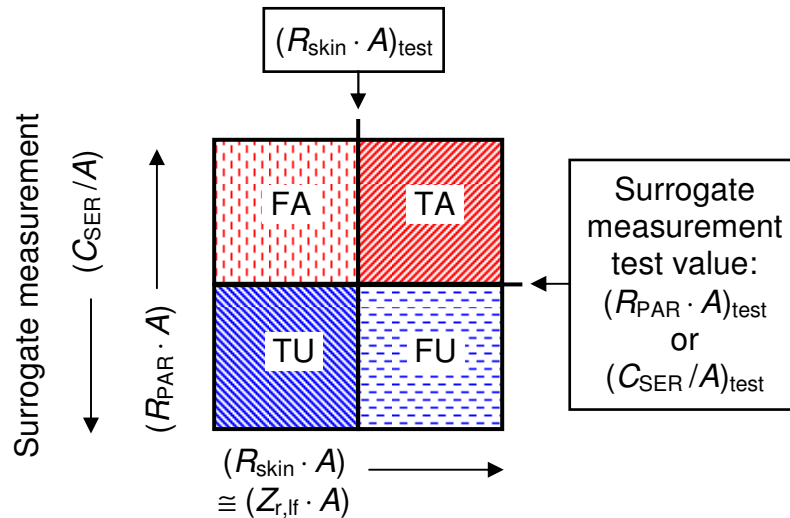
Figure 2.9 Schematic diagram illustrating the scheme for evaluating surrogate measurements for testing skin integrity.

The first surrogate criteria in Table 2.2 is $(R_{PAR} A)_{test}$ set equal to $(R_{skin} A)_{test}$, which is consistent with the assumption that R_{PAR} measured at 100 Hz is a good estimate of R_{skin}. Because R_{PAR} measured at 100 Hz is generally less than $Z_{r,lf}$ (see Figure 2.6), choosing $(R_{PAR} A)_{test}$ at 100 Hz to equal $(R_{skin} A)_{test}$ is biased toward rejecting acceptable skin samples.

To use (C_{SER}/A) measured at 100 Hz as a surrogate for recognizing skin samples with acceptable and unacceptable resistivity, suitable values for $(C_{SER}/A)_{test}$ must be determined. Assuming the cadaver skin impedance data shown in Figure 2.8 are representative of skin samples generally, criteria for $(C_{SER}/A)_{test}$ were estimated by substituting $(R_{skin} A)_{test}$ for $(Z_{r,lf} A)$ in Eq. (2.6). Overall, using $(C_{SER}/A)_{test}$ calculated using Eq. (2.6) as surrogate test criterion for $(R_{skin} A)_{test}$ was superior to using $(R_{PAR} A)_{test}$ at 100 Hz equal to $(R_{skin} A)_{test}$.

Table 2.2 Performance of $(R_{PAR}\,A)$ at 100 Hz and 1000 Hz and (C_{SER}/A) at 100 Hz as surrogate criteria for $(R_{skin}\,A)$ in testing skin integrity[a]

Surrogate Criterion								
f (Hz)	Quantity	Relationship of test value to $(R_{skin}\,A)_{test}$[b]	Test value[b]	$(R_{skin}\,A)_{test}$ kΩ cm^2	TA	TU	FA	FU
100	$(R_{PAR}\,A)$	$(R_{PAR}\,A)_{test} =$ $(R_{skin}\,A)_{test}$	10	10	93.8	5.5	0.0	0.7
			15	15	85.5	10.3	0.0	4.1
			20	20	75.2	13.8	0.0	11.0
			25	25	68.3	20.7	0.0	11.0
			30	30	64.1	26.9	0.0	9.0
			36	36	60.0	32.4	0.0	7.6
100	(C_{SER}/A)	Eq. (6): log $(C_{SER}/A)_{test} =$ -1.07 log$(R_{skin}\cdot A)_{test}$ + 3.85	598	10	92.4	4.8	0.7	2.1
			387	15	89.0	9.0	1.4	0.7
			285	20	84.8	13.1	0.7	1.4
			224	25	76.6	19.3	1.4	2.8
			185	30	73.1	26.2	0.7	0.0
			152	36	67.6	32.4	0.0	0.0
100	$(R_{PAR}\,A)$	Eq. (8): log $(R_{PAR}\,A)_{test} =$ 0.837 log$(R_{skin}\,A)_{test}$ + 0.092	8.5	10	93.8	5.5	0.0	0.7
			11.9	15	89.0	9.7	0.7	0.7
			15.1	20	84.8	13.1	0.7	1.4
			18.3	25	76.6	17.2	3.4	2.8
			21.3	30	68.3	24.1	2.8	4.8
			24.8	36	67.6	31.7	0.7	0.0
1000	$(R_{PAR}\,A)$	Eq. (9): log $(R_{PAR}\,A)_{test} =$ 0.668 log$(R_{skin}\,A)_{test}$ + 0.053	5.3	10	93.8	4.8	0.7	0.7
			6.9	15	85.5	8.3	2.1	4.1
			8.4	20	77.9	11.7	2.1	8.3
			9.7	25	71.0	15.2	5.5	8.3
			11.0	30	66.2	19.3	7.6	6.9
			12.4	36	64.8	26.9	5.5	2.8

[a] Results are reported as the percentage of the 145 skin samples that are identified by the surrogate criterion as acceptable in agreement (TA = true acceptable) or disagreement (FA = false acceptable) with $(R_{skin}\,A)$ or that are identified by the surrogate criterion as unacceptable in agreement (TU = true unacceptable) or disagreement (FU = false unacceptable) with $(R_{skin}\,A)$. For $(R_{skin}\,A)$ and $(R_{PAR}\,A)$, acceptable skin must exceed the test value; for (C_{SER}/A) acceptable skin must be less than the test value.

[b] Test value of the surrogate measurement in units of kΩ cm^2 for $(R_{PAR}\,A)_{test}$ and nF/cm^2 for $(C_{SER}/A)_{test}$.

The following regression of $(R_{PAR}\,A)$ determined at 100 Hz to $(Z_{r,lf}\,A)$,

$$\log(R_{PAR}\,A) = 0.837\log(Z_{r,lf}\,A) + 0.092 \qquad r^2 = 0.97 \qquad (2.8)$$

where the units for $(Z_{r,lf} A)$ and $(R_{PAR} A)$ are $k\Omega$ cm^2, should provide an improved criterion for $(R_{PAR} A)_{test}$. Specifically, $(R_{PAR} A)_{test}$ at 100 Hz is calculated by substituting $(R_{skin} A)_{test}$ for $(Z_{r,lf} A)$ in Eq. (2.8). A similar approach was also applied to derive $(R_{PAR} A)_{test}$ measured at 1000 Hz from the following regression for $(R_{PAR} A)_{test}$ at 1000 Hz to $(Z_{r,lf} A)$:

$$\log(R_{PAR} A) = 0.668\log(Z_{r,lf} A) + 0.053 \qquad r^2 = 0.83 \qquad (2.9)$$

Equations (2.8) and (2.9) are compared with the 145 experimental measurements in Figure 2.10. The values of $(R_{PAR} A)_{test}$ calculated according to Eqs. (2.8) and (2.9) for selected values of $(R_{skin} A)_{test}$ are listed in Table 2.2 along with a performance summary.

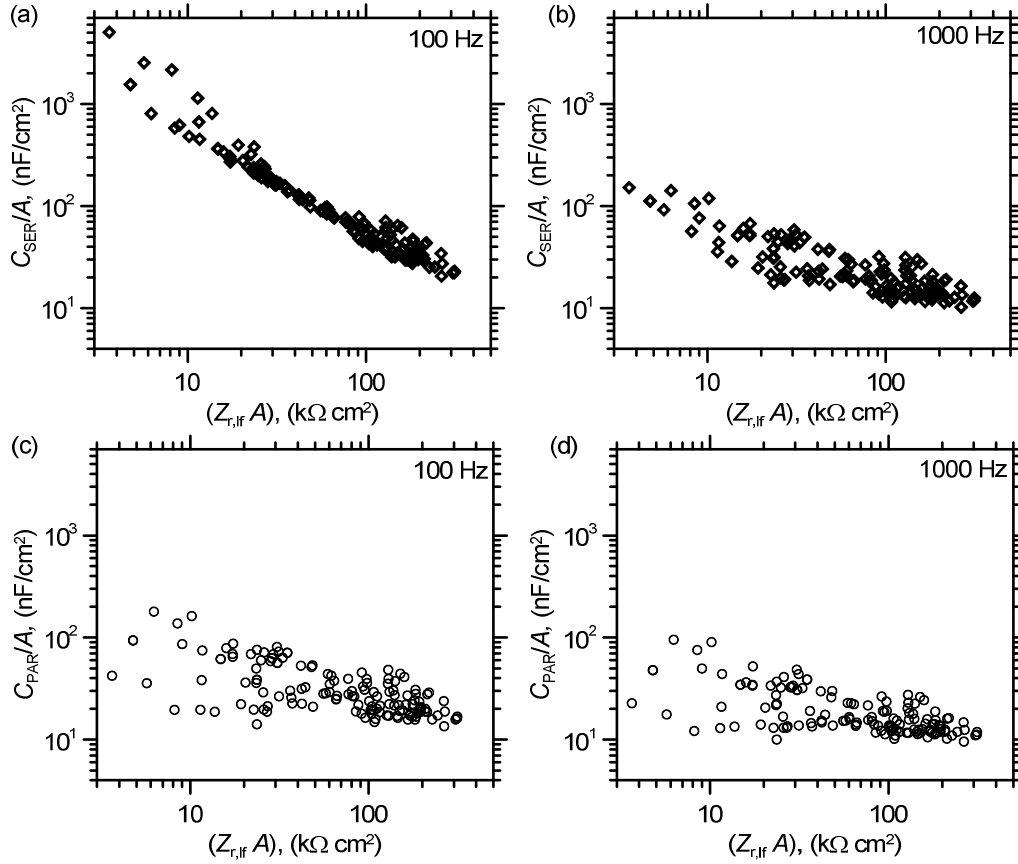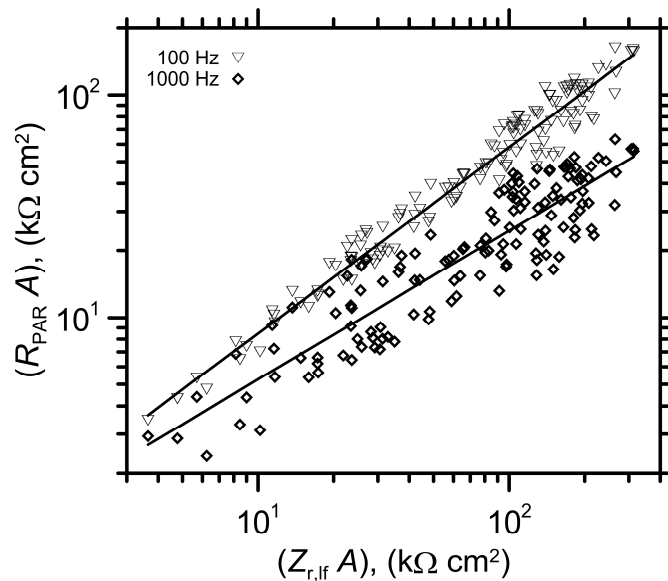
Figure 2.10 Area-normalized values of R_{PAR} calculated from the complex impedance of 145 cadaver skin samples measured at 100 Hz and 1000 Hz using the Gamry potentiostat plotted as a function of the $(Z_{r,lf} A)$. The solid lines were determined by linear regression and correspond to Eqs. (2.8) and (2.9) for the 100 Hz and 1000 Hz measurements, respectively.

Compared with the results for $(R_{PAR} A)_{test} = (R_{skin} A)_{test}$, applying $(R_{PAR} A)_{test}$ calculated from Eq. (2.8) produced fewer incorrectly identified samples, although more samples were incorrectly identified as acceptable (i.e., FA). Clearly, $(R_{PAR} A)$ measured at 1000 Hz is inferior to the other surrogate measurements listed in Table 2.2 for correctly identifying skin samples with acceptable and unacceptable integrity.

2.4.5 Comparison to the Literature

Equations (2.8) and (2.9) provide a means of estimating the DC skin resistance that corresponds with the previously proposed test values for R_{PAR} based on LCR databridge measurements. Davies et al. (2004) recommended using $(R_{PAR} A)_{test}$ of 25 kΩ cm^2 measured at 100 Hz, which corresponds to $(R_{skin} A)_{test}$ equal to about 36 kΩ cm^2 calculated using Eq. (2.8). This is not too different from $(R_{skin} A)_{test}$ equal to 30 kΩ cm^2, which is estimated for $(R_{PAR} A)_{test}$ at 1000 Hz equal to 11 kΩ cm^2 (Fasano et al., 2002). This similarity in $(R_{skin} A)_{test}$ values is expected because $(R_{PAR} A)_{test}$ in both studies was chosen to match the same value for tritiated water absorption (i.e., 1.5 mg cm^{-2} h^{-1}). Notably, Kasting and Bowman (1990) recommended 35 kΩ cm^2 for $(R_{skin} A)_{test}$ based in part on current-voltage behavior in studies of sodium ion absorption in experiments at 37°C. More recently, 13 kΩ cm^2 and 7 kΩ cm^2 have been suggested for $(R_{PAR} A)_{test}$ measured at 100 and 1000 Hz, respectively (Horne et al., 2010); these values, developed to be consistent with a tritiated water absorption of 3.5 mg cm^{-2} h^{-1}, correspond to $(R_{skin} A)_{test}$ equal to 16 kΩ cm^2.

From the ratio of urea permeability measured at 39° and 27°C, Peck et al. (1995) discovered that heat-separated human skin with ($R_{skin} A$) less than 20 kΩ cm^2 at 27°C, behaved differently than higher resistance skin and like porous Nuclepore membranes. Thus, Peck et al. (1995) selected 20 kΩ cm^2 for ($R_{skin} A$)$_{test}$. This DC resistance criteria would correspond with 15.1 and 8.4 kΩ cm^2 for ($R_{PAR} A$)$_{test}$ determined at 100 and 1000 Hz, respectively or 285 nF/cm^2 for (C_{SER}/A)$_{test}$ measured at 100 Hz.

2.5 Conclusions

Resistance and capacitance values reported by LCR databridge instruments represent manipulations of the complex impedance and are, therefore, functions of the measurement frequency. With the exception of low impedance skin samples, the R_{SER}, R_{PAR} and C_{PAR} measured at 1000 Hz and R_{SER} and C_{PAR} measured at 100 Hz will generally provide poor estimates of the skin resistivity. Measurements of R_{PAR} and C_{SER} at 100 Hz may be used as surrogate measures for skin resistivity to assess the integrity of human skin samples. While the sensitivity of R_{PAR} measured at low frequency to skin resistance is consistent with results presented in the literature, a surprising result of the present study is that the capacitance C_{SER} measured at low frequency provides an even better surrogate for skin resistivity. One should caution, however, that, depending on the chosen acceptance criteria, some skin may be falsely identified as acceptable or unacceptable.

REFERENCES

Davies, D.J., Ward, R.J., Heylings, J.R., 2004. Multi-species assessment of electrical resistance as a skin integrity marker for in vitro percutaneous absorption studies. Toxicol. In Vitro 18, 351-358.

DeNuzzio, J.D., Berner, B., 1990. Electrochemical and iontophoretic studies of human skin. Journal of Controlled Release 11, 105-112.

Fasano, W.J., Hinderliter, P.M., 2004. The Tinsley LCR Databridge Model 6401 and electrical impedance measurements to evaluate skin integrity in vitro. Toxicol. In Vitro 18, 725-729.

Fasano, W.J., Manning, L.A., Green, J.W., 2002. Rapid integrity assessment of rat and human epidermal membranes for in vitro dermal regulatory testing: correlation of electrical resistance with tritiated water permeability. Toxicol. In Vitro 16, 731-740.

Franz, T.J., Lehman, P.A., 1990. The use of water permeability as a means of validation for skin integrity in vitro percutaneous absorption studies. J. Invest. Dermatol. 94, 525.

H. Tinsley & Co, 1996. 6401 LCR Databridget Users Manual, Surrey, England.

Heylings, J.R., 2009. Personal communication, October 13,.

Heylings, J.R., Esdaile, D.J., 2007. Percutaneous absorption of pesticides, In: Roberts, M.S., Walters, K.A. (Eds.), Dermal Absorption and Toxicity Assessment, Second edition ed. Informa Healthcare, New York, pp. 575-591.

Hirschorn, B., Orazem, M.E., Tribollet, B., Vivier, V., Frateur, I., Musiani, M., 2010. Determination of effective capacitance and film thickness from constant-phase-element parameters. Electrochimica Acta 55, 6218-6227.

Horne, A., Blackstock, C., Roper, C.S., 2010. Evaluation of electrical resistance for use as a rapid method for human skin barrier integrity assessment in the flow through diffusion cell, Proceedings of the Skin Forum, 11th Annual Meeting, Edinburgh, Scotland.

Hsu, C.H., Mansfeld, F., 2001. Technical note: Concerning the conversion of the constant phase element parameter Y_0 into a capacitance. Corrosion 57, 747-748.

International Programme on Chemical Safety (IPCS), 2006. Dermal Absorption, Environmental Health Criteria 235. World Health Organization, Geneva.

Kalia, Y.N., Nonato, L.B., Lund, C.H., Guy, R.H., 1998. Development of skin barrier function in premature infants. J. Invest. Dermatol. 111, 320-326.

Kasting, G.B., Bowman, L.A., 1990. DC electrical properties of frozen, excised human skin. Pharm. Res. 7, 134-143.

Kasting, G.B., Filloon, T.G., Francis, W.R., Meredith, M.P., 1994. Improving the sensitivity of in vitro skin penetration experiments. Pharm. Res. 11, 1747-1754.

Kontturi, K., Murtomaki, L., 1994. Impedance spectroscopy in human skin. A refined model. Pharm. Res. 11, 1355-1357.

Nicander, I., Åberg, P., Ollmar, S., 2006. Bioimpedance as a noninvasive method for measuring changes in skin, In: Serup, J., Jemec, G.B.E., Grove, G.L. (Eds.), Handbook of Non-Invasive Methods and the Skin, Second ed. Taylor & Francis, Boca Raton, FL.

OECD, 2004a. OECD Guideline for Testing of Chemicals. Guideline 428: Skin Absorption: In Vitro Method (Original Guideline, adopted 13th April 2004).

OECD, 2004b. OECD Guideline for the Testing of Chemicals. Guidline 430: In Vitro Skin Corrosion: Transcutaneous Electrical Resistance Test (TER) (Original Guideline, adopted 13th April 2004).

Oh, S.Y., Guy, R.H., 1994a. Effect of enhancers on the electrical properties of skin: The effect of azone and ethanol. J. Kor. Pharm. Sci. 24, S41-S47.

Oh, S.Y., Guy, R.H., 1994b. The effect of oleic acid and propylene glycol on the electrical properties of skin. J. Kor. Pharm. Sci. 24, 281-287.

Oh, S.Y., Leung, L., Bommannan, D., Guy, R.H., Potts, R.O., 1993. Effect of current, ionic strength and temperature on the electrical properties of skin. Journal of Controlled Release 27, 115-125.

Orazem, M.E., Tribollet, B., 2008. Electrochemical Impedance Spectroscopy. Wiley-Interscience, Hoboken, NJ.

Peck, K.D., Ghanem, A.H., Higuchi, W.I., 1995. The effect of temperature upon the permeation of polar and ionic solutes through human epidermal membrane. J. Pharm. Sci. 84, 975-982.

Poon, C.S., Choy, T.T.C., 1981. Frequency dispersions of human-skin dielectrics. Biophys. J. 34, 135-147.

Scott, R.C., Batten, P.L., Clowes, H.M., Jones, B.K., Ramsey, J.D., 1992. Further validation of an in vitro method to reduce the need for in vivo studies for measuring the absorption of chemicals through rat skin. Fundam. Appl. Toxicol. 19, 484-492.

Scott, R.C., Corrigan, M.A., Smith, F., Mason, H., 1991. The influence of skin structure on permeability: an intersite and interspecies comparison with hydrophilic penetrants. J. Invest. Dermatol. 96, 921-925.

White, E.A., 2011. PhD Thesis. Colorado School of Mines, Golden, Colorado.

White, E.A., Orazem, M.E., Bunge, A.L., 2011. A critical analysis of single-frequency LCR databridge impedance measurements of human skin. Toxicol. In Vitro 25, 774-784.

Yamamoto, T., Yamamoto, Y., 1976a. Dielectric constant and resistivity of epidermal stratum corneum. Medical and Biological Engineering and Computing 14, 494-500.

Yamamoto, T., Yamamoto, Y., 1976b. Dielectric constant and resistivity of epidermal stratum corneum. Med. Biol. Eng. Comput. 14, 494-500.

Yamamoto, T., Yamamoto, Y., 1976c. Electrical properties of the epidermal stratum corneum. Med. Biol. Eng. 14, 151-158.

Yamamoto, T., Yamamoto, Y., 1981a. Non-linear electrical-properties of skin in the low-frequency range. Med. Biol. Eng. Comput. 19, 302-310.

Yamamoto, T., Yamamoto, Y., 1981b. Non-linear electrical-properties of skin in the low-frequency range. Med. Biol. Eng. Comput. 19, 302-310.

APPENDIX

The complex impedance of the R-C circuit model shown in Figure 1 is represented by the following equation:

$$Z = R_e + \frac{R_{skin}}{1 + \omega R_{skin} C_{skin}}. \tag{A.1}$$

from which the real and imaginary parts are determined to be:

$$Z_r = R_e + \frac{R_{skin}}{1 + (\omega R_{skin} C_{skin})^2} \tag{A.2}$$

and

$$Z_j = -\frac{\omega R_{skin}^2 C_{skin}}{1 + (\omega R_{skin} C_{skin})^2} \tag{A.3}$$

where the radial frequency ω is equal to $2\pi f$ for f given in cycles per time.

Although Eqs. (A.1) through (A.3) capture the essential features of skin impedance measured as a function of frequency, the R-CPE circuit model, in which a constant phase element (CPE) replaces the capacitor shown in Figure 1, provides better quantitative agreement with experimental data (Hirschorn et al., 2010; Kontturi and Murtomaki, 1994; Yamamoto and Yamamoto, 1976b, c, 1981a).

The complex impedance of the R-CPE model circuit is more complicated than the R-C model circuit because the impedance of a CPE depends on two parameters, Q and α, rather than just one (the capacitance, C_{skin}) for a capacitor. For the R-CPE model circuit, the PAR and SER modes for R and C are described by the following four equations:

$$R_{PAR} = \frac{1}{Y_r} = \frac{R_e + R + \dfrac{\left(RQR_e\omega^\alpha\right)^2}{R+R_e} + 2QRR_e\omega^\alpha \cos\left(\dfrac{\alpha\pi}{2}\right)}{1 + \dfrac{R_e\left(QR\omega^\alpha\right)^2}{\left(R+R_e\right)} + QR\omega^\alpha \cos\left(\dfrac{\alpha\pi}{2}\right)} \tag{A.4}$$

$$R_{SER} = Z_r = R_e + \frac{R + R^2 Q\omega^\alpha \cos\left(\dfrac{\alpha\pi}{2}\right)}{1 + \left(RQ\omega^\alpha\right)^2 + 2RQ\omega^\alpha \cos\left(\dfrac{\alpha\pi}{2}\right)} \tag{A.5}$$

$$C_{PAR} = \frac{Y_j}{\omega} = \frac{QR^2\omega^{(\alpha-1)} \sin\left(\dfrac{\alpha\pi}{2}\right) \Big/ \left(R+R_e\right)}{R_e + R + \dfrac{\left(RQR_e\omega^\alpha\right)^2}{R+R_e} + 2QRR_e\omega^\alpha \cos\left(\dfrac{\alpha\pi}{2}\right)} \tag{A.6}$$

and

$$C_{SER} = -\frac{1}{Z_j\omega} = \frac{1 + \left(RQ\omega^\alpha\right)^2 + 2RQ\omega^\alpha \cos\left(\dfrac{\alpha\pi}{2}\right)}{R^2 Q\omega^{2\alpha} \sin\left(\dfrac{\alpha\pi}{2}\right)} \tag{A.7}$$

The effective capacitance of an R-CPE model circuit of skin can be estimated using Eq. (2.7) from the characteristic frequency, defined here as the frequency at which the negative of the imaginary part of the impedance is at its maximum value (Orazem and Tribollet, 2008). It follows that this definition of the effective skin capacitance ($C_{skin,eff}$) is related to α and Q as follows:

$$C_{skin,eff} = Q^{1/\alpha} R_{skin}^{(1-\alpha)/\alpha} \tag{A.8}$$

As described by Hirschorn et al. (2010), Eq. (A.8) is in agreement with the development presented by Hsu and Mansfeld (2001) and used by Oh and Guy (1994a, 1994b) to estimate the capacitance of human skin.

CHAPTER 3

SINGLE-FREQUENCY IMPEDANCE MEASUREMENTS AS PREDICTORS OF HUMAN SKIN PERMEABILITY TO WATER AND OTHER HYDROPHILIC COMPOUNDS

The content of this chapter was accepted for publication in Toxicology in Vitro (White et al., 2011a) and reproduced here with consent from the publisher and co-authors (see thesis Appendix).

The objective of this study was to correlate measurements on the same pieces of skin of tritiated water permeability with impedance determined at either 100 or 1000 Hz using an LCR databridge. A previously published expression based on a simple circuit of a parallel resistor and constant phase element (CPE) was used to relate (R_{PAR} A) measured at different frequencies to the steady-state skin permeability of tritiated water. Using this analysis, tritiated water permeability (k_p) and (R_{PAR} A) data from three laboratories were shown to be consistent with each other and also with the relationship between (R_{skin} A) and k_p observed for other model hydrophilic chemicals: urea and mannitol. These results were used to compare on a consistent basis proposed tests for identifying and excluding damaged skin from chemical absorption studies. The criterion of 20 kΩ cm^2 for (R_{skin} A) corresponds to a tritiated water permeability of 3.2×10^{-3} cm/h, which should exclude damaged skin without screening undamaged but higher permeability skin samples from study.

3.1 Introduction

In vitro diffusion cell methods have been used extensively to measure the rate and extent of chemical penetration into and through skin from humans or animals. The potential exists for skin samples to be damaged during collection, storage or handling, which may affect the percutaneous absorption measurements (Scott et al., 1991). Therefore, the use of a barrier integrity test for skin penetration studies is advised and is often required if data are collected for regulatory submission (Heylings and Esdaile, 2007; International Programme on Chemical Safety (IPCS), 2006; OECD, 2004). Recommended integrity test protocols include determination of tritiated water permeability, the rate of transepidermal water loss (TEWL), and transcutaneous electrical resistance (International Programme on Chemical Safety (IPCS), 2006; OECD, 2004). Skin samples are rejected if the water permeability or water loss is considered to be too high or the electrical resistance too low for reliable determination of permeability parameters.

With respect to tritiated water permeability measured at steady state (k_p), the criteria for rejecting human skin samples have been set variously at 1.5×10^{-3} cm/h (Davies et al., 2004; Fasano et al., 2002; Scott et al., 1987), 2.0×10^{-3} cm/h (van de Sandt et al., 2000), 2.5×10^{-3} cm/h (Bronaugh and Stewart, 1986) and 4.0×10^{-3} cm/h (Buist et al., 2005). Recently, Meidan and Roper (2008) suggested that using smaller values of tritiated water permeability as integrity criteria could cause undamaged but higher permeability samples to be rejected, which could bias the permeability measurements toward underestimating

absorption. Therefore, they recommended using 4.5×10^{-3} cm/h as the tritiated water permeability criterion based on the observation that 95% of the 2390 skin samples in a study of 112 female volunteers were below this value.

Steady-state determinations of tritiated water permeability require two or more hours, which delays the start of chemical permeation measurements when used to test skin integrity. Alternative tritiated water methods requiring less time have been proposed. Kasting et al. (1994) judged skin to be acceptable for diffusion cell measurements if the amount of tritiated water collected in the receptor fluid over 1 h after a 5-minute application was less than 1.6 μL/cm^2. By comparing hourly measurements of tritiated water absorption collected for 2 h, Runciman et al. (2009), concluded that an absorption of 2.4 μL/cm^2 (i.e., calculated from 0.6% of the 400 μL/cm^2 application) in the first hour was equivalent to a permeability coefficient of 3.5×10^{-3} cm/h calculated from absorption at 2 h.

Single-frequency electrical impedance measurements are rapid and economical alternatives to tritiated water flux for skin integrity testing. The method involves measuring the potential or current response to a small-amplitude, typically sinusoidal, modulation of an input current or potential. Impedance is the ratio of the change in potential to the change in current, which for skin depends on the modulation frequency. In the limit of low frequency, the impedance measurement approaches the direct current (DC) resistance, designated for skin as R_{skin}.

Proposed criteria for *in vitro* testing of human skin integrity, several of which are listed in Table 3.1, have been selected by comparing electrical measurements on a series of samples to the percutaneous absorption measurements for tritiated water (Davies et al., 2004; Fasano et al., 2002), polar compounds (Peck et al., 1995), or ionized salts (Kasting and Bowman, 1990). For electrical resistance criteria derived from tritiated water permeability data, the chosen k_p criterion is reported. Electrical resistance test criteria vary widely, from 7 to 45 kΩ cm^2 for the studies listed in Table 3.1. Even for those derived using the same tritiated water permeability coefficient, the differences in criteria are large (e.g., 11 to 45 kΩ cm^2 for k_p of 1.5 x 10^{-3} cm/h).

The variation in the electrical resistance test criteria is due in part to the choice of the percutaneous absorption measurement method. In addition to this, skin resistance has been determined in different ways that affect the magnitude of the measurement. For example, resistances determined using an LCR databridge, like the PRISM or Tinsley instruments (Davies et al., 2004; Fasano et al., 2002; OECD, 2004b), in PAR mode (R_{PAR}) measured at different frequencies are different; in general, these are also different from resistance determined using a DC method (Fasano and Hinderliter, 2004; White et al., 2011b).

In assessing skin integrity, the meaningful quantity is electrical resistivity (ρ), which characterizes quantitatively the pathway for transport of ions, which is enhanced for damaged skin. The skin resistivity is proportional to the area-normalized skin resistance measured using a direct current method; i.e., ($R_{skin} A$) where A is the area.

Table 3.1 Recommended values of the area normalized electrical resistance ($R\,A$) for testing human skin integrity for *in-vitro* determinations of chemical permeation

Source	f^a (Hz)	($R\,A$) test criteria ($k\Omega\,cm^2$)	Tritiated water k_p test criteria [b] ($\times 10^3$ cm/h)	Estimated ($R_{skin}\,A$) [c] ($k\Omega\,cm^2$)	Estimated tritiated water k_p [d] ($\times 10^3$ cm/h)
Lawrence (1997)	12.5 [e]	45 [f]	1.5 [f]	45	1.4
Fasano et al. (2002)	1000	11	1.5	26	2.4
Davies et al. (2004)	100 [g]	25	1.5	31	2.0
Kasting & Bowman (1990)	0	35	NA [h]	35	1.8
Horne et al. (2010)	100	13	3.5	15	4.1
Horne et al. (2010)	1000	7	3.5	12	5.1
Peck et al. (1995)	0	20	NA	20	3.2

[a] Frequency of the impedance measurements upon which the recommended electrical resistance test criteria is based. A frequency of zero indicates DC measurements. All measurements at non-zero frequencies were determined in PAR mode using an LCR databridge.

[b] The tritiated water permeability coefficient criterion that was used to derive the indicated electrical resistance test criterion

[c] ($R_{skin}\,A$) value calculated using Eq. (3.4) and the corresponding electrical resistance test criterion

[d] Estimate of the tritiated water k_p corresponding to the electrical resistance test criteria calculated using ($R_{skin}\,A$) and the optimized value of b (63 $k\Omega\,cm^2$) in Eq. (3.8)

[e] The measurement frequency was not given in the paper; this value was determined from the operation manual for the instrument used in the study (World Precision Instruments, 2008).

[f] The authors did not specify a test criteria; however, they report observing that all but 4 of 111 skin samples with k_p less than 1.5 x 10^{-3} cm/h exhibited a resistance of at least 45.4 $k\Omega\,cm^2$.

[g] Davies et al. (2004) incorrectly listed the measuring frequency as 100 kHz rather than 100 Hz (J. Heylings, personal communication, 2009).

[h] Not applicable. The electrical resistance test criterion was not derived by comparing to tritiated water k_p.

The permeability of polar and ionic chemicals through skin has been shown to be inversely proportional to ($R_{skin}\,A$) (Kasting and Bowman, 1990; Peck et al., 1994, 1995; Tang et al., 2001). While impedance measured at low frequencies may be a good estimate of R_{skin}, and thus inversely proportional to the permeability coefficient of polar and ionic compounds, impedance measured at higher frequencies is not (Fasano et al., 2002; White et al., 2011b).

White et al. (2011) derived a relationship for R_{PAR} in terms of skin properties and developed a theoretical basis for describing the frequency dependence of R_{PAR}. Based on an analysis of impedance measurements of many skin samples at multiple frequencies, the authors concluded that for skin integrity testing, R_{PAR} measurements at both 100 and 1000 Hz could be used, although measurements at 100 Hz were preferred. In addition, the authors proposed equations for relating (R_{PAR} A) measured at different frequencies to (R_{skin} A). It follows that it should be possible to extend these equations to relate skin integrity test criteria based on tritiated water k_p with electrical resistance test criteria based on (R_{PAR} A) measured at various frequencies.

The objective of this study was to compare (R_{PAR} A) determined at 100 and 1000 Hz to the cumulative tritiated water absorption during 1 h of skin exposure measured on the same pieces of skin. These new measurements were then compared to previously reported correlations of steady-state tritiated water permeation and R_{PAR} determined at 100 and 1000 Hz by Davies et al. (2004) and Fasano et al. (2002), respectively. The relationship between tritiated water absorption and the estimate of skin resistivity was examined using published equations relating the DC resistance to R_{PAR} measurements determined at different frequencies using an LCR databridge (White et al., 2011). The observed linear correlation between the DC resistance estimates and tritiated water permeability coefficients was consistent among the three laboratories. These results were also consistent with the correlation in human

skin of the permeability coefficient for two model polar compounds and skin resistance, measured using DC or low frequency AC methods.

3.2 Theory

Impedance spectroscopy and permeability measurements probe, in different ways, the barrier that skin presents to the absorption of hydrophilic compounds. An overview of the two measurement techniques and the relationship between them is presented in this section.

3.2.1 Skin Impedance

Skin impedance is measured by applying a small-amplitude alternating current or potential signal across the skin and measuring the responding potential or current. The impedance is the ratio of the change in potential to the change in current. The dielectric material in the skin causes a phase shift in the measured signal relative to the applied signal, and, as a result, the measured impedance varies with the frequency of the applied signal. Mathematically, this means that the impedance is a complex number containing both real and imaginary parts. The frequency response of skin is represented reasonably by a simple equivalent circuit model consisting of a frequency-independent (Ohmic) resistance (R_e) in series with a parallel skin resistance (R_{skin}) and constant phase element (CPE) as shown in Figure 3.1 (Hirschorn et al., 2010; Kontturi and Murtomaki, 1994; Yamamoto and Yamamoto, 1976a; Yamamoto and Yamamoto, 1976b, 1981). For *in vitro* determinations of skin impedance, R_e includes

contributions from the electrolyte solution on both sides of the skin, the wires, and possibly the dermis and viable epidermis.

CPE: Q, α
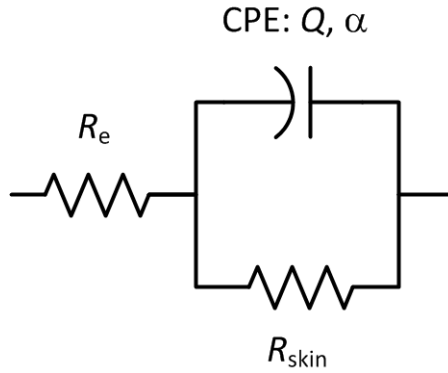
Figure 3.1 A simple R-CPE circuit model of skin.

In the skin integrity studies described below, an LCR databridge (i.e., the Tinsley 6401 or AIM 6401) was used to measure impedance at a frequency of 100 or 1000 Hz. These instruments report one component of the complex impedance as a resistance in parallel mode (R_{PAR}), which is equal to the inverse of the real part of the skin admittance (White et al., 2011b). The admittance is the alternating current analog of the DC conductance and is equal to the inverse of the impedance. Therefore, the frequency dependence of R_{PAR} is described by the following expression derived from the R-CPE equivalent circuit model (White et al., 2011b):

$$R_{PAR} = \cfrac{R_e + R_{skin} + \cfrac{\left(R_{skin}\, Q R_e \left(2\pi f \right)^\alpha \right)^2}{R_{skin} + R_e} + 2 Q R_{skin}\, R_e \left(2\pi f \right)^\alpha \cos\left(\dfrac{\alpha\pi}{2} \right)}{1 + \cfrac{R_e \left(Q R_{skin} \left(2\pi f \right)^\alpha \right)^2}{\left(R_{skin} + R_e \right)} + Q R_{skin} \left(2\pi f \right)^\alpha \cos\left(\dfrac{\alpha\pi}{2} \right)} \qquad (3.1)$$

where f is the frequency (in units of Hz, cycles per second) of the applied alternating current or potential, and Q and α are parameters quantifying the behavior of the CPE (Orazem and Tribollet, 2008). For human skin, α is approximately constant at 0.8 (Hirschorn et al., 2010; Poon and Choy, 1981) and Q is related to the resistance (R_{skin}) and the effective capacitance of the skin ($C_{skin,eff}$) by (Hirschorn et al., 2010; Hsu and Mansfeld, 2001)

$$Q = C_{skin,eff}^{\alpha}\, R_{skin}^{(\alpha-1)} \tag{3.2}$$

If R_e is small compared to R_{skin}, then Eq. (3.1) can be simplified to give

$$R_{PAR} = \frac{R_{skin}}{1 + Q R_{skin}\left(2\pi f\right)^{\alpha} \cos\left(\dfrac{\alpha\pi}{2}\right)} \tag{3.3}$$

which can be written, after substituting for Q using Eq. (3.2), as

$$R_{PAR} = \frac{R_{skin}}{1 + \left(2\pi f\, R_{skin}\, C_{skin,eff}\right)^{\alpha} \cos\left(\dfrac{\alpha\pi}{2}\right)} \tag{3.4}$$

According to Eq. (3.4), R_{PAR} is only equal to R_{skin} when it is measured at low frequency. At higher measurement frequencies, R_{PAR} is less than R_{skin} and it approaches zero in the limit of large frequency. If R_e is not small relative to R_{skin}, then R_{PAR} will approach R_e at high frequency and the sum of R_{skin} and R_e at low frequency.

3.2.2 Skin Permeability

Skin permeability to a chemical is often characterized by the permeability coefficient (k_p). It is calculated from the ratio of the steady-state flux (J_{ss}) to the

driving force for diffusion, which is the chemical concentration in the vehicle (C) when the concentration in the receptor fluid is kept close to zero, i.e.,

$$k_{\mathrm{p}} = \frac{J_{ss}}{C} \tag{3.5}$$

In many *in vitro* diffusion cell experiments, the cumulative mass of chemical delivered into the receptor solution (M) per area (A) is determined as a function of time (t). If the concentration in the vehicle C is held constant, M/A increases linearly with t after a delay that is approximately 2.4 times the lag time (t_{lag}) (Bunge and Cleek 1995). The slope of the linear (steady-state) portion of the M/A versus t curve is J_{ss}, and the time intercept is the lag time (t_{lag}), thus,

$$M / A = J_{ss}\left(t - t_{\mathrm{lag}}\right) \qquad \text{for } t > 2.4 \ t_{\mathit{lag}} \tag{3.6}$$

Experimental estimates for J_{ss} that include M/A measurements at times less than about 2.4 t_{lag}, are systematically lower than the actual value (Bunge et al., 1995).

3.2.3 Relationship Between Skin Impedance and Permeability

The electrical resistivity of (ρ), which quantitatively characterizes the resistance to ionic transport through skin, is related to the area normalized DC skin resistance R_{skin} as

$$R_{\mathrm{skin}} \ A = \rho \ \ell \tag{3.7}$$

where ℓ is the thickness of the skin layer primarily responsible for electrical resistance, which is usually the stratum corneum. The rate of ionic transport through the skin is proportional to the electrical conductivity, which is the inverse of ρ. Since k_{p} for an ionic compound is also proportional to ionic transport

through skin, the ratio of k_p and $(\rho \cdot \ell)^{-1}$ is expected to be a compound-specific

constant (b), which is defined as

$$b = \frac{k_p}{1/(\rho\,\ell)} = k_p\left(R_{\text{skin}}\,A\right) \tag{3.8}$$

The expectation that the relationship between k_p and $(R_{\text{skin}}\,A)$ is described by Eq.

(3.8) should hold for any compound that penetrates through skin primarily *via* the

pathway followed by ions has been experimentally demonstrated in studies of

several small sugars (Peck et al., 1994; Tang et al., 2001) and even water (Kalia

et al., 1996) despite evidence that water diffuses through the same pathway as

lipophilic compounds (Kasting and Barai, 2003; Potts and Francoeur, 1991; Potts

and Guy, 1992). It follows then, that for $R_e/R \ll 1$, Eqs. (3.2), (3.4) and (3.8) can

be combined to give

$$R_{\text{PAR}}A = \frac{b/k_p}{1 + \left(2\pi f\, \dfrac{C_{\text{eff}}}{A}\, \dfrac{b}{k_p}\right)^{\alpha} \cos\left(\dfrac{\alpha\pi}{2}\right)} \tag{3.9}$$

which specifies the relationship between k_p and the frequency dependent R_{PAR}

for compounds that primarily penetrate through the skin by the same pathway as

the ionic species.

3.3 Materials and Methods

Skin impedance and tritiated water absorption studies were conducted at

Charles River (Edinburgh, Scotland, UK) using Scott-Dick diffusion cells (0.64

cm^2 diffusion area) and an automated flow-through system (Newcastle

University, Newcastle, UK) described previously (Meidan and Roper, 2008). The

receptor fluid flow rate was set to 1.5 mL/h. This is referred to as the Charles

River study in the discussion below. Full thickness human skin obtained from 20

different donors (8 male abdomen, 7 female abdomen and 5 female breast, ages

19 to 66 years old) was acquired with full informed consent from the Plastic

Surgery Unit of St John's Hospital (Livingston, Scotland, UK) and stored at about

−20°C as described elsewhere (Meidan and Roper, 2008). After removal from

frozen storage, samples were dermatomed (Zimmer, Swindon, UK) to a depth of

200-400 μm and used immediately. Five skin samples from each subject were

mounted with the stratum corneum facing the donor chamber. The receptor

solution was minimum essential medium eagle (Sigma, Product No. M4655) with

added glucose (1%, weight per volume), polyoxyethylene 20 oleyl ether (6%,

weight per volume), penicillin G (100 units/ mL) and streptomycin (0.1 mg/mL).

The skin surface temperature was maintained at 32 ± 1°C (Meidan and Roper,

2008).

Phosphate buffered saline (Sigma, Product No. P4417) 1 mL, was applied

to the skin surface in the donor chamber and allowed to equilibrate for 0.5 h, after

which R_{PAR} was measured at 1000 Hz and then 100 Hz with the Tinsley 6401

LCR databridge (Surrey, England) using two 2-mm diameter stainless-steel wire

electrodes (Low Voltage Meter Probe, RS Components Limited, Corby,

Northamptonshire, UK) placed in the receptor and donor chambers, respectively.

The donor solution was then removed by pipette; the skin surface was dried with

tissue paper and left exposed to ambient air for 0.5 h while a blank sample of the

receptor solution was collected. Next, 250 μL (390 μL/cm^2) of tritiated water

(Amersham Pharmacia Biotech UK Limited, Little Chalfont, Buckinghamshire, UK) at 400,000 dpm/mL was applied to the stratum corneum surface of the skin within the donor chamber for 1 h and the receptor fluid collected. This sample was combined with 10 mL of liquid scintillation cocktail (Aquasafe 500 plus, Zinsser Analytic, Frankfurt, Germany) and analyzed by liquid scintillation counting using a Packard 2100-TR liquid scintillation analyzer (Perkin-Elmer, Beaconsfield, UK).

The fraction of the applied tritiated water collected in the receptor solution (f_{abs}) was calculated for each skin sample. The cumulative volume of water that penetrated through the skin during the 1-h exposure (equal to M divided by the density of water) was calculated from the product of f_{abs} and the volume of the tritiated donor solution applied to the skin sample (V), which was 250 μL.

For comparison to studies by Davies et al. (2004) and Fasano et al. (2002), k_p was estimated as

$$k_p = \frac{f_{abs} V}{A(t - t_{lag})} \tag{3.10}$$

where t was 1 h and t_{lag} was estimated to be 0.5 h from the results of a separate 2-h absorption study. In this study (Runciman et al., 2009), which followed procedures similar to those described above, the amount of tritiated water in the receptor solution was determined at 1 and 2 h after 400 μL/cm^2 of tritiated water was applied to 1082 split-thickness (*ca* 400 μm thick) skin samples acquired from 96 different donors (34 abdomen, 60 breast and 2 upper arm, aged 19 to 87 years old) with 2 to 47 samples from a given donor.

Davies et al. (2004) reported paired *in vitro* measurements of tritiated water k_p and R_{PAR} at 100 Hz for whole and heat separated human skin (59 and 53 samples, respectively) determined at 32°C in diffusion cells with an area of 2.54 cm^2. In these experiments, the receptor fluid (0.9% sodium chloride) was sampled at 3, 4, 5 and 6 h after application of tritiated water (also in 0.9% sodium chloride solution) and k_p was calculated from the steady-state slope of M/A versus time. Electrical impedance was measured at least 0.5 h after application of the tritiated water solution using the PRISM Electronics AIM 6401 LCR databridge connected to stainless steel wire electrodes, one each placed in the donor and receptor solutions. Skin samples that exhibited "very high" tritiated water absorption at 3 h were rejected for comparison with the electrical resistance measurements. Data from this study were derived from Figures 1A and 1D in Davies et al. (2004) using Grapher (Version 8.5, Golden Software, Inc., Golden, CO, USA).

In the study from Fasano et al. (2002), *in vitro* measurements of tritiated water k_p and R_{PAR} determined at 1000 Hz using the Tinsley model 6401 LCR Databridge (Surrey, UK) were collected on split-thickness human skin from 11 subjects in vertically oriented diffusion cells at 32°C with an area of 0.64 cm^2. The experimental procedures were similar to those followed by Davies et al. (2004), except for the timing of the receptor solution sampling, which occurred at 0.5, 1 and 2 h (Fasano et al., 2002). The data for 63 samples, which are plotted in Figure 4 of Fasano et al. (2002), were provided by W. Fasano (private communication, August 2010).

The tritiated water permeability and R_{PAR} data from this study as well as the studies from Davies et al. (2004) and Fasano et al. (2002) were compared to multi-frequency impedance scans of 145 samples of split-thickness (approximately 300 μm thick) human cadaver skin collected from 6 different subjects as described previously (White et al., 2011b). In this study, impedance of skin equilibrated for several hours with phosphate buffered saline (Sigma, Product No. P-3813) at 32°C was determined in horizontal diffusion cells as a function of frequency using four Ag-AgCl electrodes (In Vivo Metric, Healdsburg, CA, USA) by modulating the potential 10 mV rms with a Gamry potentiostat (model PCI4/300, Warminster, PA) for a range of frequencies (typically, between 1 Hz and 10 kHz) with ten measurement frequencies per logarithmic decade. The real part of the skin impedance determined at the lowest measured frequency was taken to be the DC skin resistance; this value was estimated to be within 4% of the actual DC skin resistance for skin samples in the study.

The effective capacitance of each sample ($C_{skin,eff}$) was calculated using

$$C_{skin,eff} = \frac{1}{2\pi f_c R_{skin}}$$

(3.11)

where the characteristic frequency of each skin sample (f_c) is the frequency at which the negative of the imaginary component of the impedance is maximized (Orazem and Tribollet, 2008). The log-mean average of $C_{skin,eff}$ was 39.8 nF/cm^2.

3.4 Results and Discussion

Experimental verification of the proposed relationship between electrical and permeability properties of skin are developed here for fluxes of tritiated water and

two polar compounds. This work is then extended to quantify criteria employed to assess skin integrity.

3.4.1 Application to Tritiated Water

The area-normalized volume of tritiated water collected in the receptor fluid ($f_{abs}\,V/A$) in the first hour after tritiated water was applied is compared in Figure 3.2 to ($f_{abs}\,V/A$) collected over 2 h. Under the assumption that a steady-state flux was reached within 1 h, ($f_{abs}\,V/A$) at 1 h and at 2 h should be related according to the following expression derived from Eq. (3.10):

$$k_{\mathrm{p}} = \frac{f_{abs}\,V/A}{t - t_{\mathrm{lag}}} = \frac{\left[f_{abs}\,V/A\right]_{\mathrm{at\;1\;h}}}{1\mathrm{h} - t_{\mathrm{lag}}} = \frac{\left[f_{abs}\,V/A\right]_{\mathrm{at\;2\;h}}}{2\mathrm{h} - t_{\mathrm{lag}}} \tag{3.12}$$

It follows then that a plot of ($f_{abs}\,V/A$) at 1 h compared to ($f_{abs}\,V/A$) at 2 h should be represented by a line described by

$$\left[\frac{f_{abs}\,V}{A}\right]_{\mathrm{at\;1h}} = \frac{1\mathrm{h} - t_{\mathrm{lag}}}{2\mathrm{h} - t_{\mathrm{lag}}}\left[\frac{f_{abs}\,V}{A}\right]_{\mathrm{at\;2h}} \tag{3.13}$$

which represents a line with a slope of ($1\mathrm{h} - t_{\mathrm{lag}}$)/($2\mathrm{h} - t_{\mathrm{lag}}$). The slope of the best-fit line through the data in Figure 3.2 is 0.34. From this, t_{lag} was calculated to be about 0.5 h, which indicates that a steady-state flux should be achieved in about 1.2 h (Bunge et al., 1995). In general, including data that were not at steady state in the analysis will cause t_{lag} to be underestimated. However, the difference between 1 h and 1.2 h is small enough that the 0.5 estimate for t_{lag} is reasonable within the accuracy of the measurements.
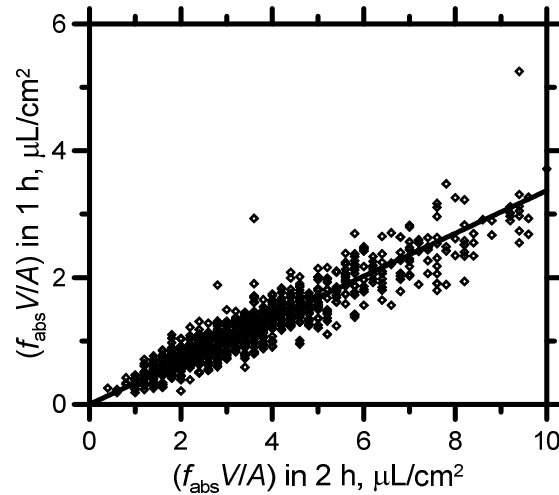
Figure 3.2 Tritiated water absorption at 1 h compared with absorption at 2 h for all samples with less than 10 μL/cm^2 of water absorbed in 2 h. The line representing the best-fit linear regression of the data forced through the origin has a slope of 0.34 (r^2 = 0.86).

Measurements of ($R_{PAR} \cdot A$) determined at 100 and 1000 Hz from the Charles River study are plotted in Figure 3.3 as functions of the inverse of k_p estimated from tritiated water absorption over 1 h under the assumption that t_{lag} was equal to 0.5 h for all skin samples. The assumption that t_{lag} was the same for all samples increases the variability of the estimated k_p. For comparison, the data reported by Davies et al. (2004) and Fasano et al. (2002) for ($R_{PAR} \cdot A$) measured at 100 and 1000 Hz, respectively (triangles) are also shown in Figure 3.3. In the Davies et al. (2004) study, there was no apparent difference in measurements from whole skin (filled triangles; R_{PAR} = 37 ± 13 kΩ cm^2 and k_p = 0.97 x 10^{-3} ± 0.41 x 10^{-3} cm/h, reported as mean ± one standard deviation) compared with human epidermal membranes (HEM) prepared by heat separation (open triangles; R_{PAR} = 53 ± 18 kΩ cm^2 and k_p = 0.81 x 10^{-3} ± 0.56 x 10^{-3} cm/h).
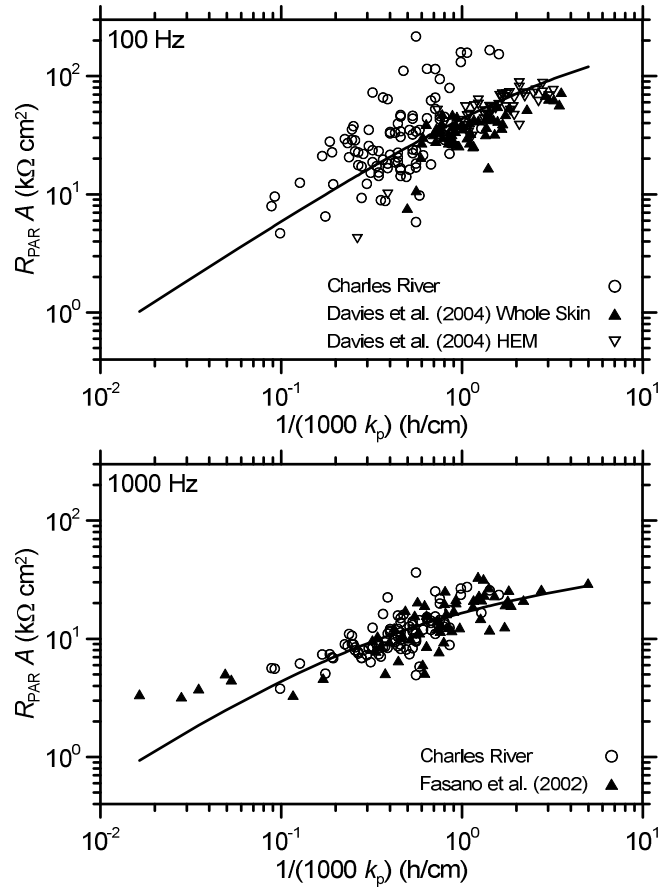
Figure 3.3 $(R_{PAR} \cdot A)$ measured at 100 and 1000 Hz plotted as a function of the inverse k_p for tritiated water determined in this study (circles) compared to data reported by Davies et al. (2004) and Fasano et al. (2002) for $(R_{PAR} \cdot A)$ measured at 100 and 1000 Hz, respectively (triangles). For Davies et al. measurements collected on whole skin and heat separated human epidermal membrane are distinguished by filled and open triangles, respectively. The curves represent the theoretical relationship for $(R_{PAR} \cdot A)$ versus $1/k_p$ described by Eq. (3.9) for the value of b (63 Ω cm^3/h) that minimized the sum of the square residuals for all the data assuming α is 0.8 and $C_{skin,eff}$ is 39.8 nF/cm^2, which is the log-mean average determined in the multi-frequency impedance study of White et al. (2011).

The curves in Figure 3.3 represent the theoretical relationship for $(R_{PAR}\ A)$

versus $1/k_p$ calculated according to Eq. (3.9) for b equal to 63 Ω cm^3/h, which is

the value of b that minimized the sum of the square residuals for all data from the

three laboratories weighted equally. In the calculation, $C_{skin,eff}/A$ was assigned a

value of 39.8 nF/cm^2, which is the log-mean average from White et al. (2011),

89

and α was assumed to be 0.8, which is a typical number for skin (Hirschorn et al., 2010; Poon and Choy, 1981).

Consistent with the impedance theory, the experimental values of R_{PAR} for a given skin sample were smaller at 1000 Hz than at 100 Hz. As a result, for the same range of k_p values, the range of observed R_{PAR} values is compressed at 1000 Hz compared with 100 Hz. Therefore, changes in the skin barrier are detected with greater sensitivity using R_{PAR} determined at lower frequency (Davies et al., 2004; Fasano and Hinderliter, 2004).

Mean values and 90% confidence intervals, ignoring the influence of different subjects, are presented in Table 3.2 for the (R_{PAR} A) and k_p data shown in Figure 3.3 as well as the values of (R_{PAR} A) reported by White et al. (2011) for frequencies of 1000, 100 and approximately zero Hz (which represents R_{skin} A). In several cases, the mean value of the same measurement collected in a different laboratory differed by a statistically significant amount. This indicates that there were differences in the skin samples between laboratories with respect to skin resistance and tritiated water permeability. One source of these differences may be the exclusion by Davies et al. (2004) of skin samples with very large tritiated water concentrations in the receptor at 3 h.

Despite the differences between laboratories, as shown in Figure 3.3, the relationship between k_p and R_{PAR} determined at both 100 and 1000 Hz are consistent between laboratories and are also consistent with the theoretical model, Eq. (3.9), which includes two parameters (α and $C_{skin,eff}$ $/A$) derived from an impedance study of a different set of skin samples (White et al., 2011b).

Table 3.2 $(R_{PAR} A)$ and k_p data from four different laboratories [a]

Study [b]	ID	f, Hz [c]	n [d]	$(R_{PAR} A)$, kΩ cm²	$(R_{PAR} A)$ differs from study ID [e]	k_p, cm/h	k_p differs from study ID [e]
White et al.		0	145				
Charles River	A	100	97	39.4 ±17.0%	C	2.78 ±11.6%	B,E
Davies et al.	B	100	112	45.2 ±6.0%	C	0.90 ±8.5%	A,E
White et al.	C	100	145	54.4 ±9.7%	A,B		
Charles River	D	1000	97	11.7 ±8.1%	E,F		
Fasano et al.	E	1000	63	14.9 ±11.2%	D,F	1.56 ±18.6%	A,B
White et al.	F	1000	145	23.1 ±8.8%	D,E		

[a] Results are reported as mean ± 90% confidence interval (reported as percent of mean), which was calculated using the Student's t-statistic.

[b] Full citation for the listed studies are: White et al. (2011), Davies et al. (2004), and Fasano et al. (2002).

[c] Frequency of the impedance measurement; for White et al. (2011), determinations at the lowest frequency measured (all less than or equal to 1 Hz) are designated as a frequency of zero

[d] Number of skin samples in study

[e] Means are considered different if the difference is statistically significant at the 5% level using the Student's t-test with different sample variances (Welch's test).

Five data points from the Fasano et al. (2004) study, all with (R_{PAR} A) determined at 1000 Hz that were less than 5 kΩ cm^2, appear to deviate systematically from the model prediction. This different behavior of low resistance skin samples compared to higher resistance samples has been observed previously. From the ratio of urea permeability measured at 39° and 27°C, Peck et al. (1995) discovered that heat-separated human skin (epidermis) with (R_{skin} A) less than 20 kΩ cm^2 at 27°C behaved more like a porous Nuclepore membranes than like higher resistance skin. Thus, Peck et al. (1995) selected 20 kΩ cm^2 as the minimum value of (R_{skin} A) for skin with acceptable integrity, which is one of the test criteria listed in Table 3.1. Notably, the value of b determined by best-fit regression of the data in Figure 3.3 to Eq. (3.9) was unaffected by the presence of the five deviant points in the Fasano et al. data set.

In the derivation of Eq. (3.9), which relates (R_{PAR} A) and k_p, it was assumed that the product of the area normalized DC skin resistance (R_{skin} A) and k_p for a given chemical is a constant, b. This hypothesis is tested directly in Figure 3.4, in which R_{PAR} measurements, determined at either 100 or 1000 Hz from each of the three laboratories, are plotted as a function of b/k_p for b at the optimum value of 63 kΩ cm^3/h. The figures also include (R_{PAR} A) data from White et al. (2011) plotted as a function of (R_{skin} A). Within the variability of the measurements, the four different sets of (R_{PAR} A) values and the k_p data from three different laboratories were in remarkable agreement with the (R_{PAR} A) and (R_{skin} A) data from White et al. (2011).

The solid curves in Figure 3.4 are plots of the frequency dependent relationship between (R_{PAR} A) and (R_{skin} A) predicted by Eq. (3.4), which represents the R-CPE circuit model for $\alpha = 0.8$ and $C_{skin,eff}/A = 39.8$ nF/cm^2 with the reasonable assumption that R_e (typically, of order 0.1 kΩ cm^2 for PBS solutions in these diffusion cells) is small relative to R_{skin} (typically, larger than 10 kΩ cm^2). (Identical curves would be generated using Eq. (3.9) to calculate (R_{PAR} A) as a function of b/k_p for b at the optimum value of 63 kΩ cm^3/h.) Although the curve closely represents the (R_{PAR} A) versus (R_{skin} A) data measured at 100 Hz, there is a systematic deviation between the theory and data measured at 1000 Hz for (R_{skin} A) larger than approximately 100 kΩ cm^2.

A likely cause of this deviation is that the R-CPE circuit model does not represent perfectly the skin impedance at all frequencies (Grimnes and Martinsen, 2005; Martinsen et al., 1997; Yamamoto and Yamamoto, 1976b). As a result, different values of $C_{skin,eff}/A$ and also α are derived when the R-CPE model equation is regressed to data from different frequency ranges. The 39.8 nF/cm^2 value for $C_{skin.eff}/A$ is the log-mean average of $C_{skin.eff}/A$ determined from the characteristic frequency for the 145 skin samples (White et al., 2011b). Upper and lower bounds calculated by adding or subtracting one standard deviation, 0.3, to the logarithm of 39.8 nF/cm^2 corresponded to 75.8 and 20.2 nF/cm^2, respectively (White et al., 2011b). The curve calculated using $C_{skin,eff}/A$ equal to 20.2 nF/cm^2 rather than 39.8 nF/cm^2 in Eq. (3.4) more closely represented the large impedance skin samples at 1000 Hz (see dashed curve in Figure 3.4).
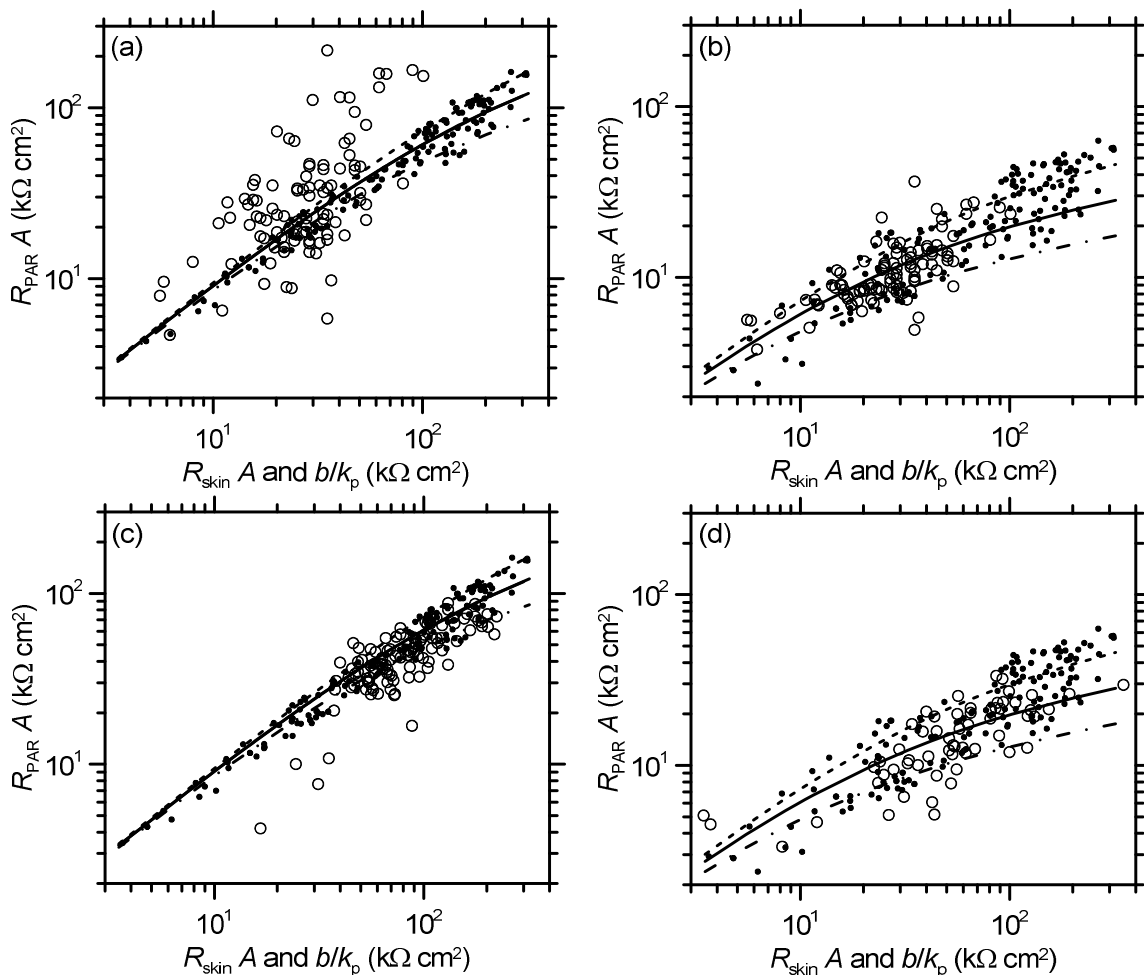
Figure 3.4 A comparison of (R_{PAR} A) versus (R_{skin} A) data (small filled circles) from the multi-frequency impedance study of White et al. (2011) with (R_{PAR} A) measured at 100 and 1000 Hz versus b/k_p data from three different laboratories (open circles) for b equal to 63 $\Omega cm^3/h$: (a) Charles River data measured at 100 Hz, (b) Charles River data measured at 1000 Hz, (c) Davies et al. (2004) data measured at 100 Hz, and (d) Fasano et al. (2002) data measured at 1000 Hz. The theoretical relationship for (R_{PAR} A) plotted as a function of (R_{skin} A) was calculated using Eq. (3.4) for α equal to 0.8 and $C_{skin,eff}/A$ equal to 39.8 nF/cm^2 (solid curves), 75.8 nF/cm^2 (dot-dashed curves), and 20.2 nF/cm^2 (dashed curves), which represent the mean and plus and minus one standard deviation of log($C_{skin,eff}/A$) determined in the multi-frequency impedance study of White et al. (2011).

Since there were only a few k_p data points with R_{PAR} determined at 1000 Hz that are larger than 100 kΩ cm^2, the systematic deviation of Eq. (3.4) calculated using 39.8 nF/cm^2 to the 1000 Hz data at large (R_{skin} A) resulted in little effect on the estimate of b. Moreover, because (R_{skin} A) values of interest for skin integrity testing are much less than 100 kΩ cm^2, Eq. (3.4) with $C_{skin,eff}/A$ equal to 39.8 nF/cm^2 can be used reliably to relate (R_{PAR} A) and (R_{skin} A) test criteria.

3.4.2 Application to Polar Compounds

The values of the proportionality constants b for different chemicals that permeate skin through the same pathway as ions should be related to their permeability coefficients: the DC resistance (R_{skin} A) for a given skin sample should equal the ratio of the chemical specific values of b and k_p for these chemicals as follows:

$$\left(R_{skin}A\right) = \left(\frac{b}{k_p}\right)_{chemical\ 1} = \left(\frac{b}{k_p}\right)_{chemical\ 2} \tag{3.14}$$

Thus, b for tritiated water should be related to b for a different polar compound and the ratio of the permeability coefficients of tritiated water to the chemical by

$$b_{water} = b_{chemical}\left(\frac{k_{p,\,water}}{k_{p,\,chemical}}\right) \tag{3.15}$$

The temperature dependence of (R_{skin} A) and $1/k_p$ should be the same, and therefore, b should be independent of temperature. However, k_p values do vary with temperature, and k_p measurements used in Eq. (3.15) should be at the same temperature.

Permeability coefficient data and the corresponding DC resistance measurements were digitally derived from Figure 7 in Peck et al. (1995) for urea ($\log K_{o/w}$ = -2.11 (Hansch et al., 1995) and MW = 60.05 Da) using Grapher and replotted in Figure 3.5. The best-fit linear regression of $\log(R_{skin} A)$ with $\log(1/k_p)$ is also shown, which, consistent with Eq. (3.8), has a slope close to 1. The expectation that temperature should not affect the relationship between ($R_{skin} A$) with ($1/k_p$) is supported by these results, which include data determined at both 27°C and 39°C (Peck et al., 1995). Under the assumption that the slope has a value exactly equal to one, $\log(b)$ was determined from the $\log (R_{skin} A)$ intercept for each data point as

$$\log(b) = \log(R_{skin} A) - \log(1/k_p) \qquad (3.16)$$

and then averaged over all data points. The resulting estimate for b was $4.9 \pm 0.7 \ \Omega \ cm^3/h$ (mean $\pm$ 1 standard deviation).

Peck et al. (1995) reported k_p values for urea of 0.201×10^{-3} cm/h and 0.272×10^{-3} cm/h at 27°C and 39°C, respectively, from which k_p at 32°C was estimated by interpolation to be approximately 0.234×10^{-3} cm/h at 32°C. This is slightly larger than 0.148×10^{-3} cm/h, which was measured by Barber et al. (1992) at 32°C. Using a k_p for tritiated water between 1.5 and 2.0×10^{-3} cm/h (see Table 3.2 and Meidan and Roper, 2008), the ratio of k_p values for water and urea is between 6.4 and 14. Multiplying b for urea by this ratio gives an estimated value of b for tritiated water between 31 and 66 $\Omega \ cm^3/h$, which is consistent with 63 $\Omega \ cm^3/h$ derived by regression to the data from three different laboratories.
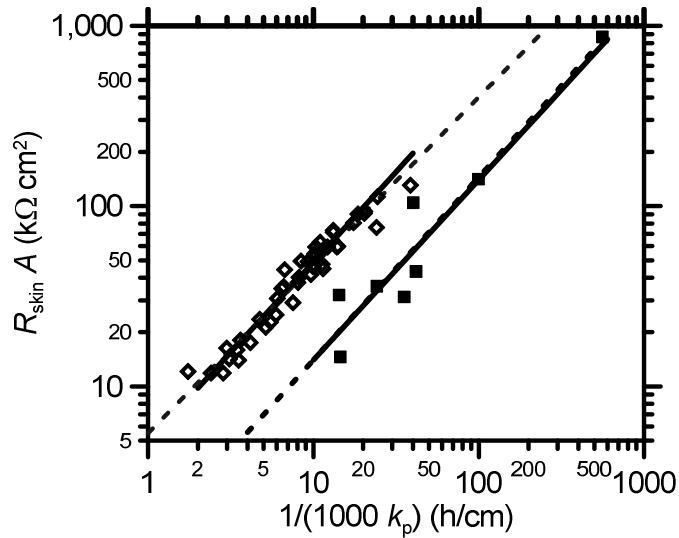
Figure 3.5 (R_{skin} A) plotted as a function of $1/k_p$ for urea (diamonds) measured at 27°C and 39°C (Peck et al., 1995) and for mannitol (squares) measured at 23°C (Tang et al., 2001). The solid lines have a slope of 1 and intercepts, log(b), equal to (log(R_{skin} A) − log ($1/k_p$)) averaged over all data for each chemical: b is 4.9 Ω cm^2 and 1.4 Ω cm^2 for urea and mannitol, respectively. For comparison, the best-fit linear regressions to the data (dashed lines) are included: for urea, log[(R_{skin} A), kΩ cm^2] = 0.93 log[1/(1000 k_p), h/cm] + log(5.5 Ω cm^2), r^2 = 0.95; for mannitol, log[((R_{skin} A)), kΩ cm^2] = 1.01 log[1/(1000 k_p), h/cm] + log(1.4 Ω cm^2), r^2 = 0.91.

From a similar analysis of low frequency impedance measurements (determined at 10 Hz, which should be close to the DC resistance) and mannitol permeation data for human skin (Tang et al., 2001), shown in Figure 3.5, b was determined to be 1.4 ± 0.6 Ω cm^3/h (digitized data from Figure 1 of Tang et al.). For mannitol (log$K_{o/w}$ = -3.10; Hansch et al., 1995) k_p at 32°C was estimated to be 0.078 x 10^{-3} cm/h from measurements of 0.067 x 10^{-3} cm/h and 0.093 x 10^{-3} cm/h at 27°C and 39°C, respectively (Peck et al., 1995). For comparison, the average k_p from Tang et al. (2001) was 0.034 x 10^{-3} cm/h measured at 23°C and Scott et al. (1991) reported a value of 0.061 x 10^{-3} cm/h at 30°C.

3.4.3 Application to Tests of Skin Integrity

A rearrangement of Eq. (3.10) along with Eqs. (3.8) and (3.4) provide a means of estimating, for a given tritiated water k_p, the corresponding values for tritiated water absorption after 1 h, (R_{skin} A), and (R_{PAR} A) measured at a given frequency. The results are presented in Table 3.3 for tritiated water k_p values that have been used variously as criteria for rejecting skin that was potentially damaged. Also listed in Table 3.3 are values for (R_{PAR} A) calculated using two equations derived by linear regression of the logarithms of (R_{PAR} A) measurements at 100 and 1000 Hz, respectively to the logarithm of (R_{skin} A) measured on the same piece of skin (White et al., 2011b). Generally, these values of (R_{PAR} A) are smaller than those estimated from Eq. (3.4), although the difference was usually less than 10%. The chief advantage of Eq. (3.4) over the linear regression equations from White et al. (2011) is that it can be used to estimate (R_{PAR} A) at any frequency. Based on the results shown in Figure 3.4, it is appropriate to restrict the use of Eq. (3.4) to frequencies less than about 1000 Hz.

Using Eq. (3.4), the (R_{skin} A) values that corresponded with the various electrical resistance integrity test criteria listed in Table 3.1 have been calculated. These are listed in Table 3.1 along with tritiated water k_p values estimated using Eq. (3.8), which can be compared to the k_p values that were used to derive the test criteria. Of the criteria in Table 3.1, the recommendation of 20 kΩ cm^2 for (R_{skin} A) from Peck et al. (1995) was based on membrane behavior that is consistent with damage rather than correlation to a selected permeability

coefficient value. Significantly, 20 kΩ cm^2 as a test criterion for (R_{skin} A)

corresponds to 17 kΩ cm^2 for (R_{PAR} A) at 100 Hz and a tritiated water k_p of 3.2 x

10^{-3} cm/h. This k_p may be large enough so that undamaged but higher

permeability skin samples are not screened from study.

Table 3.3 Calculated values of the 1-h absorption, (R_{skin} A), and (R_{PAR} A) determined at 100 Hz and 1000 Hz corresponding to different values of tritiated water permeability

Tritiated water[a]			(R_{PAR} A) from Eq. (4)		(R_{PAR} A) from White et al. 2011[c]	
k_p x 10^3	1-h absorption	(R_{skin} A) = b/k_p[b]	100 Hz	1000 Hz	100 Hz	1000 Hz
(cm/h)	(μL/cm^2)	(kΩ cm^2)	(kΩ cm^2)	(kΩ cm^2)	(kΩ cm^2)	(kΩ cm^2)
1.5	0.8	42	32	14	28	14
2.0	1.0	32	25	12	21	11
2.5	1.3	25	21	11	18	10
3.0	1.5	21	18	9.7	15	8.6
3.5	1.8	18	15	8.9	13	7.8
4.0	2.0	16	14	8.2	12	7.1
4.5	2.3	14	12	7.6	11	6.6

[a] Equal to f_{abs} V/A at 1 h calculated using Eq. (3.10) and assuming t_{lag} = 0.5 h
[b] For b equal to 63, which is the optimum value determined by minimizing the sum of the squared residuals to the prediction from Eq, (3.9) equally weighting all measurements from all studies
[c] White et al. (2011) provided the following two equations for estimating (R_{PAR}·A) from 100 Hz and 1000 Hz, respectively:
log [(R_{PAR} A) at 100 Hz] = 0.837 log(R_{skin} A) + 0.092
log [(R_{PAR} A) at 1000 Hz] = 0.668 log(R_{skin} A) + 0.053

3.5 Conclusions

Impedance measurements collected at a single frequency not larger than

1000 Hz on human skin *in vitro* are related in a predictable way to DC skin

resistance (R_{skin} A), based on a simple circuit of a parallel resistor and constant

phase element (CPE) in parallel, and therefore, after normalizing for area, to the steady-state permeability coefficient (k_p) for ionic or hydrophilic compounds. The nonlinear relationship between k_p values for tritiated water and resistances reported in parallel (PAR) mode obtained in three different laboratories at either 100 or 1000 Hz were predicted using a single equation, even though the mean values of the skin samples for permeability and resistance were significantly different for the different laboratories. The success of this equation supports the hypothesis that k_p values for tritiated water are linearly correlated with R_{skin} A, which are a measure of the barrier function to ions, even though water may permeate skin through both hydrophilic and lipophilic pathways. Moreover, the proportionality constant relating R_{skin} A and water k_p values is consistent with constants for urea and mannitol, which are known to permeate skin through a hydrophilic pathway. Using this equation relating water k_p and R_{PAR} A, previously published impedance criteria for identifying skin as acceptable for chemical absorption studies were compared on the basis of water k_p. Overall, R_{PAR} A determined at 100 Hz can be used reliably to test for skin integrity with better sensitivity than R_{PAR} A determined at 1000 Hz. The test criterion of 20 kΩ cm^2 for (R_{skin} A), has been shown to correspond with a tritiated water permeability of about 3.2×10^{-3} cm/h. This criterion could be able to exclude damaged skin without screening undamaged but higher permeability skin samples from study.

REFERENCES

Barber, E.D., Teetsel, N.M., Kolberg, K.F., Guest, D., 1992. A comparative study of the rates of in vitro percutaneous absorption of eight chemicals using rat and human skin. Fundam. Appl. Toxicol. 19, 493-497.

Bronaugh, R.L., Stewart, R.F., 1986. Methods for in vitro percutaneous absorption studies VI: Preparation of the barrier layer. J. Pharm. Sci. 75, 487-491.

Buist, H.E., van de Sandt, J.J.M., van Burgsteden, J.A., de Heer, C., 2005. Effects of single and repeated exposure to biocidal active substances on the barrier function of the skin in vitro. Regul. Toxicol. Pharm. 43, 76-84.

Bunge, A.L., Cleek , R.L., 1995. A new method for estimating dermal absorption from chemical exposure. 2. Effect of molecular weight and octanol-water partitioning. Pharm. Res. 12, 87-94.

Bunge, A.L., Cleek , R.L., Vecchia, B.E., 1995. A new method for estimating dermal absorption from chemical exposure. 3. Compared with steady-state methods for prediction and data analysis. Pharm. Res. 12, 972-982.

Davies, D.J., Ward, R.J., Heylings, J.R., 2004. Multi-species assessment of electrical resistance as a skin integrity marker for in vitro percutaneous absorption studies. Toxicol. In Vitro 18, 351-358.

Fasano, W.J., Hinderliter, P.M., 2004. The Tinsley LCR Databridge Model 6401 and electrical impedance measurements to evaluate skin integrity in vitro. Toxicol. In Vitro 18, 725-729.

Fasano, W.J., Manning, L.A., Green, J.W., 2002. Rapid integrity assessment of rat and human epidermal membranes for in vitro dermal regulatory testing: correlation of electrical resistance with tritiated water permeability. Toxicol. In Vitro 16, 731-740.

Grimnes, S., Martinsen, O.G., 2005. Cole electrical impedance model - A critique and an alternative. IEEE Trans. Biomed. Eng. 52, 132-135.

Hansch, C., Leo, A., Hoekman, D., 1995. Exploring QSAR: Hydrophobic, Electronic, and Steric Constants. American Chemical Society, Washington, DC.

Heylings, J.R., Esdaile, D.J., 2007. Percutaneous absorption of pesticides, In: Roberts, M.S., Walters, K.A. (Eds.), Dermal Absorption and Toxicity Assessment, Second edition ed. Informa Healthcare, New York, pp. 575-591.

Hirschorn, B., Orazem, M.E., Tribollet, B., Vivier, V., Frateur, I., Musiani, M., 2010. Determination of effective capacitance and film thickness from constant-phase-element parameters. Electrochimica Acta 55, 6218-6227.

Hsu, C.H., Mansfeld, F., 2001. Technical note: Concerning the conversion of the constant phase element parameter Y_0 into a capacitance. Corrosion 57, 747-748.

International Programme on Chemical Safety (IPCS), 2006. Dermal Absorption, Environmental Health Criteria 235. World Health Organization, Geneva.

Kalia, Y.N., Pirot, F., Guy, R.H., 1996. Homogeneous transport in a heterogeneous membrane: Water diffusion across human stratum corneum *in vivo*. Biophys. J. 71, 2692-2700.

Kasting, G.B., Barai, N.D., 2003. Equilibrium water sorption in human stratum corneum. J. Pharm. Sci. 92, 1624-1631.

Kasting, G.B., Bowman, L.A., 1990. DC electrical properties of frozen, excised human skin. Pharm. Res. 7, 134-143.

Kasting, G.B., Filloon, T.G., Francis, W.R., Meredith, M.P., 1994. Improving the sensitivity of in vitro skin penetration experiments. Pharm. Res. 11, 1747-1754.

Kontturi, K., Murtomaki, L., 1994. Impedance Spectroscopy in Human Skin. A Refined Model. Pharm. Res. 11, 1355-1357.

Martinsen, O.G., Grimnes, S., Sveen, O., 1997. Dielectric properties of some keratinised tissues .1. Stratum corneum and nail in situ. Med. Biol. Eng. Comput. 35, 172-176.

Meidan, V.M., Roper, C.S., 2008. Inter- and intra-individual variability in human skin barrier function: A large scale retrospective study. Toxicol. In Vitro 22, 1062-1069.

OECD, 2004. OECD Guideline for Testing of Chemicals. Guideline 428: Skin Absorption: In Vitro Method (Original Guideline, adopted 13th April 2004).

Orazem, M.E., Tribollet, B., 2008. Electrochemical Impedance Spectroscopy. Wiley-Interscience, Hoboken, NJ.

Peck, K.D., Ghanem, A.H., Higuchi, W.I., 1994. Hindered diffusion of polar molecules through and effective pore radii estimates of intact and ethanol treated human epidermal membrane. Pharm. Res. 11, 1306-1314.

Peck, K.D., Ghanem, A.H., Higuchi, W.I., 1995. The effect of temperature upon the permeation of polar and ionic solutes through human epidermal membrane. J. Pharm. Sci. 84, 975-982.

Poon, C.S., Choy, T.T.C., 1981. Frequency dispersions of human-skin dielectrics. Biophys. J. 34, 135-147.

Potts, R.O., Francoeur, M.L., 1991. The influence of stratum corneum morphology on water permeability. J. Invest. Dermatol. 96, 495-499.

Potts, R.O., Guy, R.H., 1992. Predicting skin permeability. Pharm. Res. 9, 663-669.

Runciman, J., Roper, C.S., Madden, S. Evaluation of a rapid tritiated water skin barrier integrity method for use in regulatory toxicology testing *in vitro*, Occupational and Environmental Exposure of the Skin to Chemicals (OEESC), Edinburgh, Scotland, June 14-17, 2009.

Scott, R.C., Corrigan, M.A., Smith, F., Mason, H., 1991. The influence of skin structure on permeability: an intersite and interspecies comparison with hydrophilic penetrants. J. Invest. Dermatol. 96, 921-925.

Scott, R.C., Dugard, P.H., Ramsey, J.D., Rhodes, C., 1987. In vitro absorption of some ortho-phthalate diesters through human and rat skin. Environmental Health Perspectives 74, 223-227.

Tang, H., Mitragotri, S., Blankschtein, D., Langer, R., 2001. Theoretical description of transdermal transport of hydrophilic permeants: Application to low-frequency sonophoresis. J. Pharm. Sci. 90, 545-568.

van de Sandt, J.J., Meuling, W.J., Elliott, G.R., Cnubben, N.H., Hakkert, B.C., 2000. Comparative in vitro-in vivo percutaneous absorption of the pesticide propoxur. Toxicol. Sci. 58, 15-22.

White, E.A., Horne, A., Runciman, J., Orazem, M.E., Navidi, W.C., Roper, C.S., Bunge, A.L., 2011a. Single-Frequency Impedance Measurements as Predictors of Human Skin Permeability to Water and Other Hydrophilic Compounds. Toxicol. In Vitro, in press.

White, E.A., Orazem, M.E., Bunge, A.L., 2011b. A critical analysis of single-frequency LCR databridge impedance measurements of human skin. Toxicol. In Vitro 25, 774-784.

World Precision Instruments, 2008. EVOM & EVOMX Epithelial Voltohmmeters, Instruction Manual, Sarasota, FL.

Yamamoto, T., Yamamoto, Y., 1976a. Dielectric constant and resistivity of epidermal stratum corneum. Medical and Biological Engineering and Computing 14, 494-500.

Yamamoto, T., Yamamoto, Y., 1976b. Electrical properties of the epidermal stratum corneum. Med. Biol. Eng. 14, 151-158.

Yamamoto, T., Yamamoto, Y., 1981. Non-linear electrical-properties of skin in the low-frequency range. Med. Biol. Eng. Comput. 19, 302-310.

CHAPTER 4

CHARACTERIZATION OF DMSO DAMAGED SKIN AND PINHOLE DAMAGED SKIN BY IMPEDANCE SPECTROSCOPY

Electrical impedance and the flux of non-polar compounds were measured before and after treatments that irreversibly altered human cadaver skin either chemically using dimethyl sulfoxide (DMSO) or mechanically by needle puncture. The impedance spectra collected before and after skin was treated for 1 h with DMSO exhibited a single characteristic frequency that was about 100 times larger after treatment. After DMSO exposure for only 0.25 h, the impedance spectra were consistent with two characteristic frequencies that coincided with those observed before and after DMSO treatment for 1 h. These observations are consistent with DMSO damage to a fraction of the skin, which it is shown increased proportional to the square-root of treatment time until about 0.5 h. DMSO exposure for both treatment times did not significantly change the flux of the non-polar compound, p-chloronitrobenzene, compared to the phosphate buffered saline control. The characteristic frequency of the impedance scans determined after needle puncture increased by an amount that could be predicted using a recently published theory. The flux of 4-cyanophenol increased by a small but significant amount that did not correlate with the hole resistance calculated assuming the resistance of the surrounding skin did not change.

4.1 Introduction

The outer most layer of the skin, the stratum corneum, is a matrix of dead keratinized cells suspended in lipid bilayers. It is the primary barrier to chemical penetration and electric current through the skin. Therefore, unless stated otherwise, in this chapter the word skin refers to the stratum corneum. Impedance spectroscopy, which is the measurement of the impedance for a range of frequencies, provides information about the electrical properties of skin. Impedance measurements at a given frequency involve measuring the current or potential response to small amplitude modulation of an input current or potential. The impedance is the ratio of the change in potential to the change in current, which for skin is a function of the modulation frequency. Dielectric material in skin causes the resulting signal to shift in time relative to the applied signal resulting in a complex number for impedance. Changes in the impedance spectrum of skin subsequent to chemical exposure or mechanical damage indicate changes in the structure or composition of skin.

The electrical response of the skin is related to two intrinsic properties: the resistivity and the dielectric constant. The skin resistivity is proportional to the area-normalized skin resistance measured using a direct current method; i.e., $R_s A$ where A is the skin area normal to current flow. The dielectric constant of skin is proportional to the capacitance normalized by the inverse area (C_s / A). Because the stratum corneum is heterogeneous, macroscopic electrical measurements of the skin produce effective values for the skin resistance and capacitance that combine effects from the various structures within the stratum

corneum. Hydrophilic and lipophilic molecules diffuse through skin via different pathways with different rate limiting mechanisms depending upon the octanol-water partition coefficient ($K_{o/w}$) (Bennett and Barry, 1985). For skin submerged in electrolyte solution, dissolved ions transport through the skin in response to an electric field. Thus, skin resistivity quantitatively characterizes the pathway for transport of ions through skin. Consistent with this, the permeability of hydrophilic and ionic chemicals through skin has been shown to be inversely proportional to ($R_s \cdot A$) (Kasting and Bowman, 1990; Peck et al., 1994, 1995; Tang et al., 2001).

Though the source of skin capacitance is not well understood, investigators have suggested that the skin capacitance arises from the highly ordered stratum corneum lipids (Curdy et al., 2000; DeNuzzio and Berner, 1990; Kim and Oh, 2000; Oh et al., 1993). The stratum corneum lipids are thought to be the major component of the lipophilic pathway suggesting that the effective capacitance of skin may characterize the lipophilic pathway.

High concentrations of the polar, aprotic solvent dimethyl sufoxide (DMSO) irreversibly change skin impedance and the barrier it exhibits to chemical penetration. Kurihara-Bergstrom et al. (1986) present evidence that DMSO damages rat skin - a common model for human skin - by elution of sc lipids, denaturation of sc structural proteins (keratin), and delamination of the stratum corneum layer. They showed that damage was irreversible and coincided with loss of mass, hypothesized to be extracted lipids, when skin was submerged in DMSO:water mixtures >50% strength for two hours. Allenby et al.

(1969) observed that low frequency skin impedance, which is an estimate of the skin resistance, decreased over time to a minimum value in less than 0.5 h in the presence of 100% DMSO. In light of these results, we hypothesize that impedance spectroscopy is sensitive to the changes caused by DMSO.

The objective of this study was to quantify the effect of DMSO for treatment times of 1 h or less on the impedance and flux of a model lipophilic chemical, p-chloronitrobenzene (PCNB). We present impedance data that indicate skin treated with DMSO for 0.25 h has frequency dependence consistent with a 2-time-constant model circuit, while skin treated with DMSO for 1 h has frequency dependence consistent with a 1-time-constant model circuit. We hypothesize that DMSO progressively damages a larger fraction of the skin thickness over time and that the undamaged fraction of the skin retains the intrinsic electric properties of the skin before DMSO treatment. The observed decrease in the magnitude of the impedance is due therefore, to a decrease in the thickness of undamaged skin. We then compare the impedance of DMSO treated skin to that of skin punctured with a needle, which is consistent with a 1-time-constant model. We also compare the flux of a different lipophilic compound 4-cyanophenol (CP) before and after the skin was punctured with a needle. Circuit models consistent with the nature of the skin damage are proposed and the model parameters are determined quantitatively by regression.

4.2 Theory

Skin impedance is related to the structure and composition of the stratum corneum. In this study the skin barrier is altered in two different ways and circuit models are proposed to describe the resulting skin impedance.

4.2.1 Skin Impedance Models

A common circuit model of *in-vitro* skin impedance is a resistor that represents the frequency-independent (Ohmic) resistance containing contributions from the electrolyte, wires, and possibly the dermis (R_e) in series with a parallel resistor (R_s) and constant phase element (CPE). This model, referred to here as the 1-time-constant model, is depicted in Figure 4.1a. The CPE is thought of as a non-ideal capacitor, with complex impedance, Z, defined as

$$Z = \frac{1}{Q_s \left(j2\pi f \right)^{\alpha_s}} \tag{4.1}$$

where Q_s and α_s are the CPE parameters, j is the complex number $\sqrt{-1}$, and f is the frequency with units of inverse seconds (Hz). Jorcin et al. (2006) demonstrated that, in general, CPE behavior can be the result of distributions of resistance and capacitance in the material. In skin, the CPE behavior has been attributed to the stratum corneum heterogeneity (Yamamoto and Yamamoto, 1976).
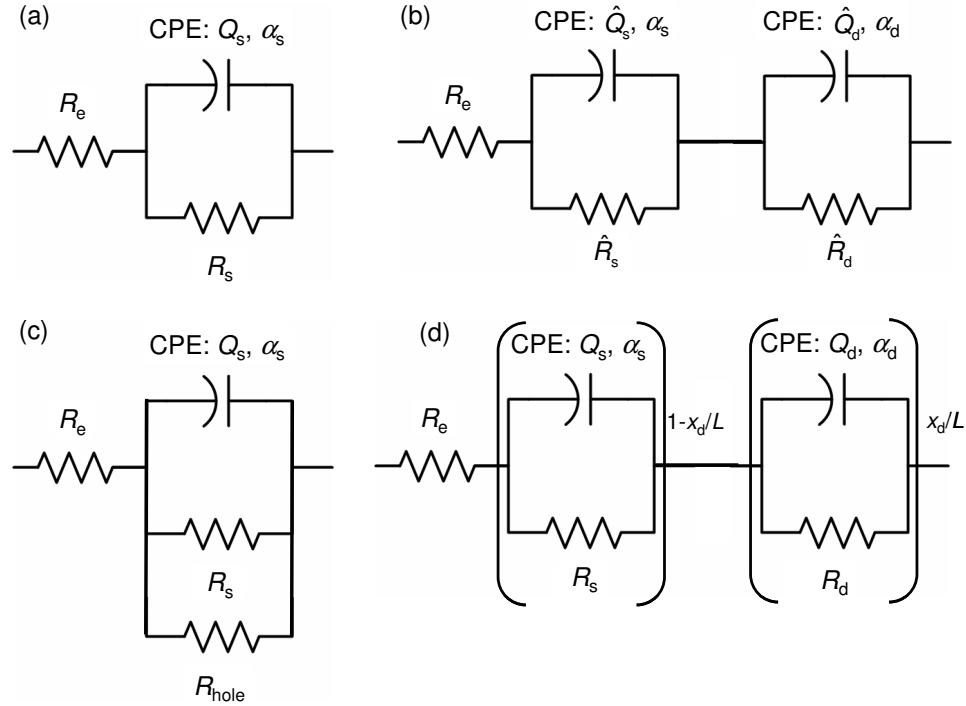
Figure 4.1 Diagrams of equivalent circuit models: (a) 1-time-constant model, (b) 2-time-constant model, (c) pinhole model, and (d) fraction-damaged model.

The impedance of the 1-time-constant model is described by Eq. (4.2).

$$Z = R_e + \frac{R_s}{1 + R_s Q_s (j2\pi f)^{\alpha_s}} \tag{4.2}$$

The characteristic frequency of the 1-time-constant model, $f_{c,s}$, which corresponds to the frequency at which the absolute value of the imaginary part of the impedance is a maximum, is calculated with Eq. (4.3).

$$f_{c,s} = \frac{1}{2\pi (R_s Q_s)^{1/\alpha_s}} \tag{4.3}$$

Eq. (4.2) is characterized by a single time constant that is equal to the inverse of this characteristic frequency ($1/f_{c,s}$).

A common simplification of the 1-time-constant model is to replace the CPE with a capacitor that has a capacitance C_s. The impedance of this

simplified R-C circuit model, in which a resistor is in series with a parallel resistor (R_s) and capacitor (C_s), is represented exactly by Eq. (4.2) for $Q_s = C_s$ and $\alpha = 1$. It follows that the characteristic frequency for the R-C circuit model is defined by Eq. (4.4).

$$f_{c,s} = \frac{1}{2\pi R_s C_s} \tag{4.4}$$

Since the dielectric constant for a material is related to the capacitance, it is useful to relate the CPE parameters in the 1-time-constant model (Q_s and α_s) to an effective capacitance. One approach for doing this is to determine the value of C_s in Eq. (4.4) that gives the same characteristic frequency as the 1-time-constant model; i.e., Eq. (4.3). The resulting expression, referred to as the Hsu and Mansfeld equation (Hsu and Mansfeld, 2001),

$$C_s = Q_s^{1/\alpha_s} R_s^{(1-\alpha_s)/\alpha_s} \tag{4.5}$$

is derived by equating Eqs. (4.3) and (4.4) and solving for C_s in terms of R_s, Q_s and α_s.

The impedance of skin treated with DMSO for shorter periods of time exhibit frequency dependence consistent with the 2-time-constant model depicted in Figure 4.1b, which we hypothesize reflects the presence of two skin layers: one undamaged and one damaged. This model consists of an electrolyte resistor, R_e, in series with two circuits each consisting of a resistor and CPE in parallel. The impedance of the 2-time-constant model is described by Eq. (4.6):

$$Z = R_e + \frac{\hat{R}_s}{1 + \hat{R}_s \hat{Q}_s (j2\pi f)^{\alpha_s}} + \frac{\hat{R}_d}{1 + \hat{R}_d \hat{Q}_d (j2\pi f)^{\alpha_d}} \tag{4.6}$$

where the R-CPE parameters, $\hat{R}_s$, $\hat{Q}_s$ and α_s represent the undamaged skin layer and $\hat{R}_d$, $\hat{Q}_d$ and α_d, the damaged skin layer. The parameters with hats indicate values that are dependent on the thickness of the respective layers. The characteristic frequency and effective capacitance of both R-CPE circuits ($f_{c,s}$, $f_{c,d}$ and $\hat{C}_s$, $\hat{C}_d$ respectively) are calculated using the parameters corresponding to each layer in Eqs. (4.3). Eq. (4.6) is characterized by two time constants that are equal to $1/f_{c,s}$ and $1/f_{c,d}$.

Figure 4.2 is a schematic diagram of partially damaged stratum corneum, which we hypothesize occurs when skin is treated with DMSO for a short time. In this diagram, the total thickness of the damaged layer (x_d) is less than the stratum corneum thickness (L). Because DMSO was applied to both sides of the skin, both sides will be affected. The schematic in Figure 4.2 depicts the thickness of the two damaged regions (i.e. the non-shaded regions) to be equal, although this is not necessarily the case. The difference between L and x_d is the length of the remaining undamaged stratum corneum; the fraction damaged is x_d/L.

An assumption in the development of the fraction-damaged equivalent circuit model is that the interface between the damaged and undamaged skin layers is distinct and uniform across the area of the DMSO treated skin. However, it is likely that DMSO does not affect the stratum corneum uniformly, resulting in a non-uniform interface between the damaged and undamaged parts of the skin. This situation is represented schematically in Figure 4.2 by the solid, wavy lines.
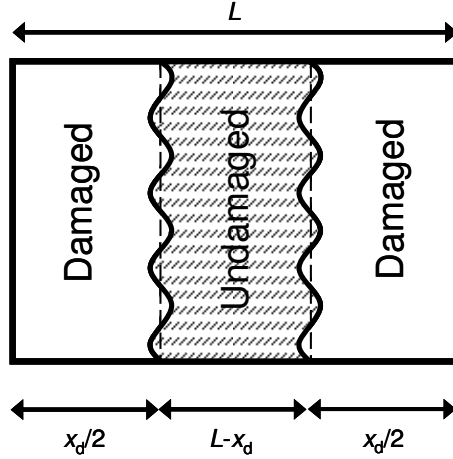
Figure 4.2 Diagram of stratum corneum that is partially damaged after exposure to DMSO on both sides. The dashed lines represent distinct and uniform boundaries between damaged and undamaged layers that may not actually exist.

The fraction damaged circuit model depicted in Figure 4.1d is described by Eq. (4.7)

$$Z = R_e + \left[\frac{R_s}{1 + R_s Q_s \left(j 2\pi f \right)^{\alpha_s}} \right] \left(1 - \frac{x_d}{L} \right) + \left[\frac{R_d}{1 + R_d Q_d \left(j 2\pi f \right)^{\alpha_d}} \right] \frac{x_d}{L} \qquad (4.7)$$

where the length-independent values of R and Q for the undamaged and damaged layers are represented as R_s, Q_s and R_d, Q_d, respectively. Comparing Eqs. (4.6) and (4.7), it is evident that

$$R_s = \frac{\hat{R}_s}{\left(1 - x_d/L \right)} \qquad (4.8)$$

$$Q_s = \hat{Q}_s \left(1 - x_d/L \right) \qquad (4.9)$$

$$R_d = \frac{\hat{R}_d}{x_d/L} \qquad (4.10)$$

$$Q_d = \hat{Q}_d \left(x_d/L \right) \qquad (4.11)$$

From these, the effective length-independent capacitance values of each layer, C_s and C_d, are calculated using the parameters for that layer by Eq. (4.5).

The impedance of punctured skin is hypothesized to vary with frequency as described by the pinhole equivalent circuit depicted in Figure 4.1c, and represented by the Eq. (4.12)

$$Z = R_e + \frac{R_t}{1 + R_t Q_s (j2\pi f)^{\alpha_t}} \tag{4.12}$$

where Q_s and α_s are the CPE parameters of the skin after the hole was punctured, and R_t is the total resistance of the skin and hole operating in parallel as defined by Eq. (4.13):

$$R_t = \left[\frac{1}{R_s} + \frac{1}{R_{hole}} \right]^{-1} \tag{4.13}$$

Like the 1-time-constant model, the pinhole equivalent circuit model has a single characteristic frequency, $f_{c,t}$, which is described by Eq.(4.14).

$$f_{c,t} = \frac{1}{2\pi (R_t Q_s)^{1/\alpha_s}} \tag{4.14}$$

From the characteristic frequency of the corresponding R-C circuit, given in Eq. (4.15)

$$f_{c,t} = \frac{1}{2\pi R_t C_s} \tag{4.15}$$

the effective capacitance of the punctured skin, C_s, is derived to be:

$$C_s = Q_s^{1/\alpha_s} R_t^{(1-\alpha_s)/\alpha_s} \tag{4.16}$$

using the procedure described above for the 1-time-constant model. If the cross-sectional area of the hole is small compared to the skin area, then the skin

resistance (R_s) and the dielectric constant of the skin before and after the pinhole are expected to be the same. If C_s represents the effective dielectric constant of the stratum corneum, it follows that C_s, measured before and after the skin is punctured should be the same.

4.2.2 Graphical Representations of Impedance

Log-log graphs of the real and imaginary components of the impedance (i.e., Z_r A and $-Z_j$ A) plotted as a function of frequency each reveal different features of the impedance response or circuit model. For the circuit models shown in Figure 4.1, the real component of the impedance approaches the total resistance of the sample at small frequencies (i.e., $(R_e + R_s)$ A for undamaged skin and $(R_e + \hat{R}_s + \hat{R}_d)$ A for fractionally damaged skin) and R_e at high frequencies. For impedance spectra that are consistent with the 1-time-constant model, Eq. (4.2), the characteristic frequency corresponds to the maximum value of the $-Z_j$ A versus frequency plot. At low and high frequencies relative to the characteristic frequency, the slope of the curve approaches α_s and $-\alpha_s$, respectively.

Impedance plane plots, also called Nyquist plots, show $-Z_j$ A plotted as a function of Z_r A on linear axes. In this plot, the 1-time-constant model looks like a single squashed semi-circle where the maximum value of $-Z_j$ A is less than half the difference of the maximum and minimum values of Z_r A. The degree to which the impedance deviates from a perfect semi-circle, which occurs when $\alpha_s = 1$, depends on how much α_s deviates from 1. In this plot, the low frequency data

appears on the right side of the $Z_r\,A$ axis and frequency increases towards the

left. Thus, the low and high impedance intercepts of the $Z_r\,A$ axis, which

correspond to high and low frequency, are equal to $R_e\,A$ and the total resistance

of the system (i.e, $(R_e + R_s)\,A$ for undamaged skin and $(R_e + \hat{R}_s + \hat{R}_d)$ for

fractionally damaged skin), respectively. The impedance values corresponding

to the characteristic frequency appear at top of the semi-circle (i.e. where $-Z_j\,A$ is

a maximum).

Occasionally, features that cannot be identified in the three plots

described above are evident in a graph of the first derivative of $\log(-Z_j\,A)$ with

respect to $\log(f)$ plotted as a function of frequency (Hirschorn et al., 2010). The

derivative is estimated numerically by the following difference equation:

$$\frac{d\log(-Z_j A)}{d\log(f)} = \frac{\log(-Z_j A)_k - \log(-Z_j A)_{k-1}}{\log(f)_k - \log(f)_{k-1}} \qquad (4.17)$$

for each $\log(f)$

$$\log(f) = \log\frac{\left(f_k + f_{k-1}\right)}{2} \qquad (4.18)$$

where k and k-1 are the indices of measurements at adjacent frequencies. For

the 1-time-constant model given by Eq. (4.2), $d\log(-Z_j\,A)/\,d\log(f)$ asymptotically

approaches α_s at low frequencies and $-\alpha_s$ at high frequencies, and equals zero at

the characteristic frequency. In this graph, systems described by two

characteristic frequencies, $f_{c,s}$ and $f_{c,d}$, will consist of the sum of the curves for

each characteristic frequency. As long as the two characteristic frequencies are

sufficiently different and the magnitudes of the impedance contributions by each

curve sufficiently similar, the presence of a second characteristic frequency will

produce a clear perturbation to the behavior of a system with only one characteristic frequency.

4.3 Materials and Methods

Chemical flux and impedance spectra were measured before and after skin was altered either chemically using DMSO or mechanically by needle puncture. The experimental procedures for these studies and the related determination of solution resistivity are described here.

4.3.1 Chemicals and Materials

Phosphate buffered saline (0.01 M) with 0.138 M NaCl, 0.0027 M KCl (pH 7.4, Sigma P-3813) was prepared in de-ionized (DI) water (Millipore Corporation, Bedford, MA). Skin was either treated with DMSO (99.9%, CAS 67-68-5, Fisher Scientific) or punctured with a needle (26S gauge, Hamilton CO., Reno, NV). The permeation of two solutes, p-chloronitrobenzene (MW = 157.56 Da, log $K_{o/w}$ = 2.4, Sigma) and 4-cyanophenol (CAS 767-00-0, MW = 119.1 Da, log $K_{o/w}$ = 1.6, pK_a = 7.97, Sigma), were measured in the DMSO and pinhole experiments, respectively. Split-thickness human cadaver skin (300-400 μm thick) identified as Q (from the back of a 77-year old Caucasian female) and AS (from either the back or abdomen of a 78-year old Caucasian male) was purchased from the National Disease Research Interchange (NDRI, Philadelphia, PA). The skin was collected within 24 h post mortem, frozen immediately and stored at temperatures less than -60 °C until used.

4.3.2 Impedance-Diffusion Cell Apparatus

Skin impedance and chemical flux were both measured in horizontally oriented glass diffusion cells from PermeGear (13 mL, Side-Bi-Side[TM] diffusion cells, Hellertown, PA) adapted to allow 4-electrode impedance measurements and to support the skin sample during manipulations requiring it to be removed from the cell. Each skin sample was mounted into one of four custom-made frames (one with area of 1.84 cm^2 and three with area of 1.65 cm^2, PDM Services, Golden, CO). This frame was then clamped between the two diffusion cell chambers modified to hold two Ag/AgCl electrodes: one working and one reference (In Vivo Meteric, Healdsburg, CA). The working electrodes were 12-mm diameter discs oriented with the face parallel to the skin surface. The cylindrical reference electrodes (1.5 mm diameter and 3 mm long) were oriented such that the long axis was parallel to the skin surface. Experiments were conducted in a temperature-controlled chamber (Electro-Tech Systems, Inc., PA) that was large enough to hold all four cells and maintained at 32 °C.

4.3.3 Analytical Instruments

Impedance was measured using a Gamry potentiostat (model PCI4/300, Warminster, PA) in a four electrode configuration over a frequency range of 1 Hz to 100 kHz for the DMSO experiments and 0.1 Hz to 20 kHz for the pinhole experiments. A 10 mV root-mean-squared, sinusoidal AC perturbation signal was used for all impedance measurements.

Chemical concentrations in solutions were measured by high pressure liquid chromatography (HPLC, Hewlett Packard 1100, Palo Alto, CA) equipped with auto-sampling and a diode array detector set to 254 nm and 274 nm for measurements of CP and PCNB, respectively. The stationary phase was a Zorbax Extend-C18 (4.6 x 250 mm, Agilent Technologies, Santa Clara, CA) column. The mobile phase was acetonitrile and water (70:30 v:v,) with flow rates of 1 and 1.5 mL/min, which correspond to retention times of about 2.3 and 3.7 minutes, for analysis of CP and PCNB, respectively. Calibration using 4 or 5 standards, with concentrations that encompass the range of sample concentrations, was conducted prior to chemical analysis.

4.3.4 Experimental Procedures

The procedures used in the DMSO and pinhole experiments as well as the determination of the PBS solution resistivity are described next.

4.3.4.1 DMSO Experiments

The DMSO experiments consisted of simultaneous measurements of impedance and PCNB flux through skin in four impedance-diffusion (ID) cells before and after four different treatments: 0.25 and 1 h treatments with 100% DMSO or with PBS, which acted as the control. The entire experiment was repeated three times. For each treatment, skin was mounted in a frame, which was then clamped into an ID cell. Both chambers were filled with PBS for an eight to twelve hour equilibration period. During the equilibration period, impedance spectra were measured hourly to establish a baseline for the

electrical properties of the skin as well as to verify that the skin was at equilibrium as indicated by insignificant differences between subsequent spectra.

After equilibration, both chambers were emptied and the receptor and donor chambers were rinsed and filled with 13 mL of PBS and PCNB-saturated PBS, respectively. To ensure saturation of the donor solution throughout the experiment, excess crystals of PCNB were added to the donor chamber solution. One-milliliter samples, collected periodically from the receptor chamber, were replaced with an equal volume of chemical-free PBS. A total of nine samples were collected over 8 h. The first sample was collected between 0 and 0.5 h after the introduction of the donor solution. The eight subsequent samples were collected approximately hourly relative to the time that the saturated donor solution was introduced to the donor chamber. Impedance scans were also collected approximately hourly during the permeation study. Next, the receptor and donor chambers were emptied and filled with either DMSO or with PBS (for the control experiments). After treatment for either 0.25 or 1 h, the frame holding each skin sample, including the PBS controls, was removed from its ID-cell assembly and soaked in approximately 1 L of fresh deionized water three times for 0.25 h and then for 1 h in about 1 L of PBS. The ID cells were rinsed thoroughly and then reassembled and filled with PBS solution for another 8-h equilibration period with hourly impedance scans. After this, the PCNB flux measurements were repeated. Impedance results reported for before and after DMSO treatment were derived from the last spectrum collected during the equilibration periods.

In a separate time-course study, four skin samples from one subject were each treated with DMSO for one of four different times: 0.25, 0.5, 0.75 and 1 h. All four experiments were conducted at the same time following the same procedure described above except that 4-CP was used in the permeation study rather than PCNB.

4.3.4.2 Pinhole Experiments

The pinhole experiments were conducted following a similar procedure to the DMSO treatment experiments. After the same initial equilibration period, solutions from both chambers were drained and 13 mL of PBS and CP-saturated PBS were placed in the receptor chamber and donor chambers, respectively. Either 1 or 2-milliliter samples were collected hourly from the receptor solution with replacement starting 4 h after introducing the saturated donor solution and continuing for 3 h. After this, the frame holding the skin was removed from the ID cells, a hole was poked with a 26 Ga needle (464 μm outside diameter), the ID cell was reassembled, and the donor and receptor chambers refilled with fresh CP-saturated PBS and PBS, respectively. Seven 2-mL samples were collected from the receptor chamber with replacement every 0.75 h after introducing the CP donor solution. Impedance spectra were collected hourly during the PCNB flux measurements and results reported before and after needle puncture were derived from the last spectrum collected during the CP flux measurements.

4.3.4.3 Steady-State Flux Determination

The cumulative mass of chemical delivered into the receptor solution (M) at a sample time (t) was calculated by summing the mass of chemical in the receptor chamber and the total mass of chemical removed from the receptor solution in previous samples. The mass of chemical in the receptor chamber at t is the product of the receptor solution volume and the measured chemical concentration in the sample collected at time t. The mass removed from the receptor chamber by sampling is the product of the concentration and volume of the sample.

The steady-state flux (J_{ss}), which is the slope of the linear portion of the area normalized cumulative mass (M/A) versus t curve, was determined by linear regression. The lag time (t_{lag}) is the ratio of the intercept to the slope of the regressed line. Experimental estimates for J_{ss} that include M/A measurements at times less than about 2.4 times the lag time, are systematically lower than the actual value (Bunge et al., 1995); thus, data points collected before $2.4t_{lag}$ were removed and the regression was repeated. In most cases, J_{ss} was determined using at least four data points: in all cases, three data points were used.

4.3.4.4 Solution Resistivity of PBS

The resistivity of the PBS solution at 32°C was determined to be 54.855 ± 0.003 Ω cm (mean ± one standard deviation, n = 6) by measuring the resistance of the PBS solution in one of the ID cells containing no skin and filled with 26-mL of PBS. Six successive impedance spectra of frequencies between 1 Hz and

100 kHz were measured in the four electrode configuration. The resistance from each spectrum was the average value of Z_r measured at frequencies where only the resistance of the PBS solution contributed to the impedance response of the system as indicated by $-Z_j = 0$ (typically between 10 - 300 Hz). The average resistance of the six scans was $93.623 \pm 0.005\ \Omega\ cm^2$ (mean $\pm$ one standard deviation). The resistivity was calculated from the product of this resistance and the electrode cell constant, which accounts for the effective area and length of the solution between the electrodes in the ID cell. The cell constant was determined by measuring the resistance of standard solutions (0.01, 0.1 and 1 molal potassium chloride in DI water) with known resistivity at $32^\circ C$ (8.19, 68.68 and 623.91 Ω cm, respectively from Pratt et al., 2001) in the same ID cell by the procedure described above. The cell constants for the three solutions, calculated from the ratio of the resistivity to the measured resistance, were independent of the potassium chloride concentration and equal to 0.586 ± 0.005 cm (average $\pm$ standard deviation).

4.3.5 Regression

Equations representing the various equivalent circuit models were regressed to the complex impedance data by minimization of the objective function (χ^2) described by Eq. (4.19)

$$\chi^2(\mathbf{p}) = \sum_{k=1}^{N_{dat}} \left[\frac{\left(Z_r(f_k) - \hat{\hat{Z}}_r(f_k|\mathbf{P})\right)^2 + \left(Z_j(f_k) - \hat{\hat{Z}}_j(f_k|\mathbf{P})\right)^2}{\bar{\sigma}(f_k)^2} \right] \tag{4.19}$$

where k is an index for the observation at each measurement frequency, N_{dat} is the total number of measurement frequencies in the spectrum, Z_r and Z_j are the real and imaginary impedance data measured at frequencies f_k, $\hat{\hat{Z}}_r(f_k \mid \mathbf{P})$ and $\hat{\hat{Z}}_j(f_k \mid \mathbf{P})$ are the real and imaginary parts of the equivalent circuit model equation evaluated at frequency f_k for the parameter vector $\mathbf{P}$ (which includes all of the model parameters being optimized), and $\bar{\sigma}(f_k)$ is the average of the stochastic error at frequency f_k determined as described below. The errors reported for tabulated values of the regressed parameters presented below are the asymptotic standard parameter errors, which is the square root of the covariance matrix (Gavin, 2011). The objective function was minimized using a Levenberg-Marquardt algorithm developed and implemented in MatLab[TM] by Gavin (2011). Orazem and Tribollet (2008) provide a description of the Levenberg-Marquardt method for regression to complex numbers.

The stochastic error in the measurements at each frequency $\bar{\sigma}(f_k)^2$ was estimated from the average of the stochastic error of the real (σ_r) and imaginary (σ_j) parts of the measured impedance at frequency f_k. The σ_r and σ_j were estimated following the measurement model approach described in the papers by Agarwal et al. and Orazem et al.(Agarwal, 1992; Agarwal et al., 1995a; Agarwal et al., 1995b; Agarwal et al., 1996; Orazem et al., 1996). Briefly, this involves fitting the impedance data to a simple equivalent circuit model (also known as the measurement model) consisting of an optimal number of R-C circuits in series to five successive impedance spectra by modulus-weighted,

complex non-linear least squares regression using the Measurement Model

Toolbox developed by Orazem (2001). The residual error between the data and

the measurement model cannot be taken as the stochastic error because the

error due to lack of fit could be significant. However, the standard deviation of

the residuals, as expressed by Eq. (4.20), is an estimate of the standard

deviation of the stochastic error as a function of frequency

$$\sigma^2\left(f_k\right) = \frac{1}{N_{scans}-1}\sum_{m=1}^{N_{scans}}\left(\varepsilon_{res,m}\left(f_k\right)-\bar{\varepsilon}_{res}\left(f_k\right)\right)^2 \tag{4.20}$$

where $\bar{\varepsilon}_{res}\left(f_k\right)$ is the mean of the residual errors at frequency f_k for all scans

(N_{scans}) included in the analysis (i.e., $N_{scans} = 5$ in this study) and $\varepsilon_{res,m}(f_k)$ is the

residual error of either the real or imaginary part of the impedance at frequency f_k

of scan m, defined as

$$\varepsilon_{res,m}\left(f_k\right) = Z\left(f_k\right) - \hat{\bar{Z}}_{MM}\left(f_k\right) \tag{4.21}$$

In Eq. (4.21), $Z(f_k)$ is the measured value of the impedance and $\hat{\bar{Z}}_{MM}\left(f_k\right)$ is the

impedance calculated from the measurement model at frequency f_k for the

optimal number of R-C circuits in series.

4.4 Results and Discussion

Using the fraction-damaged model described by Eq. (4.7), the real and

imaginary components of the impedance ($Z_r A$ and $-Z_j A$) as well as $d\log(-Z_j A)/d$

$\log(f)$, were calculated as a function of frequency for input parameter values that

are reasonable for skin. Parameter values for the undamaged skin layer are the

regression results for sample B before treatment with DMSO for 0.25 h that are

presented below: $R_s A = 167.0$ kΩ cm^2, $\alpha_s = 0.682$ and $f_{c,s} = 51$ Hz. Parameter

values for the damaged layer are the mean of regression parameters for three

samples after DMSO treatment that are presented below: $R_d A = 1.36$ kΩ cm^2,

$\alpha_d = 0.81$, $f_{c,d} = 5640$ Hz). The results are shown in the left-hand column of

Figure 4.3 for the relative thickness of the damaged layer (x_d/L) varying from zero

(i.e., no damage) to one (i.e., fully damaged).

When the skin is undamaged ($x_d/L = 0$) or completely damaged ($x_d/L = 1$),

the frequency dependence is consistent with a 1-time-constant model described

by Eq. (4.2). For x_d/L values between 0 and 1 both time constants corresponding

to the undamaged and damaged layers contribute to the total impedance. As

x_d/L increase the relative contribution to the total impedance of the undamaged

layer decreases and the impedance of the damaged layer increases.

An assumption of the fraction-damaged model is that the characteristic

frequencies of both time constants, which for the theoretical curves shown in

Figure 4.3 are 51 Hz for the undamaged layer and 5640 Hz for the damaged

layer, are independent of the fraction damaged. Although the magnitude of the

impedance changes with x_d/L, the characteristic frequency of each layer remains

unchanged. In skin, this is consistent with the relative thicknesses of the

undamaged and damaged skin layers decreasing and increasing, respectively,

while the intrinsic electric properties of each layer (i.e. resistivity and dielectric

constant) of the undamaged and damaged layers remain constant.
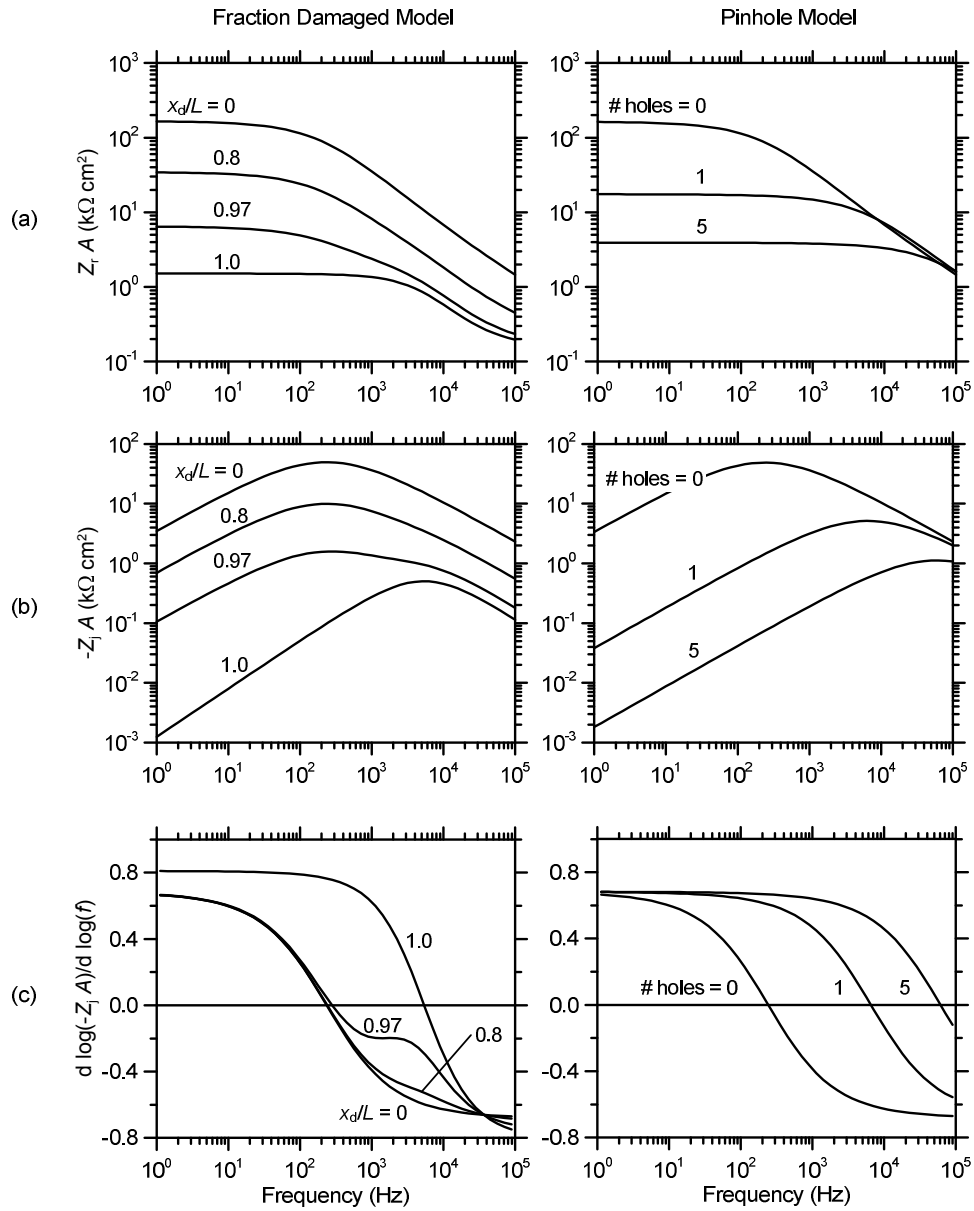
Figure 4.3 Impedance spectra calculated using either the fraction-damaged model for varying x_d/L or the pinhole model for varying numbers of holes. The model parameters are typical of those observed for human skin impedance: $R_s A$ = 167.0 kΩ cm^2, $R_d A$ = 1.36 kΩ cm^2, α_s = 0.682, α_d = 0.81, $f_{c,s}$ = 51 Hz and $f_{c,d}$ = 5640.

In plots of d log($-Z_j A$) / d log(f) versus frequency, impedance features can be identified that are not readily visible in other graphical representations. For example, when x_d/L is greater than zero but not one, the presence of a second

time constant with characteristic frequency at 5640 Hz is apparent in the plots of d log($-Z_j$ A) / d log(f) versus frequency in Figure 3c because inflection points, which are difficult to identify in the $-Z_j$ A or Z_r A plots, appear as local a minimum and maximum at frequencies greater than about 100 Hz.

If skin is partially damaged, neglecting the second time constant can produce estimates for R_s A and C_s / A that are unrealistic. For example, if the impedance spectrum of the fraction-damaged model with x_d/L = 0.8 shown in Figure 4.3 was analyzed using the 1-time-constant model with a characteristic frequency corresponding to the maximum value of $-Z_j$ A (i.e. $f_{c,s}$ = 51 Hz) and R_s A is taken to be Z_r A at the lowest measured frequency (~ 38 kΩ cm^2), then, from Eq. (4.4), the apparent C_s / A would be ~82 nF/cm^2, which is about 4-fold larger than the capacitance estimated for either the damaged or undamaged layers. This arises because Z_r A at the lowest measured frequency includes the resistances from both the damaged and undamaged layer. Thus, by not recognizing that the system consists of two layers, the resistance is estimated to be between that of the damaged and undamaged layers and the capacitance is calculated to be much larger than either the damaged or undamaged layers.

Using the pinhole model described by Eq. (4.12), Z_r A, $-Z_j$ A and d log($-Z_j$ A)/ d log(f) were calculated as a function of frequency with the same skin parameters as used for the undamaged skin layer in the fraction-damaged model described above (R_s A = 167.0 kΩ cm^2, α_s = 0.682, Q_s/A = 41.4 and $f_{c,s}$ = 51 Hz). The results are shown in the right-hand column of Figure 4.3 with the number of holes varying from 0 to 5. Each hole was assumed to not influence the

impedance of the other holes, and it was assumed that adding holes did not change the R-CPE parameters of the skin (i.e., R_s, Q_s and α_s were assumed to be constant). Each hole acted in parallel to the skin resistance with a resistance normalized by the exposed skin area (R_{hole} A) equal to 19.3 kΩ cm^2, which is similar what was seen in the experiments with one hole described below (i.e., subject III). Therefore, the total resistance attributed to the holes (R_{holes}) is the resistance of one hole (R_{hole}) divided by the number of all holes (N_{holes}) as follows

$$R_{holes} = \frac{R_{hole}}{N_{holes}} \tag{4.22}$$

For the pinhole model spectra shown in the right-hand column of Figure 4.3, the total resistance, indicated by Z_r A at low frequency, decreases with increasing number of pinholes while the characteristic frequency, which is the frequency at which the $-Z_j$ A curves are maximized or where d log($-Z_j$ A)/d log(f) equals zero, increases with the number of holes. Increasing the number of pinholes reduces the total resistance of the system causing the time constant to shift to higher frequencies.

4.4.1 DMSO Experiments

Experimental impedance spectra for six skin samples before and after DMSO treatment for either 0.25 h (samples A, B and C) or 1 h (samples D, E and F) are shown side-by-side for easy comparison in Figure 4.4. Graphs of Z_r A, $-Z_j$ A and d log($-Z_j$ A)/ d log(f) plotted as functions of frequency before treatment are shown in the left column. The impedance spectra measured after DMSO

treatment for 0.25 h and 1 h are presented in the middle and right columns,

respectively.
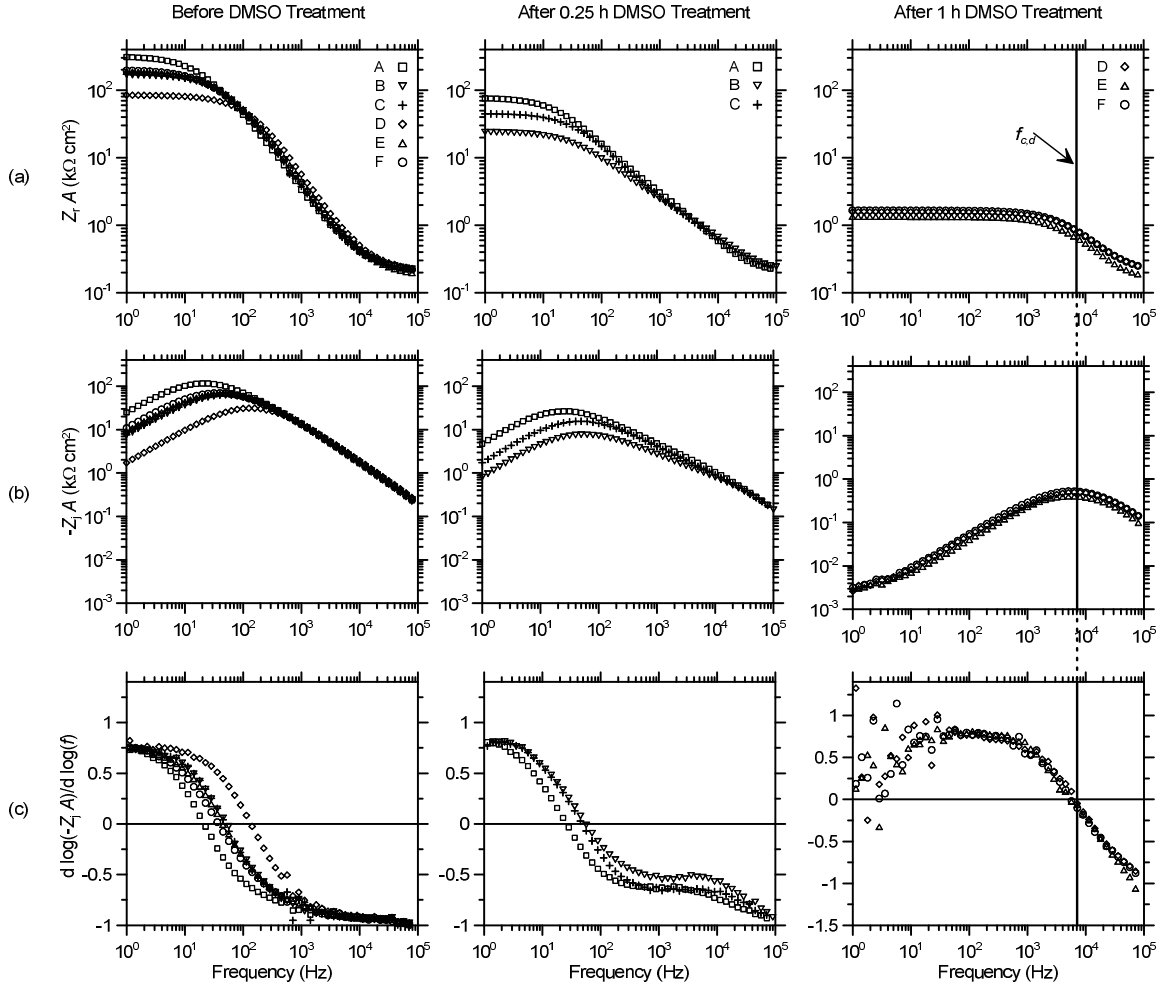
Figure 4.4 Three representations of the impedance plotted as a function of the frequency before and after skin is treated with DMSO for 0.25 and 1 h: (a) area normalized real part of the impedance, (b) area normalized imaginary part of the impedance, and (c) first derivative of the area normalized imaginary part of the impedance.

Comparing the columns of plots shown in Figure 4.4, consistent trends in

the skin impedance response subsequent to DMSO treatment for 0.25 h and 1 h

are evident. On average, $Z_r A$ at low frequency decreases by factors of ~4 and

~100 after 0.25 and 1 h DMSO treatment, respectively, while DMSO treatment at

both times had no effect on the Z_r A at the highest frequencies. Consistent with the theoretical impedance curves for the fraction-damaged model shown in Figure 4.3, the impedance spectra of skin before DMSO treatment and after DMSO treatment for 1 h each exhibit one characteristic frequency as predicted by the 1-time-constant model (corresponding to x_d/L equal to 0 and 1 respectively); while the impedance spectra of the 0.25 h DMSO treated samples behaves as predicted by the 2-time-constant model (i.e. $0 < x_d/L < 1$).

The impedance spectra before DMSO treatment show considerable sample-to-sample variation in the magnitude of the low-frequency impedance and the characteristic frequency, which corresponds to the frequency where $-Z_j$ A is a maximum or equivalently where d log($-Z_j$ A)/d log(f) is equal to zero. Variability is significantly reduced in skin that was treated with DMSO for 1 h. Consistent with this, the data for each of the three samples is in close agreement with the average $f_{c,d}$, indicated by the vertical line through the 1-h DSMO treatment data in Figure 4.4. Even the scatter in the low frequency values of d log($-Z_j$ A)/d log(f) is similar, which almost certainly arises because the magnitude of $-Z_j$ A is small enough to be affected by instrument noise.

The time-course impedance results for four skin samples after DMSO treatment for 0.25, 0.5, 0.75 and 1 h (samples G, H, I and J, respectively) are shown in Figure 4.5. The Z_r A, $-Z_j$ A and d log($-Z_j$ A) / d log (f) spectra for the two skin samples treated with DMSO for 0.25 and 1 h are consistent with the impedance spectra of the samples treated for the same times shown in Figure 4.4. Similar to the theoretical curves of the fraction-damaged model shown in

Figure 4.3, the magnitude of the skin impedance decreases with longer DMSO

treatment times and the samples treated with DMSO for less than 1 h have

frequency dependence consistent with the 2-time-constant model.
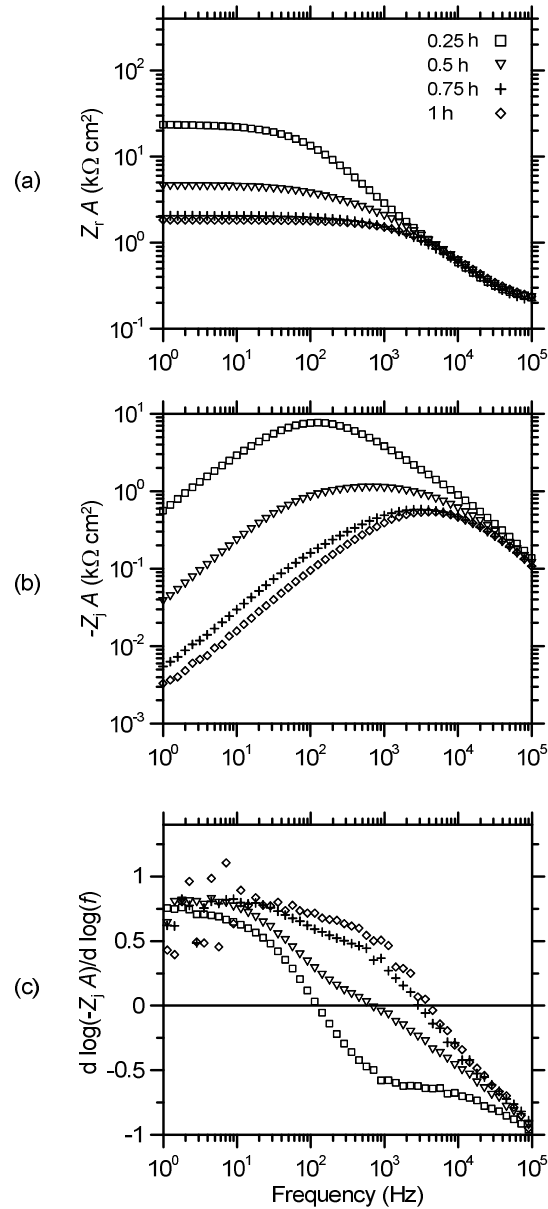
Figure 4.5 Impedance spectra after skin samples were treated with DMSO for 0.25, 0.5, 0.75 and 1 h, which corresponds to experiments G, H, I and J, respectively: (a) area normalized real part of the impedance, (b) area normalized imaginary part of the impedance, and (c) first derivative of the area normalized imaginary part of the impedance.

After 0.5 h DMSO treatment, the two convoluted time constants appear as a broad peak in the $-Z_j\,A$ spectrum. The presence of two time constants for this sample is more apparent in the d log($-Z_j\,A$) / d log (f) plot in Figure 4.5c, where the two time constants are evident by the change in slope of the d log($-Z_j\,A$) / d log (f) curve between 100 and 200 Hz.

After DMSO treatment for 0.75 h, the impedance response is consistent with a nearly completely damaged skin layer with a dominant time constant at high frequency similar to the 1 h DMSO damaged skin. There is a slight contribution from the undamaged layer at lower frequencies that is evident by the deviation of the $-Z_j\,A$ spectrum from the spectrum after 1 h DMSO treatment.

Skin impedance data were regressed to the equivalent circuit models described above to give the results reported in Tables 4.1 - 4.3. Parameters of the 1-time-constant model regressed to the skin impedance data before and after 0.25 h and 1 h treatments with either PBS or DMSO are listed in Table 4.1. The mean values (n = 3) of the regression parameters after 0.25 h PBS, 1 h PBS and 1 h DMSO treatments are given in Table 4.2 and compared to the mean values of skin before all treatments (n = 12). The parameters of the 2-time-constant model regressed to skin impedance spectra for the three samples treated with DMSO for 0.25 h are listed in Table 4.3 along with the mean and standard deviation of the parameter values. Meaningful estimates of the 2-time-constant model parameters could not be determined for skin samples treated with DSMO for 0.5 and 0.75 h because the contribution of the undamaged layer was too small to reliably resolve.

Table 4.1 Parameters of the 1-time-constant model derived by regression to impedance spectra before and after PBS (control) treatments for 0.25 and 1 h and DMSO treatment for 1 h

Treatment	Parameter (units)	Sample ID					
		A_C		B_C		C_C	
		Before	After	Before	After	Before	After
0.25 h PBS	**Regressed parameters[a]**						
	$R_e\,A$ $(k\Omega\,cm^2)$	0.13± 0.40	0.14± 0.42	0.16± 0.099	0.15± 0.09	0.18± 0.043	0.17± 0.028
	$R_s\,A$ $(k\Omega\,cm^2)$	137± 0.8	131.6± 0.8	29.7± 0.1	28.7± 0.1	13.9± 0.1	9.69± 0.04
	α_s	0.859± 0.007	0.863± 0.008	0.894± 0.006	0.884± 0.006	0.918± 0.005	0.900± 0.005
	Q_s/A $((nF\,s^\alpha)/cm^2)$	41.9± 1.8	44.3± 2.1	35.2± 1.8	40.4± 2.0	27.9± 1.3	36.0± 1.5
	Calculated parameters[b]						
	C_s/A (nF/cm^2)	17.9± 0.3	19.5± 0.3	15.5± 0.2	16.6± 0.2	13.9± 0.2	14.9± 0.2
	$f_{c,s}$ (Hz)	65± 2	62± 1	345± 5	347± 5	823± 10	1106± 12
		D_C		E_C		F_C	
		Before	After	Before	After	Before	After
1 h PBS	**Regressed parameters[a]**						
	$R_e\,A$ $(k\Omega\,cm^2)$	0.09± 0.59	0.11± 0.58	0.17± 0.10	0.17± 0.08	0.13± 0.45	0.14± 0.35
	$R_s\,A$ $(k\Omega\,cm^2)$	297.9± 1.4	258.0± 1.3	25.7± 0.1	21.2± 0.1	116.8± 0.8	105.8± 0.7
	α_s	0.856± 0.005	0.859± 0.006	0.880± 0.007	0.874± 0.007	0.866± 0.009	0.859± 0.008
	Q_s/A $((nF\,s^\alpha)/cm^2)$	37.3± 1.1	41.0± 1.3	35.8± 2.0	40.4± 2.3	41.8± 2.4	48.7± 2.4
	Calculated parameters[b]						
	C_s/A (nF/cm^2)	17.5± 0.2	19.4± 0.2	13.8± 0.2	14.6± 0.2	18.3± 0.3	20.6± 0.3
	$f_{c,s}$ (Hz)	30.5± 0.3	32.8± 0.4	448± 7	514± 8	74± 1	73± 1

Table 4.1 Continued

		Sample ID					
		A		B		C	
Treatment	Parameter (units)	Before	After	Before	After	Before	After
0.25 h DMSO	**Regressed parameters[a]**						
	$R_e A$ (kΩ cm^2)	0.14±0.59	0.12±0.13	0.15±0.46	0.12±0.10	0.16±0.53	0.15±0.10
	$R_s A$ (kΩ cm^2)	313.3±1.5	80.6±0.4	167.0±0.9	25.9±0.2	169±1	47.2±0.2
	α_s	0.85±0.01	0.72±0.01	0.682±0.007	0.64±0.01	0.879±0.008	0.72±0.01
	Q_s / A ((nF s$^{\alpha}$)/cm^2)	47.7±1.3	308±7	41.4±1.67	874±44	37±2	346±10
	Calculated parameters[b]						
	C_s / A (nF/cm^2)	22.81±0.23	75.4±0.8	18.7±0.3	108±3	18.4±0.3	72±1
	$f_{c,s}$ (Hz)	22±2	26±1	51.0±0.7	57±1.5	50.9±0.8	47±1
		D		E		F	
Treatment	Parameter (units)	Before	After	Before	After	Before	After
1 h DMSO[c]	**Regressed parameters[a]**						
	$R_e A$ (kΩ cm^2)	0.16±0.28	0.185±0.004	0.11±0.89	0.146±0.006	0.14±0.67	0.190±0.004
	$R_s A$ (kΩ cm^2)	83.4±0.4	1.396±0.004	181.6±1.8	1.194±0.007	193.9±1.5	1.480±0.004
	α_s	0.875±0.007	0.807±0.003	0.87±0.012	0.809±0.005	0.857±0.009	0.810±0.003
	Q_s / A ((nF s$^{\alpha}$)/cm^2)	33.4±1.6	143±5	34.7±2.5	190±10	45.6±2.3	140±4
	Calculated parameters[b]						
	C_s / A (nF/cm^2)	14.4±0.2	18.7±0.2	16.4±0.4	25.3±0.4	20.7±0.4	19.4±0.1
	$f_{c,s}$ (Hz)	133±2	6089 59	54 1	5263 87	40 1	5553 45

Table 4.1 Continued

<hr>

[a] Values are reported as the regressed parameters ± the standard parameter error.
[b] Values are reported as the calculated parameter ± the error estimated by propagation of the standard parameter error on the
regressed parameters contained in the calculated parameter (Orazem and Tribollet, 2008).
[c] Parameter values after DMSO treatment for 1 h represent damaged skin.

Table 4.2 Mean values of the parameters of the 1- time-constant model derived by regression to impedance spectra measured before and after PBS (control) treatments for 0.25 and 1 h and DMSO treatment for 1 h compared to mean values before all treatments

Parameter (units)		Treatment[a]						All treatments[b]
		0.25 h PBS		1 h PBS		1 h DMSO		
		Before	After	Before	After	Before	After[c]	Before
Regressed parameters								
$R_e A$	$(k\Omega\ cm^2)$	0.16± 0.03	0.15± 0.02	0.13± 0.04	0.14± 0.03	0.14± 0.03	0.17± 0.02	0.14± 0.03
$R_s A$	$(k\Omega\ cm^2)$	60± 67	57± 66	147± 139	128± 120	153± 61	1.36± 0.15	120± 94
α_s		0.89± 0.03	0.88± 0.02	0.87± 0.01	0.86± 0.01	0.87± 0.01	0.81± 0.01	0.87± 0.02
Q_s / A	$((nF\ s^{\alpha})/cm^2)$	35± 7	40± 4	38± 3.	43± 5	38± 7	158± 28	38± 6
Calculated parameters								
C_s / A	(nF/cm^2)	16± 2	17± 2	17± 2	18± 3	17± 3	21± 3	17± 3
$f_{c,s}$	(Hz)	411± 383	505± 540	184± 230	207± 277	76± 50	5640± 420	178± 244

[a] Mean ± one standard deviation of values determined in 3 skin samples for each treatment
[b] Mean ± one standard deviation of values determined in 12 skin samples before all treatments; i.e., 0.25 h and 1 h treatments with PBS and with DMSO
[c] Parameter values after DMSO treatment for 1 h represent damaged skin.

Table 4.3 Parameters of the 2-time-constant model derived by regression to impedance spectra from skin after DMSO treatment for 0.25 h

	Parameter	Units	Sample ID			All Samples[a]	
			A	B	C	Mean	Std dev
Undamaged layer	**Regressed parameters[b]**						
	$R_e A$	$k\Omega$ cm^2	0.16± 0.07	0.18 ± 0.07	0.17± 0.06	0.17	0.06
	$\hat{R}_s A$	$k\Omega$ cm^2	76.9± 0.3	24.0 ± 0.2	45.4± 0.2	48.8	39.3
	α_s	unitless	0.77± 0.01	0.72 ± 0.01	0.77± 0.01	0.75	0.43
	$\hat{Q}_s / A$	(nF s$^\alpha$)/cm^2	252± 3	583 ± 12	273± 3	369	291
	Calculated parameters[c]						
	$\hat{C}_s / A$ [b]	nF/cm^2	77.6± 1.0	111 ± 3.5	71.5± 1.1	86.6	23.4
	$f_{c,s}$	Hz	27± 0.3	60 ± 2	49± 1	45	24
Damaged layer	**Regressed parameters[b]**						
	$\hat{R}_d A$	$k\Omega$ cm^2	1.62± 0.25	0.72 ± 0.18	0.56± 0.16	0.97	0.74
	α_d	unitless	0.90± 0.09	0.89 ± 0.16	0.91± 0.20	0.9	0.40
	$\hat{Q}_d / A$	(nF s$^\alpha$)/cm^2	142± 118	125 ± 189	151± 286	139	88
	Calculated parameters[c]						
	$\hat{C}_d / A$	nF/cm^2	55± 62	39 ± 81	57± 151	50	11
	$f_{c,d}$	Hz	1790± 2040	5670 ± 11900	4990± 13200	4150	2750

[a] Values are reported as the mean ± one standard deviation of the parameter values for all three samples.
[b] Values are reported as the regressed parameters ± the standard parameter error
[c] Values are reported as the calculated parameter ± the error estimated by propagation of the standard parameter error on the regressed parameters contained in the calculated parameter (Orazem and Tribollet, 2008)

In these tables regressed parameters are reported plus or minus the standard error. Values of the characteristic frequency and effective capacitance calculated from the regressed parameters are reported with errors estimated by propagation of the standard error through the calculation. Except for $\hat{Q}_d / A$, all values of the regressed parameters listed in Table 4.3 were determined with a high degree of confidence as indicated by the small errors. The inability to resolve $\hat{Q}_d / A$ with more certainty is likely due to the convolution of the small-impedance damaged layer with the large-impedance undamaged layer. The large uncertainty of $\hat{Q}_d / A$ is reflected in large estimated errors for the calculated values of $\hat{C}_d / A$ and $f_{c,d}$.

Models and impedance data are compared in Figure 4.6 for samples B and E before and after DMSO treatment. The results for both skin samples before treatment are shown in the left column. The results after treatment for 0.25 h (sample B) and 1 h (sample E) are presented in the middle and right columns, respectively. The solid lines in Figure 4.6 represent the total impedance calculated using the regressed models to the data. The dot-dashed lines and dashed lines in the center column represent the impedance calculated for each R-CPE element of the 2-time-constant model corresponding to the undamaged and damaged skin layers. The diamonds in the impedance plane plots of Figure 4.6c represent the characteristic frequencies of the models. For skin treated with DMSO for 0.25 h, the characteristic frequencies of the undamaged and damaged layers are highlighted for both the total impedance and for the impedance of each element.
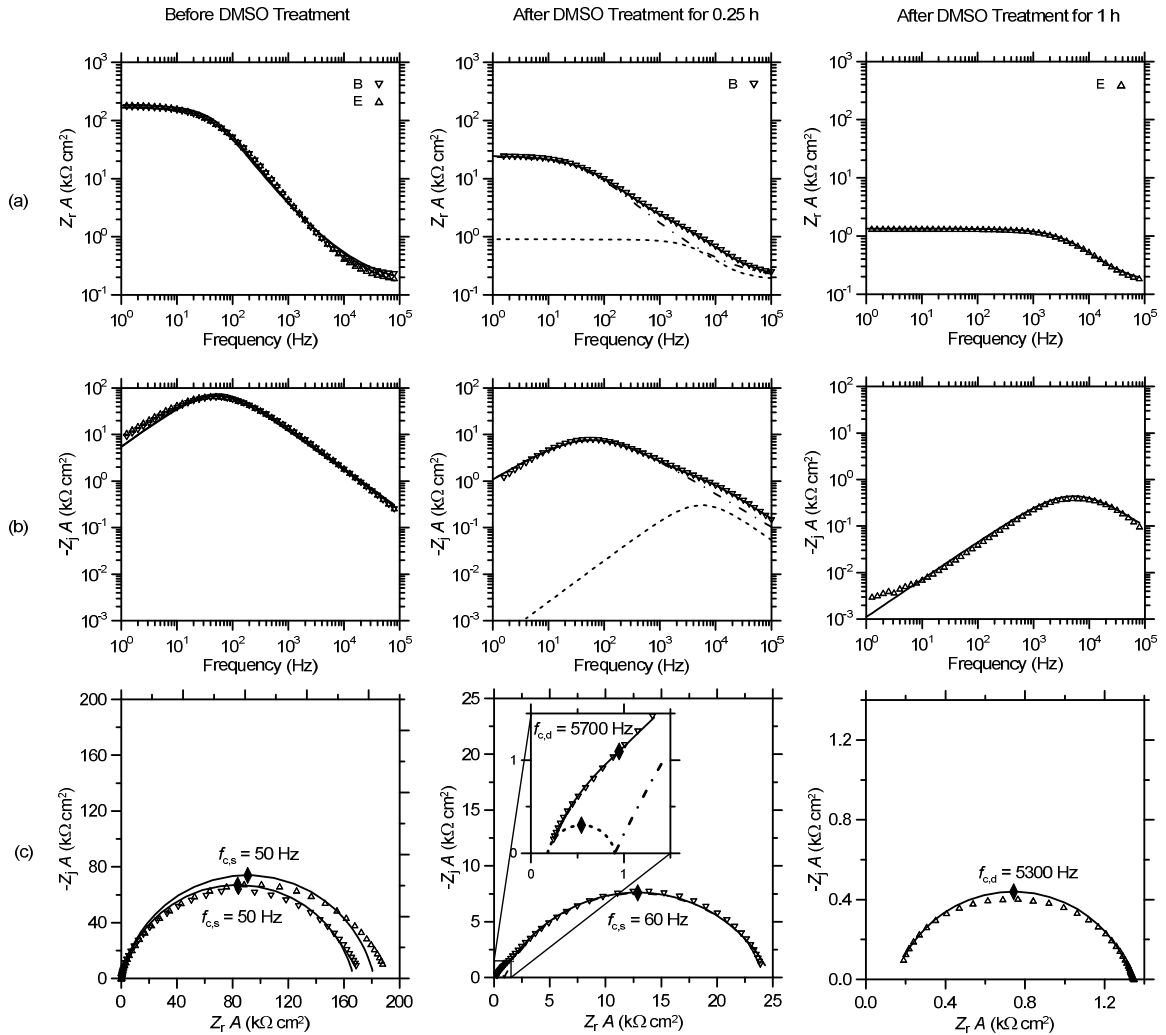
Figure 4.6 Example impedance spectra of skin before and after DMSO treatment for 0.25 h and 1 h compared to equivalent circuit models: (a) area normalized real part of the impedance, (b) area normalized imaginary part of the impedance, and (c) impedance plane (Nyquist) plot with characteristic frequencies noted. The solid lines represent the total impedance derived by regression of the 1-time-constant model to data measured before DMSO and after DMSO treatment for 1 h, and regression of the 2-time-constant model to the data measured after DMSO treatment for 0.25 h. The dot-dashed lines and the dashed lines represent respectively the impedance of the undamaged and damaged skin fractions after DMSO treatment for 0.25 hr.

Before DMSO treatment, the impedance spectra of the two skin samples

were nearly identical, with small differences that are primarily visible in the

impedance plane plot (Figure 4.6c). Although the maximum values of $Z_r A$,

139

determined at the lowest measured frequency, are noticeably different for the two samples in Figure 4.6c, the characteristic frequencies are the same, indicating that the effective capacitances were slightly different.

After 0.25 h DMSO treatment, the impedance of the damaged layer, represented by the dashed lines, contributes little to the total impedance for frequencies below ~1000 Hz. However, it is interesting to note that the shape and magnitude of the impedance response of the damaged layer is similar to that of the skin treated with DMSO for 1 h shown in the right column.

The data for skin treated with DMSO for 1 h are in good agreement with the 1-time-constant model except for $-Z_j\,A$ measured at frequencies below about 5 Hz. A similar behavior has been observed in spectra from other samples that are not shown here. Data over the entire spectrum were shown to be consistent with the Kramers-Kronig relations using the measurement model method described by Agarwal et al. (Agarwal, 1992; Agarwal et al., 1995a; Agarwal et al., 1995b; Agarwal et al., 1996). Therefore, the deviation between model and data is most probably not an experimental artifact and a different model is required to capture the low frequency dispersion observed in these samples.

The d log($-Z_j\,A$)/d log(f) spectra of samples B and E after DMSO treatment are shown in Figure 4.7 with lines representing the 2-time-constant and 1-time constant models, respectively. When the data are presented this way, the similarity in the $f_{c,d}$ values for both treatment times is evident.

If the impedance response of the 0.25 h DMSO treated skin is consistent with the fraction-damaged model given by Eq. (4.7), then the characteristic

frequency estimated for the undamaged skin layer ($f_{c,s}$) should be similar to skin

before DMSO treatment as well as to skin in the control experiments that was

treated with PBS.
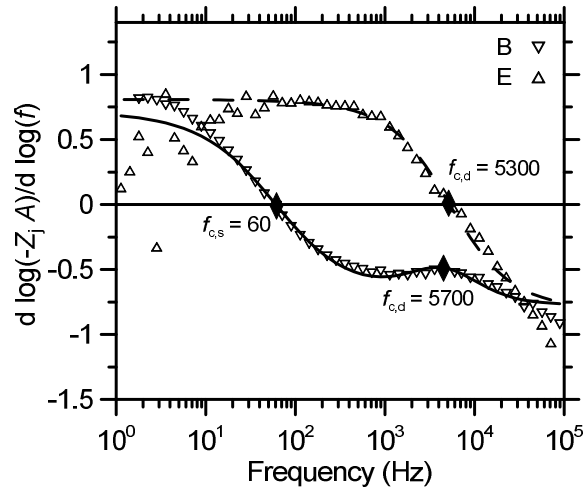
Figure 4.7 The first derivative of the logarithm of ($-Z_j\,A$) with respect to the logarithm of frequency plotted as a function of the average frequency for skin that has been treated with DMSO for 0.25 and 1 h compared respectively to the 2-time-constant (solid lines) and the 1-time-constant (dashed lines) models.

Likewise, the characteristic frequency estimated for the damaged layer ($f_{c,d}$)

should be similar to $f_{c,d}$ for skin treated with DMSO for 1 h. The mean value of $f_{c,s}$

for samples A, B and C after 0.25 h DMSO treatment, listed in Table 4.3, is

statistically indistinguishable from the mean value of $f_{c,s}$ for the same three

samples before 0.25 h DMSO treatment listed in Table 4.2 (paired student t-test,

$p < 0.05$). Also, the mean value of $f_{c,s}$ for samples A, B and C after 0.25 h DMSO

treatment is statistically indistinguishable from the mean $f_{c,s}$ for all 12 samples

before DMSO and PBS treatment, which is listed in Table 4.2 (2 sample student

t-test, $p < 0.05$). Furthermore, the mean value of $f_{c,d}$ for samples A, B and C after

0.25 h DMSO treatment, listed in Table 4.3, is statistically indistinguishable from

the mean value of $f_{c,d}$ values samples D, E and F after 1 h DMSO treatment (student t-test, $p < 0.05$).

In Figure 4.8 the characteristic frequencies are compared graphically as the ratios of $f_{c,s}$ and $f_{c,d}$ after treatment to $f_{c,s}$ before treatment (i.e., $f_{c,s}/f_{c,s\ before}$ and $f_{c,d}/f_{c,s\ before}$) for 0.25 h and 1 h treatments with either DMSO or PBS. The dashed line, plotted on the left-hand axis at 1.1, represents the mean value of $f_{c,s}/f_{c,s\ before}$ for the six PBS control experiments; the solid line, the mean value of 94 for $f_{c,d}/f_{c,s\ before}$ from the three skin samples treated with DMSO for 1 h plotted on the right-hand axis. Consistent with the assumption of the fraction-damaged model, the after-to-before ratios of the characteristic frequencies for the undamaged and damaged layers of skin treated with DMSO for 0.25 h are similar to the ratios observed after treatment with PBS at both treatment times and with DMSO for 1 h, respectively.

Values for x_d/L for skin treated with DMSO for 0.25 h were estimated by requiring that the resistances of the two skin layers sum to give the total resistance observed experimentally as specified by Eq. (4.23):

$$\hat{R}_s + \hat{R}_d = R_s\left(1 - x_d/L\right) + R_d\, x_d/L \tag{4.23}$$

which after rearrangement gives

$$x_d/L = \frac{R_s - \left(\hat{R}_s + \hat{R}_d\right)}{R_s - R_d} \tag{4.24}$$

In addition, it was assumed that: (a) $R_d\, A$ is equal to the mean value of the resistance measured in skin treated with DMSO for 1 h, and (b) $R_s\, A$ is equal to the resistance determined in the same piece of skin before treatment multiplied

by 0.86, which was the average change in $R_s A$ observed in treatment with PBS

for 0.25 and 1 h combined (no difference was observed in 0.25 h compared to

1 h).
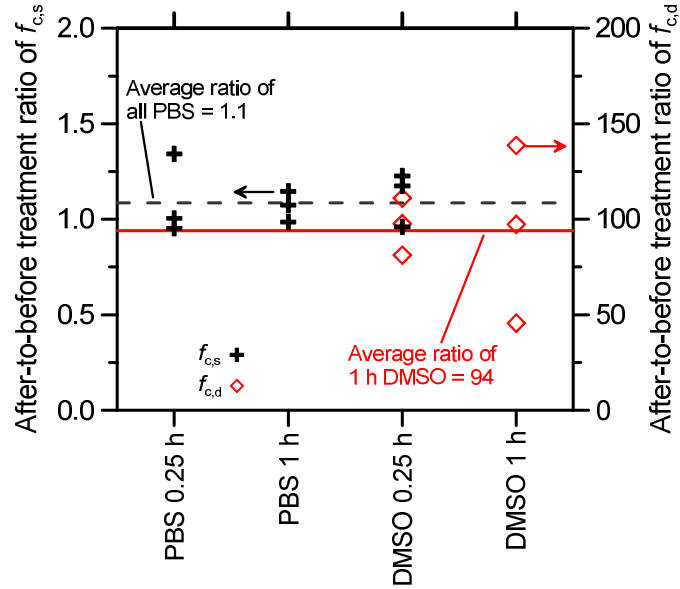
Figure 4.8 The after-to-before treatment ratio of the characteristic frequencies estimated for the undamaged and damaged layers of skin treated with DMSO for 0.25 h compared to skin treated with PBS and with DMSO for 1 h. The dashed line indicates the mean value of the ratio for all of the PBS control experiments ($f_{c,s}/f_{c,s\,before}$ = 1.1), and the solid line represents the mean value of the ratio for skin treated with DMSO for 1 h DMSO experiments ($f_{c,d}/f_{c,s\,before}$ = 94).

Calculated values for x_d/L as well as the length-independent values for the

area normalized capacitance for three samples treated with DMSO for 0.25 h are

summarized in Table 4.4. Interestingly, the mean C_s / A estimated for the

undamaged layer (21 ± 2 nF/cm^2) is the same as before DMSO treatment (20 ± 2

nF/cm^2). For the damaged layer, the mean C_s / A, increased by a factor of about

2 (37 ± 4 nF/cm^2), which could be consistent with increased lipid disorder or a

change in the dielectric property towards a less lipophilic character.

143

Table 4.4 Estimated values for the fraction damaged (x_d/L) and model parameters of the damaged and undamaged skin layers for skin treated with DMSO for 0.25 h

	Parameter	Units	Sample ID A Before[a]	After[b]	B Before[a]	After[b]	C Before[a]	After[b]	All samples Before[c]	After[c]
Damaged layer	$R_e\,A$	$k\Omega\ cm^2$	0.14	0.16	0.15	0.18	0.16	0.17	0.15± 0.01	0.17± 0.01
	x_d/L			0.71		0.83		0.69		0.74± 0.076
	$R_d\,A$	$k\Omega\ cm^2$		2.3		0.9		0.8		1.3± 0.8
	$C_d\,/\,A$	nF/cm^2		39		32		39		37± 4
	α_d			0.90		0.89		0.91		0.90± 0.01
	$Q_d\,/\,A$	$(nF\ s^\alpha)/cm^2$		101		104		103		103± 2
	$f_{c,d}$	Hz		1790		5670		4990		4150± 2070
Undamaged layer	$R_s\,A$	$k\Omega\ cm^2$	313	269	167	144	169	145	216± 84	186± 72
	$C_s\,/\,A$	nF/cm^2	23	22	19	18	19	22	20± 2	21± 2
	α_s		0.85	0.77	0.86	0.72	0.88	0.77	0.86± 0.02	0.75± 0.03
	$Q_s\,/\,A$	$(nF\ s^\alpha)/cm^2$	48	72	41	97	37	85	42± 6	84.7± 12.5
	$f_{c,s}$	Hz	22	27	51	60	51	49	41± 17	45± 17

[a] Calculated using the 1-time constant model.
[b] Calculated parameters, normalized for the fraction damaged, for skin after DMSO treatment assuming $R_s/R_{s,before} = 0.86$
[c] Values are reported as mean ± one standard deviation of values determined in 3 skin samples

Values of x_d/L were estimated for the 0.25, 0.5 and 0.75 h treatments with DSMO from the time-course study using Eq. (4.24) where the high frequency determinations of Z_r were used as estimates R_s and $\hat{R}_s + \hat{R}_d$ before and after DMSO respectively. Estimates of $R_s A$ before DMSO and $(\hat{R}_s + \hat{R}_d) A$ after DMSO treatment for 0.25, 0.5 and 0.75 are listed in Table 4.5. The x_d/L for the time-course study and the three other skin samples treated with DMSO for 0.25 h listed in Table 4.4 are shown as a function of the square-root of the DMSO treatment time in Figure 4.9.

Table 4.5 Estimates of the area normalized total skin resistance before and after DMSO treatment for the time-course study[a]

Treatment time	Before DMSO	After DMSO
	$R_s A$	$\left(\hat{R}_s + \hat{R}_d\right) A$
h	$(k\Omega\ cm^2)$	$(k\Omega\ cm^2)$
0.25	114.0	23.4
0.50	185.7	4.34
0.75	340.7	1.87

[a] Values determined from $Z_r A$ measured at low frequency.

As discussed earlier, x_d/L was essentially 1 for the sample treated with DMSO for 0.75 h. As expected for a diffusion process, the plot of x_d/L from the time-course study versus the square-root of time forced through the origin is linear. The slope of the line through the intercept is 1.5 $h^{-1/2}$, from which it can be

estimated that x_d/L should be equal to one for treatment times longer than about 0.5 h.
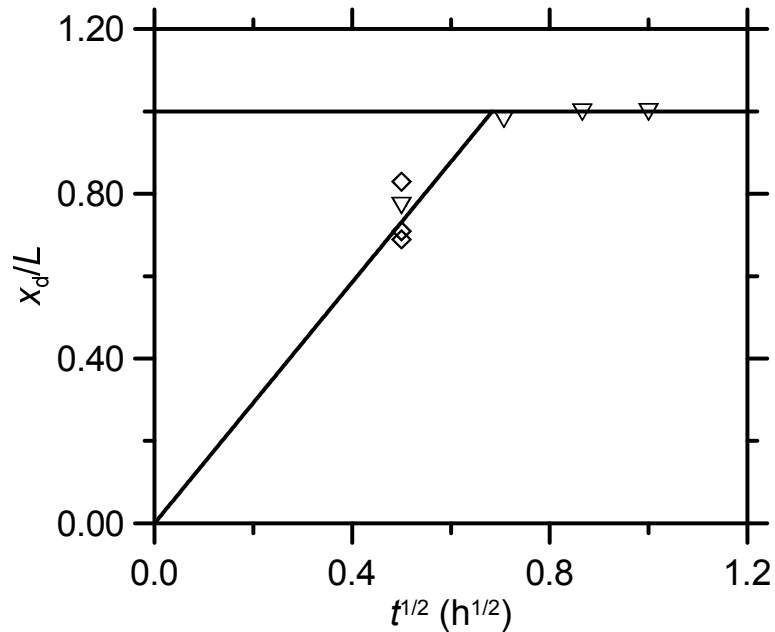
Figure 4.9 The fraction damaged plotted as a function of the square root of treatment time for the time-course study (triangles) and the 0.25 h DMSO experiments listed in Table 4.4 (diamonds).

To estimate the lag time for the growth of the damaged layer requires an assumption about the smallest DMSO concentration relative to the maximum that causes an irreversible change in the electrical properties of the stratum corneum (see Appendix). For example, the lag time of the growth in the damaged layer thickness is almost 6 minutes if the concentration of DMSO in the damaged layer must be at least 50% of the maximum. For comparison, estimates for the lag time increase to about 25 minutes if the DMSO concentration needs to be at least 75% of the maximum, and decreases to 2 minutes if the concentration only needs to be 25% of the maximum.

The steady-state flux of PCNB through skin measured before and after treatments with DMSO and PBS treatment for 0.25 h and 1 h are reported in Table 4.6. The change in PCNB flux after treatment is also listed. The flux increased after treatment for all samples except for one sample treated with PBS for 0.25 h and one sample treated with PBS for 1 h. The average change in flux after DMSO treatment for 1 h was insignificantly larger than the average change in flux after DMSO treatment for 0.25 h and PBS treatment for 0.25 h and 1 h (student t-test, $p < 0.05$). Neither treatment time nor treatment type had a discernable effect on PCNB flux through skin. Thus, although the impedance of skin decreased significantly when treated with DMSO, and the change was larger after 1 h compared to 0.25 h, the flux of PCNB did not change significantly after DMSO treatment for either 0.25 h or 1 h compared to the PBS control experiments. This differed from the time course study in which the ratio of the flux of CP after to before DMSO treatment did increase with increasing treatment time from almost 2 at 0.25 h to about 4 at 1 h. However, it is difficult to know if these differences would have been significant if the experiment had been replicated.

4.4.2 Pinhole Experiments

Values of the parameters determined by regression to the pinhole model are listed in Table 4.7 for seven skin samples from two subjects before and after pinhole. For all samples, the impedance response of the skin, both before and after pinhole, is adequately represented by the 1-time-constant model as illustrated by the $Z_r A$ and $-Z_j A$ spectra, and the impedance plane plot shown for

sample IV in Figure 4.10. The regression parameters for the control experiment,

in which the skin was treated in the same way as the other samples except that it

was not punctured, are reported in Table 4.8.

Table 4.6 Comparing the steady-state flux of PCNB ($\mu g/cm^2/h$) measured before and after treatments with DMSO and PBS (control) for 0.25 and 1 h

Treatment time (h)	Sample ID	DMSO treatment			PBS Control		
		Before	After	Change[a]	Before	After	Change
0.25	A	4.65	6.24	1.60	7.08	8.81	1.73
	B	5.31	5.46	0.15	5.96	4.69	-1.27
	C	3.69	4.33	0.64	5.35	5.42	0.07
	Mean[b,c]	4.55+	5.34	0.80	6.13*	6.31	0.18
	Std dev[d]	0.81	0.96	0.74	0.88	2.20	1.50
1	D	4.14	5.55	1.41	5.71	6.87	1.16
	E	7.46	8.49	1.03	5.09	4.52	-0.57
	F	2.54	3.44	0.90	3.77	3.82	0.05
	Mean[c]	4.71	5.83	1.11	4.86	5.07	0.21
	Std dev[d]	2.51	2.53	0.27	0.99	1.60	0.88

[a] Defined as the value after treatment minus the value before treatment
[b] Comparing the flux before, the flux after, or the change in flux for a given treatment (either DSMO or PBS control); only the flux values before 0.25 and 1 h PBS control treatments were significantly different from each other.
[c] Comparing the flux before, the flux after, or the change in flux for a given treatment time (either 0.25 or 1 h); only the flux values before the 0.25 h treatment with DMSO were statistically significantly different from the PBS control.
[d] Comparing the flux before, the flux after, or the change in flux, the variance for treatment times and treatment types are not statistically different from each other according to single-factor ANOVA.

Because the needle used to puncture the skin was small compared to the

total skin area, the pinhole was expected to have little effect on the impedance

properties of the remaining skin. From the control experimental results, it was

confirmed that the electrical properties of skin did not change during the other

skin handling steps. Therefore, the resistance and the dielectric constant for the

skin were assumed to be the same before and after pinhole. Assuming that a pinhole adds a low frequency shunt resistance (i.e. R_{hole}) in parallel with the skin, the values of R_{hole} listed in Table 4.7 were calculated by rearrangement of Eq. (4.13) assuming $R_s A$ was equal to the before pinhole value.

The resistance of a hole through a membrane (R_{hole}) is related to the solution resistivity (ρ), the hole diameter (d_{hole}) and the length of the hole (L_{hole}) as described by Eq. (4.25).

$$R_{hole} = \frac{\rho}{2d_{hole}} + \frac{4L_{hole}\rho}{\pi d_{hole}^2} \tag{4.25}$$

where the first term on the right hand side of Eq. (4.25) represents the constriction of the flux lines from a semi-infinite bulk electrolyte solution to the hole, and the second term represents the resistance of the electrolyte solution in the hole assuming the surrounding skin is impermeable to ions (Carslaw and Jaeger, 1959). Assuming the length of the hole is the total thickness of the skin sample (i.e., approximately 350 μm for the split-thickness skin used in this study) and that it is completely filled with PBS solution, d_{hole} for the pinhole in each sample was estimated from R_{hole} using the measured resistivity of PBS solution ($\rho = 54.9 \ \Omega$ cm). The results are listed in Table 4.7. The average resistance of the pinholes in 7 skin samples corresponds 180 μm for d_{hole} (range from 126 to 241 μm). If the hole resistance of 19.76 kΩ (sample II) is discarded as an outlier, then the average value for R_{hole} is 10.25 $\pm$ 2.80 kΩ, which corresponds to 189 μm for d_{hole} (range from 150 μm to 241 μm).

Table 4.7 Parameter values of the 1-time-constant model regressed to skin data before and after pinhole and estimates of the pinhole resistance and diameter

Parameter	Units	Sample ID[a] I Before	I After	II Before	II After	III Before	III After	IV Before	IV After
Regressed parameters[b]									
$R_t\,A$	$k\Omega\ cm^2$	141.8±0.2	9.94±0.01	93.6±0.1	24.07±0.03	93.4±0.1	15.96±0.02	55.2±0.1	11.78±0.01
α_s	unitless	0.81±0.002	0.82±0.002	0.82±0.01	0.82±0.003	0.79±0.01	0.82±0.003	0.83±0.01	0.83±0.002
$Q_s\,/\,A$	$nF\ s^{\alpha}/cm^2$	79.8±1.0	67.7±1.5	68.5±1.3	73.5±1.4	99.7±1.1	83.0±1.4	66.5±1.4	63.7±1.1
Calculated parameters[c]									
$R_s\,A$[d]	$k\Omega\ cm^2$	141.8±0.2	141.8 0.2	93.6±0.1	93.6 0.1	93.4±0.1	93.4 0.1	55.2±0.1	55.2 0.1
$C_s\,/\,A$	nF/cm^2	27.4±0.1	14.3 0.8	23.1±0.2	18.2 1.3	28.8±0.1	18.9 1.1	20.5±0.1	14.4 0.8
$R_{hole}\,A$[e]	$k\Omega\ cm^2$		10.7±0.01		32.4±0.07		19.3±0.03		15.0±0.02
R_{hole}	$k\Omega$		6.48±0.01		19.76±0.04		11.67±0.02		8.14±0.01
d_{hole}[f]	μm		241		126		170		210

Table 4.7 Continued

Parameter	Units	Sample ID[a] V Before	V After	VI Before	VI After	VII Before	VII After	All samples[f] Before	All samples After
Regressed parameters[b]									
$R_t A$	kΩ cm²	179±0.3	15.63±0.02	192±0.3	21.20±0.04	69.2±0.1	14.88±0.02	118±54	16.21±4.96
α_s	unitless	0.83±0.01	0.85±0.003	0.81±0.01	0.84±0.004	0.82±0.01	0.83±0.003	0.8±0.01	0.83±0.01
Q_s / A	nF s$^\alpha$/cm²	61.8±1.2	51.3±0.9	70.5±1.2	57.3±1.3	74.3±1.7	69.5±1.3	74.4±12.5	66.6±10.5
Calculated parameters[c]									
$R_s A$[d]	kΩ cm²	179±0.3	179±0.3	192±0.3	192±0.3	69.2±0.1	69.2±0.1	118±54	118±54
C_s / A	nF/cm²	23.8±0.2	14.1±0.9	26.4±0.2	15.7±1.3	23.6±0.2	16.5±1.3	24.8±2.9	16.0±1.9
$R_{hole} A$[e]	kΩ cm²		17.1±0.02		23.8±0.05		19.0±0.03		19.6±6.9
R_{hole}	(kΩ)		10.38±0.01		14.54±0.03		10.30±0.02		11.6±4.4
$f_{c,t}$	Hz	37±1.0	721±0.9	31±0	477±0.8	98±1	648±0.8	68.7±39.4	685±266
d_{hole}[f]	μm		182		150		183		180±35

[a] Samples I to IV are from subject Q; samples V to VII are from subject AS
[b] Values are reported as the regressed parameters ± the standard parameter error
[c] Values are reported as the calculated parameter ± the error estimated by propagation of the standard parameter error on the regressed parameters contained in the calculated parameter (Orazem and Tribollet, 2008).
[d] $R_s A$ before and after the pinhole is assumed to be unchanged for purposes of calculating R_{hole}.
[e] $R_{hole} A$ is calculated from $R_t A$ and $R_s A$ according to Eq. (4.13)
[f] Hole diameter was estimated using Eq. (4.25).
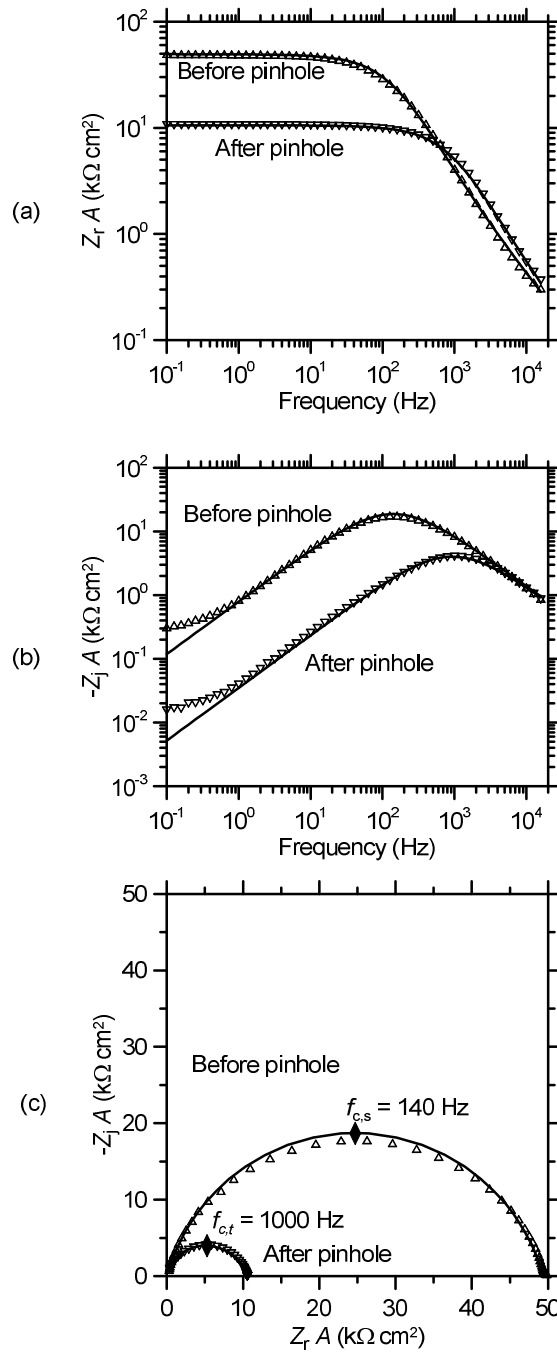
Figure 4.10 Typical impedance spectra measured before (point-up triangles) and after (point-down triangles) pinhole (subject IV): (a) area normalized real part of the impedance, (b) area normalized imaginary part of the impedance, and (c) impedance plane (Nyquist) plot with characteristic frequencies noted with diamonds.

Table 4.8 Parameter values of the 1-time-constant model regressed to skin data for the control sample in the pinhole experiment[a]

Parameter	Units	Before	After
Regressed parameters[b]			
$R_t A$	$k\Omega\ cm^2$	103.2± 0.2	102.6± 0.16
α_s	Unitless	0.80± 0.002	0.81± 0.002
Q_s / A	$nF\ s^{\alpha}/cm^2$	85.6± 1	83± 1
Calculated parameters[c]			
$R_s A$	$k\Omega\ cm^2$	103.2± 0.2	102.6± 0.2
C_s / A	nF/cm^2	26.6± 0.1	26.5± 0.8
$R_{hole} A$	$k\Omega\ cm^2$		
$f_{c,t}$	Hz	58± 0.1	58± 0.1

[a] Skin sample from subject Q was treated the same as all other skin samples in the pinhole experiment but without puncturing a hole.
[b] Values are reported as the regressed parameters ± the standard parameter error
[c] Values are reported as the calculated parameter ± the error estimated by propagation of the standard parameter error on the regressed parameters contained in the calculated parameter (Orazem and Tribollet, 2008)

Overall, these estimates for d_{hole} are a little smaller than half of the needle

diameter (464 μm). This is not surprising since the hole left by pushing a needle

through the skin will certainly be smaller than the needle diameter. Also, if the

hole is not completely filled with PBS, then the resistivity of the material in the

hole would be larger than for PBS, which will lead to a larger estimate for d_{hole}.

Turning now to the effective capacitance, values of C_s / A calculated using

Eq. (4.16) are listed in Table 4.7. Consistently, for all seven skin samples, C_s / A

after the pinhole is about two-thirds the value before pinhole. This result

contradicts the expectation that adding a pinhole does not change the skin

properties if the assumption that C_s represents the effective dielectric constant of skin is correct.

Assuming C_s is related to R_t, Q_s and α_s as described by Eq. (4.16), then the characteristic frequency of the skin is represented by Eq. (4.15), and the ratio of the characteristic frequencies after to before pinhole ($f_{c,t} / f_{c,s}$) is expressed as:

$$\frac{f_{c,t}}{f_{c,s}} = \frac{R_s\, C_{s,before}}{R_t\, C_{s,after}} \tag{4.26}$$

in which $C_{s,before}$ and $C_{s,after}$ designate the effective capacitance before and after pinhole. In fact, the differences listed in Table 4.7 for C_s before and after are consistent with the observed change in characteristic frequency. If it is assumed instead that $C_{s,before} = C_{s,after}$, then the predicted ratio of the characteristic frequencies is given by the ratio of the resistances, which is about two-thirds the observed ratio (and consistent with observed two-thirds ratio in C_s); see Table 4.9.

Recently, Hirschorn et al. (2010) proposed a different approach for estimating the dielectric constant of a material with impedance behavior that is consistent with an R-CPE circuit model (i.e., with the 1-time-constant and pinhole models). Under the assumption that the dielectric constant is independent of position, they demonstrate that the behavior of an R-CPE circuit is consistent with a power-law decay of skin resistivity through the skin thickness. Based on their results (cf. Eqs. 28 and 29 in Hirschorn et al., 2010), the following alternative expression for the effective capacitance can be derived:

$$C_{s,alt} = g^{1/\alpha_s}\, Q_s^{1/\alpha_s}\, R_L^{(1-\alpha_s)/\alpha_s} \tag{4.27}$$

in which the resistivity of the inner most interface of the dominant resistive layer (i.e.,the stratum corneum in the case of skin) is equal to $R_L \, A/L$ and the parameter g is defined as

$$g = 1 + 2.88(1 - \alpha_s)^{2.375} \qquad (4.28)$$

For α_s between 0.8 and 0.7, which are typical values for skin, g is between 1.06 and 1.17. Since R_L is a property of the stratum corneum, to satisfy the assumption that skin properties including $C_{s,alt}$ do not change after needle puncture, both Q_s and α_s in the pinhole model must remain constant. Therefore, according to Eq. (4.14), the ratio of the characteristic frequencies after-to-before pinhole is predicted to be related to the after-to-before resistance ratio as:

$$\frac{f_{c,t}}{f_{c,s}} = \left(\frac{R_s}{R_t} \right)^{1/\alpha_s} \qquad (4.29)$$

As shown in Table 4.9, Eq. (4.29) is consistent with the experimental observations. This result supports the hypothesis that values of C_s estimated using Eq. (4.5) and Eq. (4.16) may not accurately reflect the dielectric constant of the skin when the skin resistance cannot be attributed solely to the dielectric properties of the skin.

An additional observation is that the magnitude of the dielectric constant calculated assuming C_s represents the capacitance of skin according to the definition given in Eq. (4.30)

$$\varepsilon = \frac{C_s L}{A \varepsilon_o} \qquad (4.30)$$

is physically unrealistic. In Eq. (4.30), ε is the dielectric constant, L is the stratum corneum thickness, ε_o is the permittivity of vacuum (8.8542×10^{-5} nF/cm), and A is the sample area.

Table 4.9 Comparing predictions and experimental values for the ratio of the characteristic frequencies after to before skin is punctured with a needle

| | Sample ID | | | | | | | |
Quantity[a]	I	II	III	IV	V	VI	VII	All Samples[b]
$\left(f_{c,t}/f_{c,s}\right)$	27.2	4.9	8.9	6.7	19.5	15.4	6.6	12.8 ± 8.3
$\left(R_{s}/R_{t}\right)$	14.3	3.9	5.9	4.7	11.5	9.1	4.7	7.69 ± 4.0
$\left(f_{c,t}/f_{c,s}\right)/\left(R_{s}/R_{t}\right)$	0.52	0.79	0.65	0.70	0.59	0.59	0.70	0.65 ± 0.1
$\left(R_{s}/R_{t}\right)^{1/\alpha_{s}}$	26.1	5.2	9.0	6.4	18.2	14.5	6.4	12.26 ± 7.7
$\left(f_{c,t}/f_{c,s}\right)/\left(R_{s}/R_{t}\right)^{1/\alpha_{s}}$	0.96	1.07	1.00	0.97	0.94	0.94	0.97	0.98 ± 0.04

[a] For quantities that involve α_s, the value used is the average of the value before and after a pinhole was made. Values before pinhole are designated with subscript s; after pinhole are designated with subscript t.
[b] Values are mean ± one standard deviation of the parameter values for all seven samples.

In this study, the average C_s / A calculated for all skin samples before treatment with DMSO, PBS or pinhole (i.e., from Tables 4.1 and 4.7) was 20.2 ± 4.5 nF/cm^2 (mean ± one standard deviation for 19 samples from two subjects) with a range of 13.8 to 28.8 nF/cm^2, respectively. These results generally agree with 18.6 nF/cm^2 reported for heat separated skin in 50 mM buffered $CaCl_2$ (Hirschorn et al., 2010) and 39.8 nF/cm^2 for 145 samples of split-thickness skin in PBS (White et al., 2011). Assuming L is 15 μm, then the average dielectric constant of the samples presented in this study is 341 (with standard deviation of 77). This value for ε is high by a factor of 5 to 10 given the expected range between about

156

2 for several oils and about 76 for water at 32°C (Weast, 1968). According to Eq. (4.27), $C_{s,alt}$ would be a factor of 3 to 10-fold smaller than C_s calculated using Eq. (4.5) if R_s / R_L is between 100 and 10000 assuming α_s is 0.8. If α_s is 0.75, then $C_{s,alt}$ is 5 to 10-fold smaller than C_s for R_s / R_L between 100 and 1000. Based on low frequency impedance measurements determined as a function of increasing amounts of skin removed by tape stripping, R_s / R_L between 100 and 1000 and perhaps 10000 may be reasonable (Yamamoto and Yamamoto, 1976).

The steady-state flux of CP before and after pinhole and the change in CP flux after pinhole are listed in Table 4.10. Assuming all seven samples belong to the same population, the CP flux after pinhole is not significantly different than before pinhole. However samples I-IV (mean flux 113 ± 14 µg/cm^2/h) are from a different subject than samples V-VII (mean flux 55 ± 4 µg/cm^2/h). Within each subject group the mean CP flux after pinhole is significantly larger than the CP flux before pinhole (student t-test, $p < 0.05$). As an experimental control, one sample was treated in the same way as the pinhole samples except no pinhole was made (Table 4.10). The CP flux for the control sample did not change, suggesting that the observed changes in flux were due only to the hole or to changes in the skin incurred while making the hole. Despite this, the change in CP flux was not correlated with either the hole resistance or diameter, perhaps because the changes were too small relative to the experimental variability.

4.5 Conclusions

Skin impedance measurements are sensitive to irreversible damage caused by exposure to the polar solvent DMSO or by puncture with a needle.

Table 4.10 Steady-state flux of 4-CP ($\mu g/cm^2/h$) before and after pinhole

| | Sample ID[a] | | | | | | | | All samples[b] | |
	Control	I	II	III	IV	V	VI	VII	Mean	Std dev
Before	0.164	101.8	109.8	134.5	107.6	50.9	58.5	55.4	88.4	33.0
After	0.164	120.0	135.4	149.1	127.2	61.8	62.2	62.0	102.5	38.9
Change[b]	0	18.2	25.6	14.5	19.6	10.9	3.7	6.5	14.1	7.7

[a] Samples I to IV are from subject Q; samples V to VII are from subject AS
[b] Values are the mean ± one standard deviation of the parameter values for all seven skin samples.
[c] Change is the value after treatment minus the value before treatment

Moreover, the impedance responses to the two treatments provide insights into differences in the mechanism of damage for DMSO and needle puncture. Impedance measurements after DMSO treatment for various times between 0.25 h and 1 h were consistent with a circuit model in which it was assumed that DMSO progressively damaged a larger fraction of the skin thickness over time and that the undamaged fraction retained the electric properties of the skin before DMSO treatment. The skin appeared to be completely damaged after DMSO treatment times greater than about 0.5 h. Despite changes in skin impedance, treating skin with DMSO for either 0.25 or 1 h did not change the flux of the moderately lipophilic molecule PCNB by a statistically significant amount. This indicates that exposure to DMSO for 1 h or less did not alter significantly the diffusion pathway for this lipophilic compound, but did affect the pathway of ions and presumably other hydrophilic molecules. The change in the skin impedance after DMSO treatment is likely due to changes in the R-CPE parameters of the skin rather than the creation of low resistance shunt pathways.

The impedance of skin before and after puncture with a needle is represented by an R-CPE circuit model that is characterized by a single

characteristic frequency. The characteristic frequency of the impedance scans

determined after needle puncture increased by an amount that could be

predicted using a theory, recently publish by Hirshorn et al. (2010), which

predicts that the CPE parameters of the skin (α_s and Q_s) should not change if the

dielectric constant and resistivity do not. After pinhole, flux of CP increased by a

small but significant amount that was not correlated with the hole resistance or

diameter estimated by assuming that the skin resistance was unchanged after

the pinhole.

REFERENCES

Agarwal, P., Crisalle, O., Orazem, M.E., Garcia-Rubio, L., 1995a. Application of measurement models to impedance spectroscopy, II. Determination of the stochastic contribution to the error structure. Journal of the Electrochemical Society 142, 4149-4158.

Agarwal, P., Orazem, M.E., Garcia-Rubio, L., 1995b. Application of measurement models to impedance spectroscopy, III. Evaluation of consistency with Kramers-kronig relations. Journal of the Electrochemical Society 142, 4159-4168.

Agarwal, P., Orazem, M.E., Garcia-Rubio, L.H., 1996. The influence of error structure on interpretation of impedance spectra. Electrochim. Acta 41, 1017-1022.

Agarwal, P., Orazem, M. E. & Garcia-Rubio, L. H., 1992. Measurement models for electrochemical impedance spectroscopy I. Demonstration of applicability. Journal of Electrochemical Society 139, 1917-1926.

Allenby, A.C., Fletcher, J., Schock, C., Tees, T.F.S., 1969. The effect of heat, pH and organic solvents on the electrical impedance and permeability of excised human skin. Br. J. Dermatol. 81, 31-39.

Bennett, S.L., Barry, B.W., 1985. Effectiveness of skin penetration enhancers propylene glycol, azone, decylmethylsulphoxide and oleic acid with model polar (mannitol) and nonpolar (hydrocortisone) penetrants. Journal of Pharmacy and Pharmacology 37, 84P.

Bunge, A.L., Cleek , R.L., Vecchia, B.E., 1995. A new method for estimating dermal absorption from chemical exposure. 3. Compared with steady-state methods for prediction and data analysis. Pharm. Res. 12, 972-982.

Carslaw, H.S., Jaeger, J.C., 1959. Conduction of Heat in Solids. Oxford University Press, Oxford, Great Britain.

Crank, J., 1975. The Mathematics of Diffusion, 2nd ed. Oxford Science Publication, Oxford.

Curdy, C., Kalia, Y.N., Falson-Rieg, F., Guy, R.H., 2000. Recovery of human skin impedance in vivo after iontophoresis: Effect of metal ions. AAPS PharmSci 2, article 23.

DeNuzzio, J.D., Berner, B., 1990. Electrochemical and iontophoretic studies of human skin. Journal of Controlled Release 11, 105-112.

Gavin, H., 2011. The Levenberg-Marquardt method for nonlinear least squares curve-fitting problems. Department of Civil and Environmental Engineering, Duke University, p. 15.

Hirschorn, B., Orazem, M.E., Tribollet, B., Vivier, V., Frateur, I., Musiani, M., 2010. Determination of effective capacitance and film thickness from constant-phase-element parameters. Electrochim. Acta 55, 6218-6227.

Hsu, C.H., Mansfeld, F., 2001. Technical note: Concerning the conversion of the constant phase element parameter Y_0 into a capacitance. Corrosion 57, 747-748.

Jorcin, J.-B., Orazem, M.E., Pebere, N., Tribollet, B., 2006. CPE analysis by local electrochemical impedance spectroscopy. Electrochemica Acta 51, 1473-1479.

Kasting, G.B., Bowman, L.A., 1990. DC electrical properties of frozen, excised human skin. Pharm. Res. 7, 134-143.

Kim, H.S., Oh, S.Y. Effect of nonionic surfactants on the transdermal flux of ketoprofen, American Association of Pharmaceutical Scientists (AAPS) Annual Meeting, Indianapolis, IN, Oct. 29 - Nov. 2, 2000.

Kurihara-Bergstrom, T., Flynn, G.L., Higuchi, W.I., 1986. Physicochemical study of percutaneous absorption enhancement by dimethyl sulfoxide: kinetic and thermodynamic determinants of dimethyl sulfoxide mediated mass transfer of alkanols. J. Pharm. Sci. 75, 479-486.

Oh, S.Y., Leung, L., Bommannan, D., Guy, R.H., Potts, R.O., 1993. Effect of current, ionic strength and temperature on the electrical properties of skin. Journal of Controlled Release 27, 115-125.

Orazem, M.E., 2001. User Manual for the Measurement Model Toolbox for Impedance Spectroscopy. University of Florida, Gainesville, FL.

Orazem, M.E., Moustafid, T.E., Deslouis, C., Tribollet, B., 1996. The Error Structure of Impedance Spectra for Systems with a Large Ohmic Resistance with Respect to the Polarization Impedance. Journal of The Electrochemical Society 143, 3880-3890.

Orazem, M.E., Tribollet, B., 2008. Electrochemical Impedance Spectroscopy. Wiley-Interscience, Hoboken, NJ.

Peck, K.D., Ghanem, A.H., Higuchi, W.I., 1994. Hindered diffusion of polar molecules through and effective pore radii estimates of intact and ethanol treated human epidermal membrane. Pharm. Res. 11, 1306-1314.

Peck, K.D., Ghanem, A.H., Higuchi, W.I., 1995. The effect of temperature upon the permeation of polar and ionic solutes through human epidermal membrane. J. Pharm. Sci. 84, 975-982.

Pratt, K.W., Koch, W.F., Wu, Y.C., Berezansky, P.A., 2001. Molality-based primary standards of electrolytic conductivity - (IUPAC technical report). Pure and Applied Chemistry 73, 1783-1793.

Tang, H., Mitragotri, S., Blankschtein, D., Langer, R., 2001. Theoretical description of transdermal transport of hydrophilic permeants: Application to low-frequency sonophoresis. J. Pharm. Sci. 90, 545-568.

Weast, R.C., 1968. Handbook of Chemistry and Physics, 49th ed. CRC Press, Cleveland, OH.

White, E.A., Orazem, M.E., Bunge, A.L., 2011. A critical analysis of single-frequency LCR databridge impedance measurements of human skin. Toxicol. In Vitro.

Yamamoto, T., Yamamoto, Y., 1976. Electrical properties of the epidermal stratum corneum. Med. Biol. Eng. 14, 151-158.

APPENDIX

The concentration of a chemical (C) within an initially chemical free membrane at time (t) soon after it is exposed to a chemical solution at constant concentration is described by the following expression (Crank, 1975).

$$\frac{C}{C_o} = 1 - erf\left(\frac{x/L}{2\sqrt{Dt/L^2}}\right) \tag{A.1}$$

in which C_o is the concentration of chemical in the membrane at the surface in contact with the solution, x is the position in the membrane from the surface in contact with the solution, L is the membrane thickness, and D is the diffusion coefficient of the chemical in the membrane. The growth in the thickness of the damaged layer (x_d), defined as the position within the membrane where C is equal to C_d, defined as the minimum value required to alter the measured membrane properties, can be written by a rearrangement of Eq. (A.1) as:

$$x_d/L = 2\sqrt{Dt/L^2}\; \mathrm{erf}^{-1}\left(1 - C_d/C_o\right) \tag{A.2}$$

It follows that the lag time for the growth in the damaged layer thickness ($t_{lag,d}$) can be expressed as

$$t_{lag,d} = \frac{L^2}{6D} = \frac{1}{24\left[\mathrm{erf}^{-1}\left(1 - C_d/C_o\right)\right]^2 \left(\dfrac{x_d/L}{\sqrt{t}}\right)^2} \tag{A.3}$$

Given C_d/C_o, estimates for $t_{lag,d}$ can be calculated by substituting the slope of a plot of x_d/L versus the square-root of time for $(x_d/L)/\sqrt{t}$ in Eq. (A.3).

CHAPTER 5

SUMMARY OF FINDINGS AND RECOMMENDATIONS FOR

FUTURE WORK

The objective of this work was to develop a quantitative foundation for evaluating impedance measurements of skin and to relate the results of the impedance analysis to the skin barrier to chemical transport. To that end, equivalent circuit models of skin impedance were used to calculate the electrical properties of intact and intentionally damaged skin. The parameters from the equivalent circuit models of the impedance were compared with the flux of tritiated water and two lipophilic compounds: 4-cyanophenol (CP) and parachloronitrobenzene (PCNB). A summary of the major findings from this work are described first followed by recommendations for future work.

5.1 Summary of Findings

In this work, numerous impedance spectra were collected from fully hydrated skin samples that had not been intentionally damaged. These data were analyzed, as described in the previous chapters, using an R-CPE equivalent circuit model consisting of a resistor (R_e) in series with a parallel resistor (R_s) and constant phase element (CPE), which is characterized by two parameters, Q and α_s. An effective capacitance (C_{eff}) was calculated from these parameters, using the following expression from Hsu and Mansfeld (2001)

$$C_{eff}/A = \left(Q_s/A\right)^{1/\alpha_s} \left(R_s A\right)^{(1-\alpha_s)/\alpha_s} \tag{5.1}$$

As described in Chapter 4 (see discussion related to Eq. 4.5), this expression was derived by equating the characteristic frequencies for the R-CPE model to the R-C circuit model, in which the CPE is replaced by a capacitor with capacitance C_{eff}.

Estimates of the effective capacitance calculated using Eq. (5.1) were remarkably similar for all samples studied (see Chapters 2 and 4). For example, estimates of C_{eff} for 145 samples from 6 different subjects presented in Chapter 2 had a log mean of 39.8 nF/cm^2 with upper and lower bounds at 75.8 nF/cm^2 and 20.2 nF/cm^2, which correspond to the mean plus and minus one standard deviation of log C_{eff}. In the experiments described in Chapter 4, C_{eff} for all skin samples before treatment with dimethyl sulfoxide (DMSO), phosphate buffered saline (PBS) or needle puncture was 20.2 ± 4.5 nF/cm^2 (mean ± one standard deviation for 19 samples from two subjects) with a range of 13.8 to 28.8 nF/cm^2.

The outermost layer of the skin, called the stratum corneum, is the primary barrier to the transport of ions. It is a heterogeneous membrane consisting of keratin-filled corneocytes surrounded by lamellar lipids, which are about 10 to 20% of the mass of dry stratum corneum (Raykar et al., 1988; Romonchuk and Bunge, 2010). In fully hydrated stratum corneum, the corneocytes contain more than their dry weight in water (Kasting and Barai, 2003). It is expected then that the effective dielectric constant (ε_{eff}) should depend on the dielectric constants, and the amounts and geometric configuration of the main components of the stratum corneum, which are water and lipids. However, because the lipid fraction of fully hydrated stratum corneum is less than 10%, changes in dielectric

constant arising from changes in the lipid composition or configuration may be difficult to measure.

Values of ε_{eff} can be calculated from the definition of C_{eff} given in Eq. (5.2)

$$\varepsilon_{eff} = \frac{C_{eff} \, L}{A \varepsilon_o} \tag{5.2}$$

in which L is the stratum corneum thickness, ε_o is the permittivity of a vacuum (8.8542×10^{-5} nF/cm), and A is the sample area. Consistent with a prior study (Hirschorn et al., 2010b), estimates of ε_{eff} for a typical stratum corneum thickness of 15 μm are an order of magnitude larger than expected (i.e., 674 and 342 for C_{eff} equal to 39.8 and 20.2 nF/cm^2, respectively) based on the range of about 2 to 80 for the dielectric constants of the lipids and water in the stratum corneum. While the reason for this discrepancy remains unknown, Hirschorn et al. (2010a) suggested that, contrary to the approach used to develop Eq. (5.1), the specific geometry and composition of the system should be considered in order to obtain accurate estimates of C_{eff}. Specifically, they showed that under the assumption that the dielectric constant does not change with depth in the stratum corneum, the R-CPE behavior for skin is consistent with a power-law decay of resistivity with depth in the stratum corneum.

While the model developed by Hircshorn et al. (2010b) was based on experimental observations, the actual spatial and chemical properties of the skin that give rise to the R-CPE behavior have not been established. For example, given the heterogeneity of the stratum corneum, it seems reasonable that the electrical properties of the stratum corneum would vary over the skin area as well

as with the depth of the skin. This could be the subject of future modeling efforts described in the Section 5.2.

The pinhole experiments in Chapter 4 provide a quantitative test for using Eq. (5.1) to calculate the C_{eff} of skin. In the pinhole experiments, the skin impedance spectrum was measured before and after the skin was punctured with a needle and in both cases the frequency dependence was determined to be consistent with an R-CPE circuit. Because the cross-sectional area of the needle was small compared to the area of the skin sample, the amount of dielectric material in the punctured skin was essentially unchanged. Despite this, C_{eff} calculated by Eq. (5.1) of the punctured skin was about two thirds the value of C_{eff} calculated for the skin before puncture. Thus, C_{eff} calculated using Eq. (5.1) does not reflect the dielectric constant of the skin when a parallel shunt resistance is added, although the impedance spectrum is still described by an R-CPE circuit.

In Chapters 2 and 3 the single frequency impedance measurements made with an LCR databridge instrument were analyzed. The LCR databridge is a device that has been used to characterize the skin barrier, though there is confusion in the literature about the interpretation of these measurements. In making impedance measurements with the LCR databridge, the user selects three settings: (1) the reported value, either resistance or capacitance; (2) the measurement frequency, either 100 or 1000 Hz; and (3) the measurement mode, either parallel (PAR) or series (SER). In Chapter 2, it was demonstrated that the resistance and capacitance measured in parallel and series modes (i.e. R_{PAR},

R_{SER}, C_{PAR} and C_{SER}) are representations of the complex impedance and

admittance and which are given in Table 5.1.

Table 5.1 Interpretation of the LCR databridge
measurements in terms of the complex impedance (Z) and
admittance (Y)

Settings	Impedance[a]
R_{PAR}	$\dfrac{1}{Y_r}$
R_{SER}	Z_r
C_{PAR}	$\dfrac{Y_j}{2\pi f}$
C_{SER}	$-\dfrac{1}{2\pi f Z_j}$

[a] The subscripts r and j designate the real and imaginary part; the
symbol f designates the frequency at which the measurement
was made in Hz.

From the relationships between the LCR databridge measurements and

the impedance shown in Table 5.1, the frequency dependence for R_{PAR}, R_{SER},

C_{PAR} and C_{SER} measurements was derived in terms of the R-CPE model

parameters in Chapter 2. Also in Chapter 2, an analysis of a large data set of

impedance spectra from fully hydrated skin revealed that R_{PAR} and C_{SER}

measured at 100 Hz are more sensitive to changes in the DC skin resistance

than LCR databridge measurements made with other settings.

In Chapter 3, a large data set of paired measurements of tritiated water

permeability coefficient and R_{PAR} measured with an LCR databridge at either 100

or 1000 Hz, from three different laboratories, was analyzed. Using the equation

for R_{PAR} derived in Chapter 2 and assuming $C_{eff} = 39.8$ nF/cm^2 and $\alpha = 0.8$ for all

skin samples, the DC resistance was estimated from the R_{PAR} measurements.

The estimated DC resistance, normalized by the area, was shown to be inversely

proportional to the tritiated water permeability coefficient. This linear relationship

has been demonstrated for molecules that transport through skin by primarily a

polar pathway (Peck et al., 1995). Thus, the observed linear relationship

between the area normalized DC skin resistance and the inverse of the tritiated

water permeability coefficient supports the hypothesis that water transports

through skin via the polar pathway, despite evidence supporting the lipid pathway

for water (Kasting et al., 2003; Peck et al., 1994, 1995; Potts and Guy, 1992)

In Chapter 4, the skin impedance, measured over a range of frequencies,

was shown to be sensitive to damage caused by chemical treatment with the

aprotic, polar solvent DMSO. In these experiments, the skin impedance and the

flux of PCNB, a model lipophilic compound, were measured simultaneously

before and after treatment with DMSO for various amounts of time up to 1 h. The

most significant result from these experiments was that DMSO appeared to

progressively damage a larger fraction of the skin over time. The impedance

spectrum of DMSO treated skin was consistent with a circuit model that

represents a damaged layer in series with an undamaged layer, where the

undamaged layer retains the electrical properties of the skin before DMSO

treatment. Also, the electrical properties of the DMSO damaged layer, while

different than for undamaged layer, did not appear to change with increased

DMSO treatment time, although the thickness of the damaged layer increased at

a rate that was proportional to the square root of the treatment time. When both

sides of the skin were treated with DMSO, the skin was completely damaged

after about 0.5 h. Interestingly, the flux of PCNB did not change after DMSO

treatment for up to 1 h. From the impedance and flux experiments combined, it

appears that DMSO treatment changed the pathway for ions through skin, as

indicated by the decreased skin resistance, but did not significantly alter the

lipophilic pathway, as indicated by the insignificant change in PCNB flux.

5.2 Recommendations for Future Work

In this section recommendations for future work are presented that follow

naturally from this work. First, additional experiments are recommended to

clarify the results of the pinhole experiments and to further explore the

mechanism by which skin is damaged by DMSO. Next, further investigations are

recommended of two observations made over the course of this work that were

not explored due to limited time. Finally, future modeling efforts are

recommended that would provide insight into the underlying processes affecting

the impedance response of skin.

In Chapter 4, results of the pinhole experiments are presented for seven

samples taken from two subjects. In these experiments, the flux of 4-

cyanophenol before the skin was punctured was about 2-fold larger for one

subject compared to the other. After the pinhole, the flux increased by an

amount proportional to the flux before the pinhole. If the skin remaining after the

pinhole was unchanged, which was supported by the control experiment, then

the change in flux after the pinhole should depend on the size of the hole, which

was independent of the flux before the pinhole. To resolve this discrepancy, it is

recommended that the pinhole experiment be repeated using many samples

from several subjects, to control for variations in skin permeability and mechanical properties that might affect the pinhole size. Also, the skin thickness should be measured at the site of the puncture, which will reduce uncertainty in the pinhole area estimate from the skin resistance measurements.

In the study of DMSO treated skin described in Chapter 4, both sides of the skin had contact with DMSO. The impedance results of these experiments indicate that the skin was completely damaged after about 0.5 h treatment with DMSO. Changes in impedance reflect change in the stratum corneum because it is the skin layer that primarily limits ion transport. Since the stratum corneum lies on top of two layers, the viable epidermis and dermis, which are much more hydrophilic and less restrictive to diffusion, DMSO may not affect both sides of the stratum corneum at the same rate. Therefore, it is recommended that the study of DMSO treatment time described in Chapter 4 be repeated with only one side of the skin in contact with DMSO. Differences in the rate of skin damage for DSMO contact to the stratum corneum compared to contact with the dermis would indicate whether one side of the stratum corneum is more susceptible to DMSO damage than the other.

The first unexplored observation of this study was that skin impedance increased in the presence of CP. Specifically, the impedance of skin equilibrated in 0.01 M phosphate buffered saline (PBS, with 0.138 M NaCl, 0.0027 M KCl, pH 7.4) increased when PBS in the donor chamber was replaced with PBS that was saturated with 4-cyanophenol (CP, MW = 119.1 Da, log $K_{o/w}$ = 1.6). This change in impedance was reversed when the donor chamber was again filled with only

PBS. In similar experiments with PCNB (MW = 157.56 Da, log $K_{o/w}$ = 2.4) saturated PBS, there was no measureable change in impedance from PBS alone.

One possible explanation for this phenomenon is that CP, with a pK_a of 7.97, dissociates in the PBS donor solution (pH = 7.4), while PCNB does not. If the pH of the saturated CP solution is maintained at pH of 7.4, then approximately 20% of the dissolved CP is ionized. It is possible, however, that because of the large CP solubility (18.4 mg/mL from Romonchuk and Bunge (2010) which corresponds to 0.15 M), the partially dissociated CP acid may have overwhelmed the buffering capacity of the PBS. The CP ions would carry some fraction of the charge through the skin. Because the mobility of the CP ions in skin will be smaller than the mobility of the NaCl ions (which is the primary electrolyte in PBS), the impedance of the skin in the presence of CP would appear to increase compared to PBS solution alone.

Though the effect of CP was observed to be reversible, a controlled experiment designed specifically to observe this phenomenon is recommended. The recommended experiment would involve measuring impedance of skin after it has been successively: (1) equilibrated in PBS, (2) equilibrated in CP-saturated PBS, and (3) thoroughly rinsed to remove all CP and equilibrated in PBS again. The control experiment would follow the same steps except that in step 2 the CP-saturated PBS would be replaced with plain PBS. The effect would be considered reversible if the impedance measured in steps 1 and 3 are the same or the impedance changes between steps 1 and 3 in the same way as for the

control experiment. If the phenomenon is not reversible, then the effect is likely related to changes in the skin rather than due to the solution chemistry.

If the effect of the CP saturated PBS on the skin impedance is reversible, the next recommended experiments would examine whether the magnitude of the increase in skin impedance is related to the concentration of ionized CP. In these experiments, the concentration of ionized CP would be controlled by adjusting the CP concentration in PBS solution keeping pH and ionic strength constant by addition of NaOH and NaCl. First, a baseline would be established by measuring the impedance of the skin equilibrated in the buffer solution without CP. Next, the skin would be equilibrated in successively larger concentrations of CP-buffer solution and the impedance measured. As long as the CP solutions are maintained at the same pH, the concentration of CP ions is proportional to the amount of CP dissolved in solution. If the impedance of the skin increases in proportion to the concentration of CP ions in solution, then the effect is likely due to the low mobility of the CP ions through the skin compared to the other ions in solution.

Also recommended is a parallel study that follows the same procedure except that the CP is dissolved in a pH 6 buffer solution, for which only 1% of the dissolved CP is ionized. In these experiments increasing the CP concentration would be expected to have a much smaller effect on the skin impedance.

The second unexplored observation from the work presented here is that the skin impedance consistently deviated from the simple R-CPE circuit model at frequencies below about 1 Hz, as shown most clearly in the plot of $-Z_j A$ in Figure

173

4.10. This low frequency dispersion was also noted by Hirschorn et al. (2010b) for heat separated skin, which includes the stratum corneum and part of the viable epidermis. The impedance over the entire frequency range was consistent with the Kramers-Kronig relations; therefore, the low frequency dispersion is most probably a real feature of the skin and not an experimental artifact. Since this low frequency dispersion was observed for both split-thickness skin and heat-separated skin, it could be caused by the viable epidermis, perhaps in combination with the dermis. This could be confirmed experimentally by measuring the impedance of isolated stratum corneum, which is prepared by soaking the skin in trypsin, an enzyme solution that dissolves the viable epidermis and any remaining dermis to leave only the stratum corneum (Liron et al., 1994a; Liron et al., 1994b). Because isolated stratum corneum is very fragile, the samples would need to be supported during impedance-diffusion experiments.

Finally, additional mathematical modeling is recommended. In general, a simple R-CPE circuit model describes the frequency dependence of skin impedance under a variety of conditions, such as before and after the skin has been treated with DMSO or punctured with a needle. It was shown in this research that equations describing the R-CPE circuit model could be used to relate single frequency impedance measurements to the DC skin resistance and for quantifying changes caused by chemical or mechanical insults. However, it is important to note that the R-CPE circuit model, and equivalent circuits in general, are not based on specific physical and chemical properties that cause the

impedance response to vary with frequency. An alternative approach to modeling the skin impedance is to develop a model based on the structures and composition of the skin that control the mass transfer of ions. A number of questions could be answered with such a model, especially if effects of hydration could be represented. These include: (1) how is the impedance response related to the dielectric constants of the individual components of the stratum corneum (e.g., lipids and corneocytes) and how would this change with hydration? (2) what would be the effect of ion binding to components of the stratum corneum? (3) can the variation of skin hydration explain the hypothesized decrease of resistivity with depth from the stratum corneum surface? and (4) Do the electrical properties vary across the sample area? Answers to these questions would inform further experimental efforts and help to establish how the individual structures of the stratum corneum contribute to the electrical properties represented by equivalent circuit models of the skin.

REFERENCES

Hirschorn, B., Orazem, M.E., Tribollet, B., Vivier, V., Frateur, I., Musiani, M., 2010a. Constant-Phase-Element Behavior Caused by Resistivity Distributions in Films II. Applications. Journal Of The Electrochemical Society 157, C458-C463.

Hirschorn, B., Orazem, M.E., Tribollet, B., Vivier, V., Frateur, I., Musiani, M., 2010b. Determination of effective capacitance and film thickness from constant-phase-element parameters. Electrochim. Acta 55, 6218-6227.

Hsu, C.H., Mansfeld, F., 2001. Technical note: Concerning the conversion of the constant phase element parameter Y_0 into a capacitance. Corrosion 57, 747-748.

Kasting, G.B., Barai, N.D., 2003. Equilibrium water sorption in human stratum corneum. J. Pharm. Sci. 92, 1624-1631.

Kasting, G.B., Barai, N.D., Wang, T.-F., Nitsche, J.M., 2003. Mobility of water in human stratum corneum J. Pharm. Sci. 92, 2326-2340.

Liron, Z., Clewell, H.J., McDougal, J.N., 1994a. Kinetics Of Water-Vapor Sorption In Porcine Stratum-Corneum. J. Pharm. Sci. 83, 692-698.

Liron, Z., Wright, R.L., McDougal, J.N., 1994b. Water Diffusivity In Porcine Stratum-Corneum Measured By A Thermal Gravimetric Analysis Technique. J. Pharm. Sci. 83, 457-462.

Peck, K.D., Ghanem, A.H., Higuchi, W.I., 1994. Hindered diffusion of polar molecules through and effective pore radii estimates of intact and ethanol treated human epidermal membrane. Pharm. Res. 11, 1306-1314.

Peck, K.D., Ghanem, A.H., Higuchi, W.I., 1995. The effect of temperature upon the permeation of polar and ionic solutes through human epidermal membrane. J. Pharm. Sci. 84, 975-982.

Potts, R.O., Guy, R.H., 1992. Predicting skin permeability. Pharm. Res. 9, 663-669.

Raykar, P.V., Fung, M.C., Anderson, B.D., 1988. The role of protein and lipid domains in the uptake of solutes by human stratum corneum. Pharm. Res. 5, 140-150.

Romonchuk, W.J., Bunge, A.L., 2010. Mechanism of enhanced dermal permeation of 4-cyanophenol and methyl paraben from saturated aqueous solutions containing both solutes. Skin Pharamcology and Physiology 23, 152-163.

APPENDIX

PERMISSIONS TO USE COPYRIGHTED MATERIAL

Chapter 2 was published in the Elsevier journal *Toxicology In Vitro*.

Chapter 3 has been accepted for publication in the same journal. Authors who

publish in Elsevier journals retain the right "to include the article in full or in part in

a thesis or dissertation … with full acknowledgement of its original publication in

the journal."

I am a co-author on the paper titled, "Single-Frequency Impedance Measurements as Predictors of Human Skin Permeability to Water and Other Hydrophilic Compounds Toxicology in Vitro," which has been accepted for publication in *In Vitro Toxicology*

I grant Eric A. White permission to publish this paper as a chapter in his thesis for the degree Doctor of Philosophy at the Colorado School of Mines.

Signed: _Runciman_____

Jill Runciman

Date: _20 Jul 2011_____

I am a co-author on the paper titled, "Single-Frequency Impedance Measurements as Predictors of Human Skin Permeability to Water and Other Hydrophilic Compounds Toxicology in Vitro," which has been accepted for publication in *In Vitro Toxicology*

I grant Eric A. White permission to publish this paper as a chapter in his thesis for the degree Doctor of Philosophy at the Colorado School of Mines.

Signed: _____*Alan Horne*_____
Alan Horne

Date:_____20 July 2011_____

I am a co-author on the paper titled, "Single-Frequency Impedance Measurements as Predictors of Human Skin Permeability to Water and Other Hydrophilic Compounds Toxicology in Vitro," which has been accepted for publication in *In Vitro Toxicology*

I grant Eric A. White permission to publish this paper as a chapter in his thesis for the degree Doctor of Philosophy at the Colorado School of Mines.

Signed: _____

Clive S. Roper

Date: _20 July 2011_____

180